Exploring Lower-Limb Motor Control with a Custom Fabricated High Power Haptic Robot

By

Alexander R. Dawson-Elli

A dissertation submitted in partial fulfillment of

the requirements for the degree of

Doctor of Philosophy

(Mechanical Engineering)

at the

UNIVERSITY OF WISCONSIN-MADISON

2022

Date of final oral examination: 11/2/2022

The dissertation is approved by the following members of the Final Oral Committee:

Peter G. Adamczyk, Associate Professor, Mechanical Engineering
Michael R. Zinn, Associate Professor, Mechanical Engineering
Kreg G. Gruben, Professor, Kinesiology
Darryl G. Thelen, Professor, Mechanical Engineering
Joshua D. Roth, Assistant Professor, Mechanical Engineering

Acknowledgements

Thank you to Rebecca Ross for supporting and encouraging me towards a scientific career from a young age. Thank you Paco Lopez for showing me by example what good mentorship looks like and instilling that by putting your people before the work, good work will follow. Dan Phillips, for sharing words of wisdom with me, many of which I came to appreciate the truth of years after they were spoken to me. Thank you Michal Niedzielski – for sharing with me your curiosity, optimism, clinical expertise, and relentless pursuit of the truth. You are without a doubt the reason I am now studying biomechanics.

Thank you to my advisor Peter Adamczyk, for your financial support and for the interesting conversations we have had over the years. Thank you to my committee, Mike Zinn, Kreg Gruben, Darryl Thelen, Josh Roth, for your time and input through this process.

Thank you to my colleagues and office mates Patrick Dills and Mike Hagenow, I've learned a tremendous amount from both of you and will miss the intellectual enjoyment of our conversations. Thanks to Samuel Acuña, for taking me under your wing in my first year.

Thanks to my BADGER Lab mates, Jenna Thorp, Evan Glanzer, Mike Greene, Weixin Wang, Hannah Mrazsko, Kieran Nichols, Becca Roembke, Yisen Wang, Heidi Fehr, Stephanie Hernández-Hernández. I have fond memories with each of you that I will take with me.

I would like to thank my funding sources including the National Science Foundation and their National Robotics Initiative program, NCSRR's pilot projects program, and UW Mechanical Engineering fellowships for supporting this research.

Finally, a huge thanks to all of my family and friends, and most of all my soon to be wife Alana Stempien for your boundless support throughout this experience.

Abstract

Stroke impacts 7 million people in US. Of the disabilities induced by stroke, mobility limitations are among the strongest factors limiting quality of life. Robotic approaches to stroke rehabilitation in the lower-limb have historically focused on rhythmic movements and activities which replicate gait kinematics. These approaches have not yet yielded better outcomes than standard therapy. A reason for this could be the lack of volitional engagement and goal-directed behavior in these activities. This Dissertation explores the design of robotic and software systems required for the study of goal-directed lower-limb motor control and the application of these systems to derive new insights through controlled experiments. The outcomes of this Dissertation aim towards facilitating future studies of rehabilitation in stroke affected populations.

The First chapter describes the design, development, and validation of NOTTABIKE, a high-power haptic robot developed for the study of motor control and the delivery of lower-limb therapy. The second chapter explores the results of experiments on healthy subjects performing lower-limb reaching tasks in a dynamic environments. The results center around the time course of adaptation to these varied environments and an optimal control model of adaptation. The third chapter details an experiment investigating the effect of cognitive models on the skill learning in the lower-limb, an important yet understudied aspect of rehabilitation with robotic systems. Finally, the fourth chapter documents the optimal design of the linkage system for a 2DOF high power haptic robot using a novel force-space matching approach. This Dissertation lays the foundation for a Research Program in the BADGER Lab oriented towards the study of lower-limb motor control and the application of rehabilitative therapy in the lower-limb that focuses on the training of volitional movements.

Table of Contents

List of Figures

Chapter 4

List of Tables

Introduction

This section covers the research motivation, background, approach, a summary of the research contributions, and an overview of the chapters of this Dissertation.

Research Motivation

Rehabilitation after neural injury such as stroke is an important aspect of health care for aging populations due to the high prevalence of stroke and incidence of stroke-related disability [1]. Mobility impairments are among the effects of stroke that most limit survivors' participation and quality of life [2], [3]. Robotics for gait therapy have been touted as a breakthrough technology that could significantly reduce this burden. But, outcomes from those therapies have not been as successful as expected [4].

One possible reason for this could be the emphasis placed on task-specific gait training in the rehabilitation on the lower-limb. The idea that training must be task-specific is often traced to a classic study in which two balance interventions with different effects on standing symmetry did not have differential effects on gait symmetry [5]. This finding is commonly interpreted as evidence that motor skills do not transfer across activities, and therefore full tasks must be practiced in an all-at-once fashion. However, there are clear examples in which improvements in one task transfers into practical and transferable skills, such as the finding that practicing tai chi helps reduce all falls in older adults (not just falls while practicing tai chi) [6], [7]. A potential difference may be that tai chi improves an underlying, general sensorimotor capacity whereas training a specific pattern may simply train a preference.

Additionally, approaching lower-limb rehabilitation training in an all-at-once fashion often takes the form of replicating the kinematics of gait. This neglects a fundamental tenet of cognitive neuroscience that neuroplastic change in the adult brain requires volitional engagement via top down cortical control [8]. Training sub-movements that are goal-directed requires conscious control and the development of precursory movements is an alternative that has not been sufficiently explored in the lower-limb.

The motivation of this research program is to use the robotic systems we have developed to expand understanding of volitional, goal-directed activities in the lower-limb, with the idea that this understanding will help inform future rehabilitation interventions.

Background

Rehabilitation robotics for the lower-limb have mostly focused exoskeletons and pedal systems targeting gait and cycling training [3], [4], [9]–[12]. The Hocoma Lokomat [13] system originally executed a simple playback of a pre-recorded gait pattern, with the idea of providing normal proprioceptive signals that could help the brain relearn control [14]–[17]. Unfortunately, such open-loop motion playback failed to engage patients volitionally in the task, and many simply allowed their legs to be passively moved. In addition to the Lokomat, other lower limb exoskeleton robots including the walkTrainer [18], [19], AutoAmbulator [20], LOPES [21], and MindWalker [22] have been created to provide different forms of assistance and rehabilitative intervention. Efforts have been made to add compliance in order to implement virtual tunnels where correction is only done “as needed”, or by adding a biofeedback component [23].

Kinematic variability during training [17] has also been shown to alter post training coordination. One approach with reasonable success is split-belt treadmill gait training [24], [25]

which leverages an adaptation process to temporarily restore gait symmetry during washout. Split-Belt treadmill training evokes high involvement from the participant but remains coupled to a walking activity and so in not feasible for the pre-ambulatory subject without weight support. In summary, apart from split-belt treadmill training, robotic gait training has shown little benefit beyond conventional training (body weight-supported treadmill training, BWSTT).

Robots used to study motor control in the lower-limb have focused on cycling activities and developing understanding of inter-limb connections, believed to exist at the level of the spinal cord. These ideas were likely motivated by animal studies conducted in the 1970's in the tradition of Bernstein on decerebrate cats [26], which showed that in cats, machine stabilized locomotion was possible without cortical involvement, through the presence of Central Pattern Generators (CPGs). Studies by Ting [27] revealed that static extensor contraction of one leg could alter the phasing and magnitude of the flexor muscles of the contralateral leg, further suggesting that this brainstem level connection exists in man. This finding however does not preclude the fact that cortical involvement is an essential component of gait in man – as cortical level damage can certainly induce gait deficit [28]. Thus, it appears that goal-directed reaching activities which require cortical involvement and full integration of the planning sensory and the visuo-motor systems remain understudied in the lower-limb.

In contrast, the study of motor control and the application of therapy in the upper-limb using robots has been based around the activity of planar reaching. Early work in this area centered around studying the distortions imposed on straight line reaching when interacting in a 2D forcefield [29]. The forcefield of choice for early investigators was the cross-axis damper which produces force orthogonal to the direction of movement and in proportion to the velocity of the end effector. After a period of time, subjects would adapt to this environment, and when the

environment was taken away would experience after-effects from the continued anticipation of interaction with the environment. This is similar to the behavior seen during de-adaptation in split-belt treadmill walking. Other approaches included the creation of virtual channels, and the concept of error augmentation, which improves learning rate by amplifying error and providing it in a force feedback channel [30], [31]. Evidence from the cognitive neuroscience of learning suggests that in adults, attention is required for neuroplasticity, as well as the involvement of motivational rewards systems in the dopaminergic system of the basal ganglia [8]. While the approaches to upper-limb study and rehabilitation integrate the motivational system through goal directed behavior, those that are commonplace in the rehabilitation of gait do not.

Approach

Our approach to rehabilitation and the study of motor control is to explore the goal-directed activities popularized in the study of the upper-limb, in the lower-limb. We have and continue to construct specialized hardware such as NOTTABIKE and the follow-on 2DOF robot which are capable of generating the forces required to study the lower-limb. We have conducted studies in reaching in dynamic environment in healthy subjects to establish behavior norms and determine how motor adaptation in reaching task compares between the upper and lower limbs. Future BADGER Lab research will extend this work to stroke subject populations and compare learning rates and principles between healthy and stroke effected populations.

Statement of Contributions

The key contributions of this research are summarized below:

- Designed, built, and validated NOTTABIKE hardware system, a robotic platform built on an exercise cycle but motorized with an industrial servomotor and instrumented with two, 5 axis force-torque sensing pedals, crank and pedal encoders, and integrating EMG sensors.
- Developed the software system for NOTTABIKE which enables rendering impedance and admittance based haptic environments, specification, and automation of extended experimental protocols, as well as the visualization of real-time feedback.
- Published a manuscript (Chapter 1) characterizing NOTTABIKE performance, usage, rendering capabilities in TNSRE
- Developed experimental protocol to investigate adaptation of lower-limb control strategies to springs of different stiffnesses.
- Analyzed the impact of changing spring environments on lower-limb reaching performance, and modeled reaching performance as a Model Identification adaptive control process.
- Submitted manuscript (Chapter 2) for publication in HMS.
- Created a protocol for quantitatively studying the role of cognitive models on the time course of skill acquisition in the lower-limb in a novel half-reversed cycling task.
- Executed HRC experimental protocol in 20 subjects and developed a proposed analysis pipeline (Chapter 3).
- Developed a methodology for designing a 2DOF lower-limb parallel haptic robot based on the novel concept of force-space congruence matching between a robot model and a human model in the sagittal plane.

- Implemented a custom software library defining human and robot model kinematics, inverse kinematics, and instantaneous kinematics / statics.
- Integrated human and robot and performed a joint optimization using the DIRECT method to select optimal robot design parameters under various constraints.
- Developed a dynamic model of the 2DOF robot using the Chrono Engine.

Summary of Chapters

In chapter 1, we describe the design and validation of NOTTABIKE, a recumbent cycle ergometer that has been motorized and instrumented for the study of lower-limb motor control and the application of rehabilitative exercise. We emphasize the design of the hardware system, the software architecture of the controller and experimental scripting platform, and performance metrics for haptic rendering.

In chapter 2, we present the results of an experiment investigating adaptation to a reaching task in a spring environment. The questions evaluated include the temporal dynamics of adaptation, the influence of visual precursory information on performance, and modeling of the adaptation process using an optimal control approach.

In chapter 3, we present an experiment to quantify of cognitive models and explicit knowledge in lower-limb skill acquisition. The training task under evaluation is termed half-reversed cycling (HRC) and represents a novel environment in which skill must be progressively developed over multiple sessions to gain and retain proficiency. We also evaluate the extent of interlimb transfer.

In chapter 4, we detail the optimal design of a 2DOF parallel rehabilitation robot for the lower-limb based on a novel technique of force-space congruence matching. We also present a dynamic model of the robot, and auxiliary mechanical design details.

References

[1] D. Mozaffarian *et al.*, "Executive Summary: Heart Disease and Stroke Statistics—2015 Update:: A Report From the American Heart Association," *Circulation*, vol. 131, no. 4, pp. 434–441, Jan. 2015, doi: 10.1161/CIR.0000000000000157.

[2] M. A. Muren, M. Hütler, and and J. Hooper, "Functional Capacity and Health-Related Quality of Life in Individuals Post Stroke," *Top. Stroke Rehabil*, vol. 15, no. 1, pp. 51–58, Jan. 2008.

[3] P. Langhorne, F. Coupar, and and A. Pollock, "Motor recovery after stroke: a systematic review," *Lancet Neurol*, vol. 8, no. 8, pp. 741–754, 2009.

[4] C. M. Stretton, S. Mudge, N. M. Kayes, and and K. M. McPherson, "Interventions to improve real-world walking after stroke: a systematic review and meta-analysis," *Clin. Rehabil*, vol. 31, no. 3, pp. 310–318, Mar. 2017.

[5] C. J. Winstein, E. R. Gardner, D. R. McNeal, P. S. Barto, and D. E. Nicholson, "Standing balance training: effect on balance and locomotion in hemiparetic adults," *Arch Phys Med Rehabil*, vol. 70, no. 10, pp. 755–62, 1989.

[6] F. Li *et al.*, "Tai Chi and Fall Reductions in Older Adults: A Randomized Controlled Trial," *J Gerontol A Biol Sci Med Sci*, vol. 60, no. 2, pp. 187–194, Feb. 2005, doi: 10.1093/gerona/60.2.187.

[7] S. Low, L. W. Ang, K. S. Goh, and S. K. Chew, "A systematic review of the effectiveness of Tai Chi on fall reduction among the elderly," *Archives of Gerontology and Geriatrics*, vol. 48, no. 3, pp. 325–331, May 2009, doi: 10.1016/j.archger.2008.02.018.

[8] M. S. Gazzaniga, *The cognitive neurosciences*. MIT press, 2009.

[9] S. Hesse and D. Uhlenbrock, "A mechanized gait trainer for restoration of gait," *Journal of rehabilitation research and development*, vol. 37, no. 6, pp. 701–708, 2000.

[10] J. Mehrholz and M. Pohl, "Electromechanical-Assisted Gait Training After Stroke: A Systematic Review Comparing End-Effector and Exoskeleton Devices," *Journal of Rehabilitation Medicine*, vol. 44, no. 3, pp. 193–199, Mar. 2012, doi: 10.2340/16501977-0943.

[11] D. A. Brown, S. Nagpal, and S. Chi, "Limb-Loaded Cycling Program for Locomotor Intervention Following Stroke," *Phys Ther*, vol. 85, no. 2, pp. 159–168, Feb. 2005, doi: 10.1093/ptj/85.2.159.

[12] T. Tatemoto, S. Tanaka, K. Maeda, S. Tanabe, K. Kondo, and T. Yamaguchi, "Skillful Cycling Training Induces Cortical Plasticity in the Lower Extremity Motor Cortex Area in Healthy Persons," *Front. Neurosci.*, vol. 13, 2019, doi: 10.3389/fnins.2019.00927.

[13] "Lokomat®," *Hocoma*. https://www.hocoma.com/solutions/lokomat/ (accessed Jul. 20, 2017).

[14] M. Alcobendas-Maestro, "Lokomat Robotic-Assisted Versus Overground Training Within 3 to 6 Months of Incomplete Spinal Cord Lesion Randomized Controlled Trial," *Neurorehabil. Neural Repair*, vol. 26, no. 9, pp. 1058–1063, Nov. 2012.

[15] J. Hidler, "Multicenter Randomized Clinical Trial Evaluating the Effectiveness of the Lokomat in Subacute Stroke," *Neurorehabil. Neural Repair*, vol. 23, no. 1, pp. 5–13, Jan. 2009.

[16] C. Bonnyaud, D. Pradon, J. Boudarham, J. Robertson, N. Vuillerme, and and N. Roche, "Effects of Gait Training Using a Robotic Constraint (Lokomat®) on Gait Kinematics and Kinetics in Chronic Stroke Patients," *J. Rehabil. Med*, vol. 46, no. 2, pp. 132–138, Feb. 2014.

[17] M. D. Lewek, T. H. Cruz, J. L. Moore, H. R. Roth, Y. Y. Dhaher, and and T. G. Hornby, "Allowing Intralimb Kinematic Variability During Locomotor Training Poststroke Improves Kinematic Consistency: A Subgroup Analysis From a Randomized Clinical Trial," *Phys. Ther*, vol. 89, no. 8, pp. 829–839, Aug. 2009.

[18] M. Bouri *et al.*, "The WalkTrainer: A Robotic System for Walking Rehabilitation," in *2006 IEEE International Conference on Robotics and Biomimetics*, Dec. 2006, pp. 1616–1621. doi: 10.1109/ROBIO.2006.340186.

[19] Y. Stauffer *et al.*, "The WalkTrainer - A New Generation of Walking Reeducation Device Combining Orthoses and Muscle Stimulation," *IEEE Transactions on Neural Systems and Rehabilitation Engineering*, vol. 17, no. 1, pp. 38–45, Feb. 2009, doi: 10.1109/TNSRE.2008.2008288.

[20] "AutoAmbulator," *Encompass Health*. http://encompasshealth.com/inpatient-rehabilitation/irf-our-technology/autoambulator (accessed Aug. 09, 2020).

[21] J. F. Veneman, R. Kruidhof, E. E. G. Hekman, R. Ekkelenkamp, E. H. F. Van Asseldonk, and H. van der Kooij, "Design and Evaluation of the LOPES Exoskeleton Robot for

Interactive Gait Rehabilitation," *IEEE Transactions on Neural Systems and Rehabilitation Engineering*, vol. 15, no. 3, pp. 379–386, Sep. 2007, doi: 10.1109/TNSRE.2007.903919.

[22] S. Wang, "Design and Control of the MINDWALKER Exoskeleton," *IEEE Trans. Neural Syst. Rehabil. Eng*, vol. 23, no. 2, pp. 277–286, 2015.

[23] C. Krishnan, R. Ranganathan, Y. Y. Dhaher, and and W. Z. Rymer, "A pilot study on the feasibility of robot-aided leg motor training to facilitate active participation," *PloS One*, vol. 8, no. 10, p. 77370, 2013.

[24] D. S. Reisman, H. McLean, J. Keller, K. A. Danks, and A. J. Bastian, "Repeated Split-Belt Treadmill Training Improves Poststroke Step Length Asymmetry," *Neurorehabil Neural Repair*, vol. 27, no. 5, pp. 460–468, Jun. 2013, doi: 10.1177/1545968312474118.

[25] D. S. Reisman, H. McLean, J. Keller, K. A. Danks, and and A. J. Bastian, "Repeated Split-Belt Treadmill Training Improves Poststroke Step Length Asymmetry," *Neurorehabil. Neural Repair*, vol. 27, no. 5, pp. 460–468, Jun. 2013.

[26] M. L. Latash, *Progress in motor control: Bernstein's traditions in movement studies*, vol. 1. Human kinetics, 1998.

[27] L. H. Ting, S. A. Kautz, D. A. Brown, and F. E. Zajac, "Contralateral movement and extensor force generation alter flexion phase muscle coordination in pedaling," *Journal of Neurophysiology*, vol. 83, no. 6, pp. 3351–3365, 2000.

[28] L. D. Alexander, S. E. Black, K. K. Patterson, F. Gao, C. J. Danells, and W. E. McIlroy, "Association between gait asymmetry and brain lesion location in stroke patients," *Stroke*, vol. 40, no. 2, pp. 537–544, 2009.

[29] R. Shadmehr and F. Mussa-Ivaldi, "Adaptive representation of dynamics during learning of a motor task," *The Journal of Neuroscience*, vol. 14, no. 5, pp. 3208–3224, May 1994, Accessed: Aug. 12, 2011. [Online]. Available: http://www.jneurosci.org/content/14/5/3208.abstract

[30] F. Abdollahi *et al.*, "Arm control recovery enhanced by error augmentation," in *2011 IEEE International Conference on Rehabilitation Robotics*, Jun. 2011, pp. 1–6. doi: 10.1109/ICORR.2011.5975504.

[31] F. Abdollahi *et al.*, "Error Augmentation Enhancing Arm Recovery in Individuals With Chronic Stroke: A Randomized Crossover Design," *Neurorehabil Neural Repair*, vol. 28, no. 2, pp. 120–128, Feb. 2014, doi: 10.1177/1545968313498649.

Chapter 1

Design and Validation of a Lower - Limb Haptic Rehabilitation Robot

Alexander R. Dawson-Elli and Peter G. Adamczyk
(This Chapter is published in the Journal IEEE TNSRE)

1.1 Abstract

Present robots for investigating lower-limb motor control and rehabilitation focus on gait training. An alternative approach is to focus on restoring precursor abilities such as motor adaptation and volitional movement, as is common in upper-limb robotic therapy. Here we describe NOTTABIKE, a one degree-of-freedom rehabilitation robot designed to probe and promote these underlying capabilities. A recumbent exercise cycle platform is powered with a servomotor and instrumented with angular encoders, force-torque sensing pedals, and a wireless EMG system. Virtual environments ranging from spring-mass-damper systems to novel foot-to-crank mechanical laws present variants of leg-reaching and pedaling tasks that challenge perception, cognition, motion planning, and motor control systems. This paper characterizes the dynamic performance and haptic rendering accuracy of NOTTABIKE and presents an example motor adaptation task to illustrate its use. Torque and velocity mode controllers showed near unity magnitude ratio and phase loss less than 60 degrees up to 10 Hz. Spring rendering demonstrated 1% mean error in stiffness, and damper rendering performed comparably at 2.5%. Virtual mass rendering was less accurate but successful in varying perceived mass. NOTTABIKE will be used to study lower-limb motor adaptation in intact and impaired persons and to develop rehabilitation protocols that promote volitional movement recovery.

1.2 Introduction

Most information about motor control and rehabilitation has been derived from studies of upper limb reaching and manipulation. Haptic robotics have played a key role in establishing motor learning principles from experiment. The ability to control the mechanical environment of the limb and hand allows experimenters to present subjects with tasks they have not encountered previously, and then observe the processes of motor adaptation and learning. This approach has led to a set of motor control insights and guiding principles for rehabilitation intervention [1]. First, the brain can build internal models of limb dynamics [2] and multiple such models coexist or interfere in predictable ways. Second, amplifying error can accelerate motor learning [3]–[5]. Third, dynamically manipulating task success rate can optimize patient motivation [6]–[9] leading to higher self-selected work volumes. Finally, task assistance should only be applied as needed [10]–[12], not continuously. An implicit principle common to upper-limb rehabilitation approaches is volitional control [13]: movements – typically reaching – are initiated by the user; the tasks require cognitive engagement to respond to visual and mechanical stimuli; and completing the task requires a full chain of neural control including perception, cognition, planning, initiation, execution, and feedback. This circuit of afferent and efferent neural activity is thought to be important for neural plasticity [14], [15].

By contrast, approaches to lower limb rehabilitation have focused almost exclusively on cyclic tasks, especially gait and gait-like tasks. For instance, early training approaches on the Hocoma Lokomat [16] exoskeleton played back pre-recorded gait patterns to provide proprioceptive input similar to normal gait [17]. Extensions to improve the volitional engagement of these activities have included the Lokomat as well as a variety of other machines, ranging from haptic foot plates to whole-limb or single-joint exoskeletons (for excellent reviews, see [18], [19])

Fig 1.1. NOTTABIKE System Overview.
NOTTABIKE is a one degree-of-freedom robot used to study human motor control and to deliver rehabilitation in the lower-limb. Measurements of subject endpoint kinematics and kinetics are used by a computer controller to create virtual haptic environments.

These systems have been used to explore different control strategies including assist-as-needed control, impedance control, adaptive control that responds to user success, or electromyography-driven control [18].

These strategies comport with best practices in motor rehabilitation, but the overwhelming focus on using them within a walking context leads to fundamental challenges to accessibility and therefore scalability in final application. Such problems include high device complexity (and therefore cost, space and dedicated personnel), substantial time and effort in mounting the device to the user or the user to the device, and in some cases a substantial minimum functional level of the user prior to therapy. There remains a need for solutions that are simple, easy to use, and usable early in the recovery process, while still using motor rehabilitation principles to evoke high volitional engagement.

A recumbent pedal-based robot could meet this need, building upon past [20] use of recumbent cycles and steppers. In clinical use, powered cycle ergometers such as the MOTOmed [21] and RT300 [22] are used to move subjects through cyclic motions, though without explicitly requiring volitional muscle activation. In research, pedaling backward has been shown to require a change in timing for a subset of muscles [23], [24]. Studies of split-crank pedaling [25] have shown ipsilateral motor coordination pattern is altered by the state of the contralateral leg [26], [27] suggesting cross-couplings between extensor and flexor muscle groups. Recent cycling research suggests skillful cycling leads to longer lasting cortical activation changes than constant speed pedaling [28]. And, experiments on the NuStep [29] recumbent stepper have demonstrated an excitatory effect of upper limb activity on lower limb EMG during rhythmic tasks [30], [31]. In hemiparetic subjects, pedaling studies have shown reduced work generation on the affected side

[32], [33] but retained ability to increase force output against an increased work load when demanded [34]. Other studies indicate that it is foot force direction, rather than magnitude that is primarily affected after stroke [35]. These studies and rehabilitation approaches are frequently based on the idea that much of lower limb control is managed by subcortical neural structures that are adapted to cyclic motion [36]. But, rehabilitation that relies exclusively on cyclic motions, without compelling volitional engagement, may miss a critical step by failing to engage cortical structures that need to recover or adapt [37].

Our goal is to combine the simplicity of a pedaling system with motor rehabilitation principles gleaned from upper limb reaching, emphasizing engagement of cortical structures through volitional movements in the lower limb. As opposed to an all-at-once approach of directly emulating gait, we propose to use lower-limb reaching in different haptic environments to develop motor competency through a series of subtasks related to gait. The large forces inherent in lower limb movement prevent the direct application of upper limb reaching robots to studying motor control in the lower limb. To address this gap, we built a powered, instrumented robotic exercise cycle (NOTTABIKE) to present cognitively demanding reaching and pedaling tasks in novel haptic mechanical environments in the lower limb.

Haptic environments are important because they enable a researcher to present specific mechanical conditions to a moving limb. These environments may be designed to present conditions that the motor system has never experienced before (to study motor learning), or conditions that incentivize specific aspects of motor control that need to be improved (for rehabilitation). In the upper limb, environments such as viscous curl [2], haptic tunnels [38], and error augmentation [39] have been used to derive motor learning principles. NOTTABIKE was created to facilitate the study of similar haptic environments in the lower limb. A few haptic lower

limb robots have been implemented before [40]–[42], but none in the context of pedaling-like movement.

This paper describes the design and performance of the NOTTABIKE platform. The system is built on a recumbent exercise cycle frame and has a single actuated degree-of-freedom powered by an industrial servomotor. An array of sensors record foot reaction forces and moments, crank and pedal kinematics, and muscle electromyographic (EMG) activity, which are used to compute state and control the motor. We evaluate the performance of the system using ramp-input, step-input and frequency response tests, and demonstrate human interaction with multiple haptic environments. We conclude with a demonstration of using NOTTABIKE to probe adaptation to haptic rendering of different spring stiffnesses. A preliminary version of this work has been reported [43].

1.3 Methods

The Neuromotor Optimization Testbed for Training in Atypical Behavior-Inducing Kinetic Environments (NOTTABIKE; Fig 1.1) is based on a recumbent exercise cycle platform, but its purpose is not pedaling exercise. Rather, it is a one degree-of-freedom haptic leg rehabilitation robot designed to render customized virtual environments defining the foot-to crank mechanical interaction. The recumbent posture is intended to enable early intervention following neuromotor injury, before ambulatory capacity is reestablished. The haptic environments are intended to demand active motor exploration and volitional engagement in non-cyclic tasks like targeted leg reaching, foot force control or manipulation of a dynamic system, and to provide proprioceptive afferent neural activity to encourage neural plasticity. The goals are to explore motor control in volitional leg movements, characterize deficits and capacity in performance and motor learning in

impaired and unimpaired persons and develop therapeutic exercises that promote targeted improvement in these deficits.

The NOTTABIKE system is designed to render impedance- and admittance-based haptic environments. Mechatronic subsystems include a high-performance industrial servomotor, a custom drivetrain, and kinetic and kinematic sensors. A custom multi-threaded software framework enables setting up and running rehabilitation exercises and human motor control experiments. The following sections present the mechatronic design, control architecture, and system performance characterization in a series of electromechanical and human interaction tests.

1.3.1 Mechatronic Design – Drivetrain and Communication

The frame of the robot is a retrofitted recumbent stationary bicycle. The frame consists of square steel tube construction with an adjustable padded seat and bilateral hand holds with integral grip-actuated safety switches.

The power subsystem is based on a brushless DC servomotor with integrated high-bandwidth velocity and torque mode controllers (ClearPath CPM-MCVC-3441S-RLN, Teknic Inc., Victor, NY, USA). The motor can provide peak torque of 13 Nm at the spindle, and peak assistive power of 350 W. This motor was chosen for its high torque density and low peak velocity (840RPM). A 75 VDC, 350 W continuous power supply was used (IPC-5, Teknic Inc., Victor, NY, USA) to source power during assistive operation, and an 800W regeneration clamp and power resistor dissipates power during resistive operation (Applied Motion Products, Watsonville, CA, USA).

The drivetrain transfers power between the motor and the crank. It consists of a motor mount, a two-stage chain transmission, and a bottom-bracket and crank assembly (Fig 1.2). This

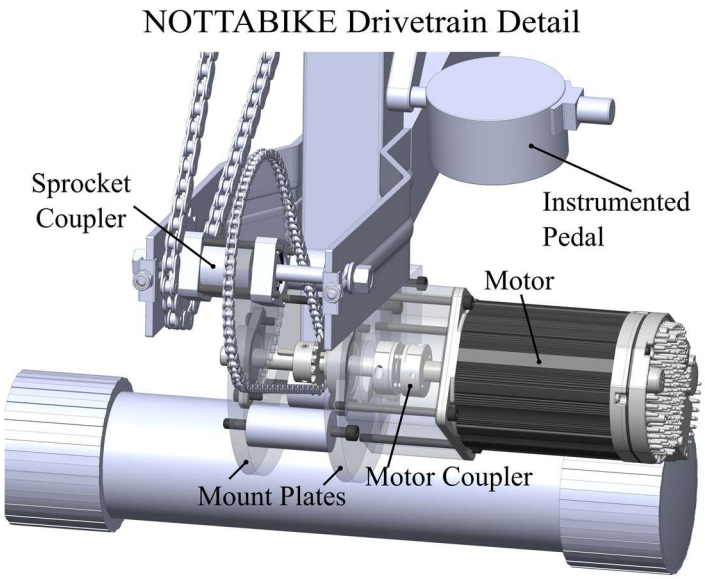

Fig 1.2. Two-Stage Mechanical Drivetrain.
The drivetrain provides efficient power transfer between the user, who interacts through the pedals, and the industrial servomotor.

design was selected over alternative approaches because high drivetrain efficiency and back drivability are required for accurate impedance-based haptic renderings. The motor is attached to the steel frame by a custom aluminum mounting bracket which is pinch fit to the frame to allow freedom for chain tensioning. A 10mm diameter steel driveshaft rests between bearing blocks and connects to the motor through a rotary shaft coupler. A two-stage chain-and-sprocket reduction transfers power from the drive shaft to the pedal crank. The overall gear ratio between the rotation of the motor and the crank is 3128:320 or 9.775:1.

Communication to the integrated controller on the servomotor is achieved through Pulse Width Modulation (PWM) of control lines. A dedicated microcontroller (Atmega 2560, Atmel Corp. San Jose, CA, USA) converts command packets received over a serial communication port into 8 kHz PWM control signals. The motor controller interprets these PWM signals as velocity or torque commands. The motor's integrated controller may be placed into either velocity or torque mode via commands sent over USB from the host computer.

The motor system has several safety features that protect the user from encountering excessive torque or velocity. First, software limits on torque and velocity are set on the motor's embedded controller (nominal settings for this application are equivalent to 70 Nm and 30 RPM at the crank). Second, we installed two safety switches, one under each hand, that must both be depressed for the motor to receive power from the power supply. If at any time one of these safety switches is released, power to the motor is cut and the system enters a passive damped state facilitated by the motor back-EMF.

1.3.2 Mechatronic Design – Sensors

The robot is instrumented with sensors to measure forces and moments at the pedal interface, angular rotations of the crank and pedals, and Electromyographic (EMG) activity of the user's leg muscles. These data are sampled by a 16-bit data acquisition (DAQ) card (PCIE-6343, National Instruments, Austin, TX, USA) and are used for High-Level control (see section C) and logged for analysis through a desktop computer (Windows 10 operating system, Microsoft Corp., Redmond WA). Foot endpoint forces, moments, and pedal angular positions are measured by instrumented pedals (I-Crankset, Sensix, Poitiers, France). Each pedal contains a six-component force-torque load cell with internal amplification and signal conditioning. Maximum simultaneous force measurement is 250 N in the F_x (lateral) and F_y (anterior) directions and 2000 N in F_z. (normal to the pedal) – more than adequate for experimentation in healthy subjects. Optical quadrature encoders on each pedal axis generate 20000 counts per revolution. Crank kinematics are measured with a magnetic quadrature encoder ring fixed to the left crank and a reader fixed to the frame, which generate 24000 counts per revolution. The amplified analog signals from each pedal and quadrature channels are collected in a junction box and output over a VHDCI cable into the DAC card. A wireless EMG system (Trigno Avanti Research+, Delsys, Natick, MA, USA) records up to 16 channels of EMG and relays them onto analog lines for synchronized recording on the DAC. EMG System relay delay is 42 ms.

1.3.3 Control and Software Architecture

The control system of the robot is implemented with a cascaded architecture across multiple processors connected by communication interfaces. A high-level control law rendering a specified haptic environment runs on a desktop computer at 100Hz. From that virtually rendered

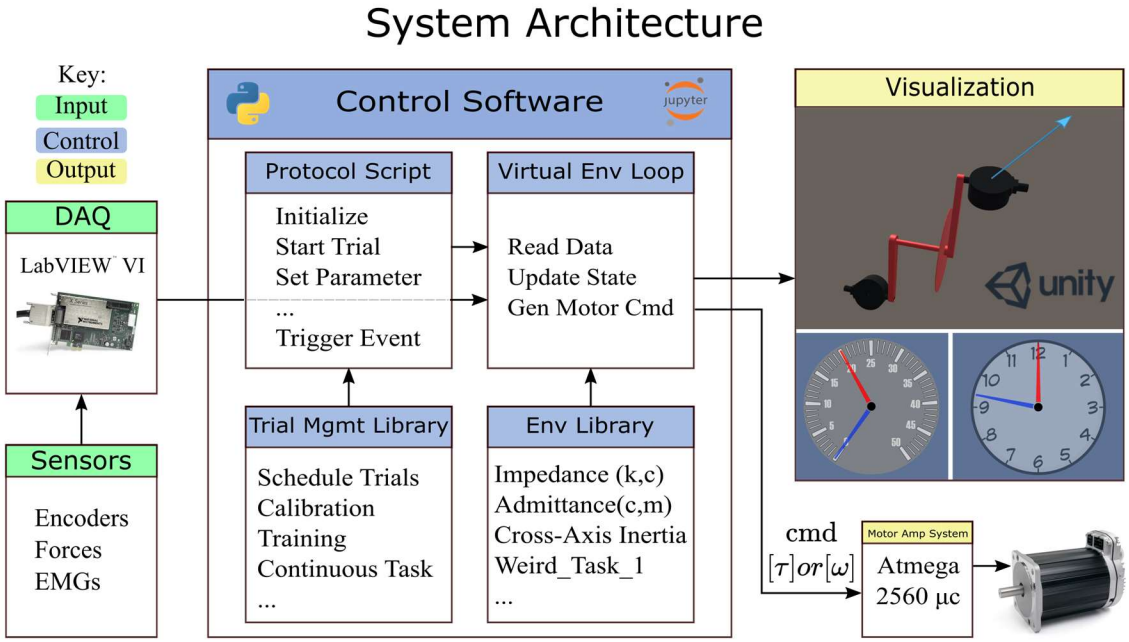

Fig 1.3. Schematic Representation of the System Architecture.
Measurements from encoders, force sensors, and EMG sensors are read through a LabVIEW Virtual Instrument at 1000Hz and are streamed to a virtual environment loop running in (Python) Jupyter Notebook at 100Hz. The state of the robot is updated, and a command torque or velocity is calculated based on the currently selected haptic environment from the Environment Library. Experiments may be designed and executed in the Protocol Script using tools from the Trial Management Library. Outputs are then sent to the motor amplifier and a visualization program to provide performance feedback to the user.

haptic environment, a torque or velocity is calculated and commanded to a low-level processor integrated into the servomotor. The servomotor controller then performs closed-loop control on the specified variable using internal collocated sensors. This architecture combines the benefit of the high-performance timing of a microcontroller with the flexibility of programming a desktop computer.

The software system is comprised of several modules. Data is acquired from the DAQ card using a dedicated LabVIEW virtual instrument (VI). These data are streamed to a Python control software responsible for facilitating experiment execution and haptic environment rendering. Finally, data are streamed from the Python control software to a visualization program and the low-level servomotor controller. (Fig 1.3).

The LabVIEW VI collects data at 1 kHz using a hardware clock on the DAC. The three angle encoders (crank and both pedals), forces, and EMG data are buffered into an array for transmission at 100 Hz to the Python controller over an internal UDP communications socket.

Data from LabVIEW are received by the virtual environment loop and parsed to update the state of the robot. High-level control laws are defined within the Environments library to specify desired crank output parameters from present system state. Two haptic rendering approaches are used under different circumstances – impedance- and admittance-based rendering. Impedance-based rendering measures robot kinematics and controls motor torque, while admittance-based rendering does the converse. Impedance-based environments excel at rendering springs, while admittance based environments are better at rendering masses [44]. In general, high-level control laws take the form of any constraint between a measured and a commanded variable. This generic architecture enables many potential targeted and precise learning environments. (see Discussion section).

After data are received and the system state is updated, the motor command is calculated based on the currently enabled virtual environment and is sent to the motor where collocated control is performed using the motor's integrated controller and sensors. Collocated control is preferred over non-collocated control for stability when there exists compliance between the motor and the load. Additional state information may be sent to the visualization loop to provide the subject with biofeedback.

Visual feedback is provided by two-dimensional or three- dimensional user interfaces built with Unity Engine (Unity Technologies, San Francisco, CA, USA). Two-dimensional visual feedback is displayed on a computer monitor directly in front of the subject. 2D widgets convey information about position, velocity, and other trial conditions using intuitive displays such as a clock face or speedometer dial. Other information may also be displayed, including dials to indicate system parameters on subsequent trials, vectors to indicate desired vs. actual force direction and magnitude, graphs of muscle EMG envelope, and scores to increase motivation and decrease subject slacking [45]–[47].

Experiments may be performed through a protocol scripting interface in Python running within the Jupyter Notebook environment. We developed a variety of tools for specifying, tuning, and recording trials, which are contained within the Trial Management library. The protocol script sends messages to the virtual environment loop to change system behavior. An example of such a script might enable recording, set a system parameter to a particular value, wait for an end condition such as time or accomplishment of a task goal, and then increment the trial. This design enables complex and precise experimental protocols to be specified and executed.

1.3.4 Evaluation – Machine Performance Testing

We conducted a series of tests to characterize device performance, including quantifying torque and velocity measurement accuracy, step-input response, and frequency response. Investigating the performance limits of the device allowed us to benchmark its capabilities against other lower limb robotic systems.

We fashioned a jig to lock the rotation of the crank during testing. We made a cantilever beam of steel plate backed by a wooden board and clamped it perpendicular to the robot frame in line with the right pedal (Fig 1.4B inset). We placed the right pedal in contact with the beam so it could measure the force between the beam and the pedal face. The reaction force supplied by the beam prevented the crank from rotating in the backward direction.

We first evaluated the torque command accuracy of the robot. We sent a ramp torque command from 0 Nm to 30 Nm over a period of 30 seconds to the motor controller. We calculated RMS error between commanded and measured torque (Fig 1.4A). It is important to note that the sensor feedback from the pedal was not used to control torque: torque was controlled independently by the motor's integrated controller using onboard collocated sensors, and performance was evaluated using the torque measured separately through the instrumented pedals. Thus, from the perspective of the high-level control law, the motor may be treated as a torque source, and the response may be viewed as an open-loop response. It was therefore important to establish congruence between the torque command and torque measurement.

We next evaluated torque step response. We applied a baseline torque (15 Nm) to assure that the pedal face was firmly in contact with the cantilever beam. We then applied a step command (40 Nm) to the servomotor and measured the resulting forces on the pedal. We recorded 10 trials and plotted the average response (mean ± SD) (Fig 1.4B). We evaluated performance in each trial

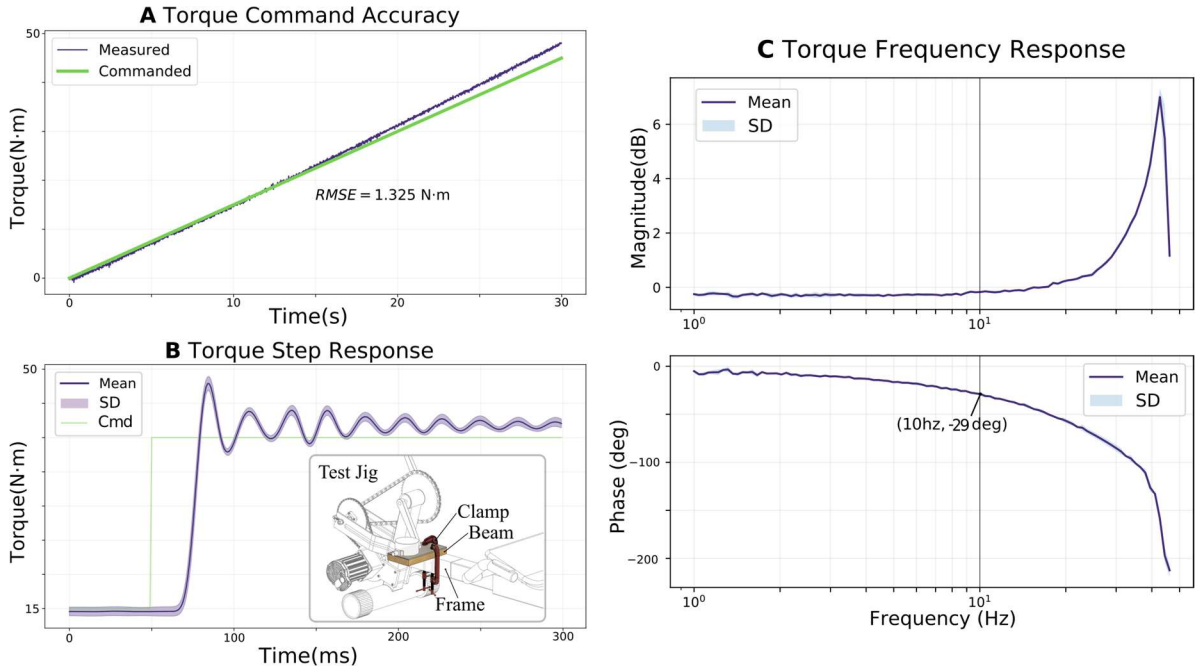

Fig 1.4.Torque Command Accuracy, Step Response, and Frequency Response. (A) Torque command accuracy to a ramp function over a 30 second trial. (B) Average torque step response from a baseline torque of 15 Nm to a target torque of 40 Nm. Rise time was determined to be 29 ms. (B inset) Pedal fixation arrangement for torque response testing. Torque was controlled by the motor's internal circuitry only, and measured with the pedal load cell. (C) Average frequency response function to a torque chirp input baseline torque was 20Nm with 10Nm peak-to-peak magnitude. Notable features include magnitude of approximately unity and phase lag less than 29 degrees up to 10 Hz.

with rise time (time between when the command was issued 50ms into the trial and 100% of final value) and settling time (time to settle within 5% of the final value) criteria.

We next evaluated torque frequency response. We created a linear torque chirp signal with a peak-to-peak magnitude of 10 Nm and an offset of 20 Nm. The initial frequency was set to 0.05 Hz and the terminal frequency was 50 Hz, with a duration of 90 s.

Next, we calculated the frequency response function (FRF) for torque control. We calculated magnitude ratio as the quotient of the RMS torque output over the RMS torque command. For each evaluated frequency in the chirp signal, we used a half-second (500 sample) window centered at the time when the test frequency was commanded. We also calculated phase using the lag at maximum cross-correlation between output and input signals within the same window. We performed this analysis on each of the 10 trials, and we plotted the magnitude and phase as a function of frequency (mean ± SD) (Fig 1.4C).

To evaluate velocity command accuracy, we applied a speed ramp command starting at 0 rad/s and ending at 3.14 rad/sec (30 RPM) after 30 seconds. We measured crank position from the encoder and used the central difference method to estimate crank velocity. We applied a 50 Hz bandwidth linear IIR filter and calculated RMS error between the commanded and measured velocities (Fig 1.5A). It is important to note that the sensor feedback from the crank encoder was not used to control velocity: velocity was controlled independently by the servomotor's integrated controller, and performance was evaluated using the crank encoder.

We also evaluated the velocity step response between a baseline velocity of 1.05 rad/s and a final velocity of 3.14 rad/s. We averaged 10 trials and plotted the resulting velocity ± SD (Fig 1.5B). We evaluated response time and settling time using 100% final value and 5% settling error criteria, as in the torque step test.

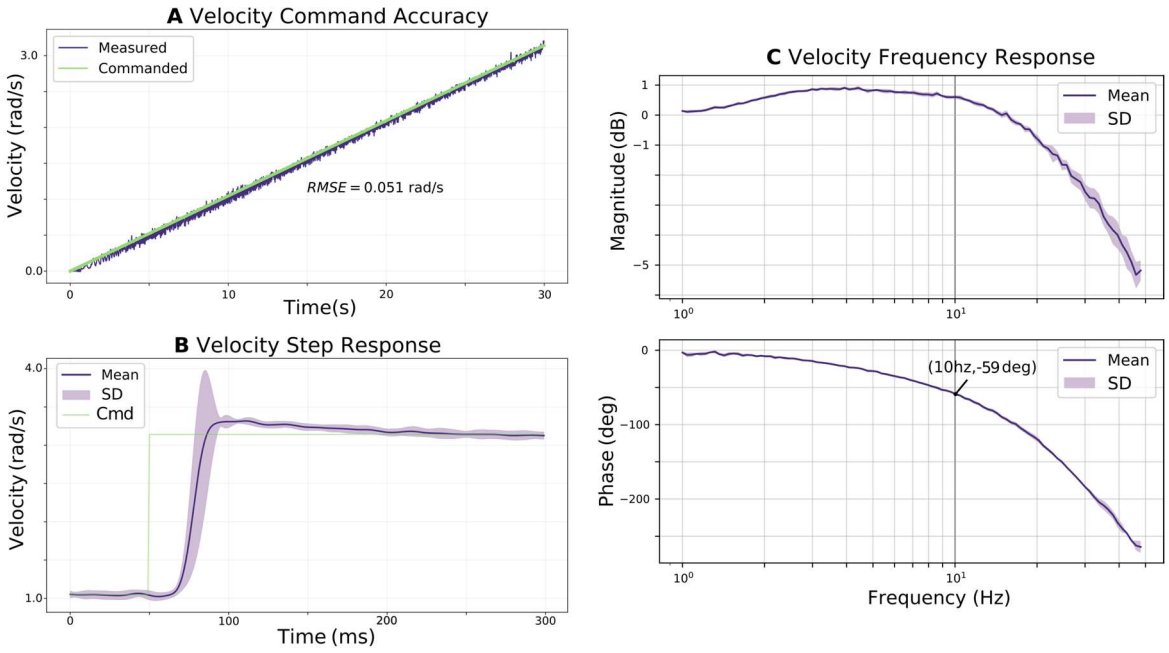

Fig 1.5. Velocity Command Accuracy, Step Response, and Frequency Response. (A) Velocity command accuracy to a ramp function over a 30 second trial. (B) Average velocity step-response from a baseline velocity of 1.0 rad/s to a target velocity of 3.14 rad/s (30 RPM). Rise time was determined to be 36 ms. (C) Average frequency response function to a velocity chirp input. Notable features include magnitude ratio within 1dB (12%) of unity and phase lag less than 59 degrees up to 10Hz.

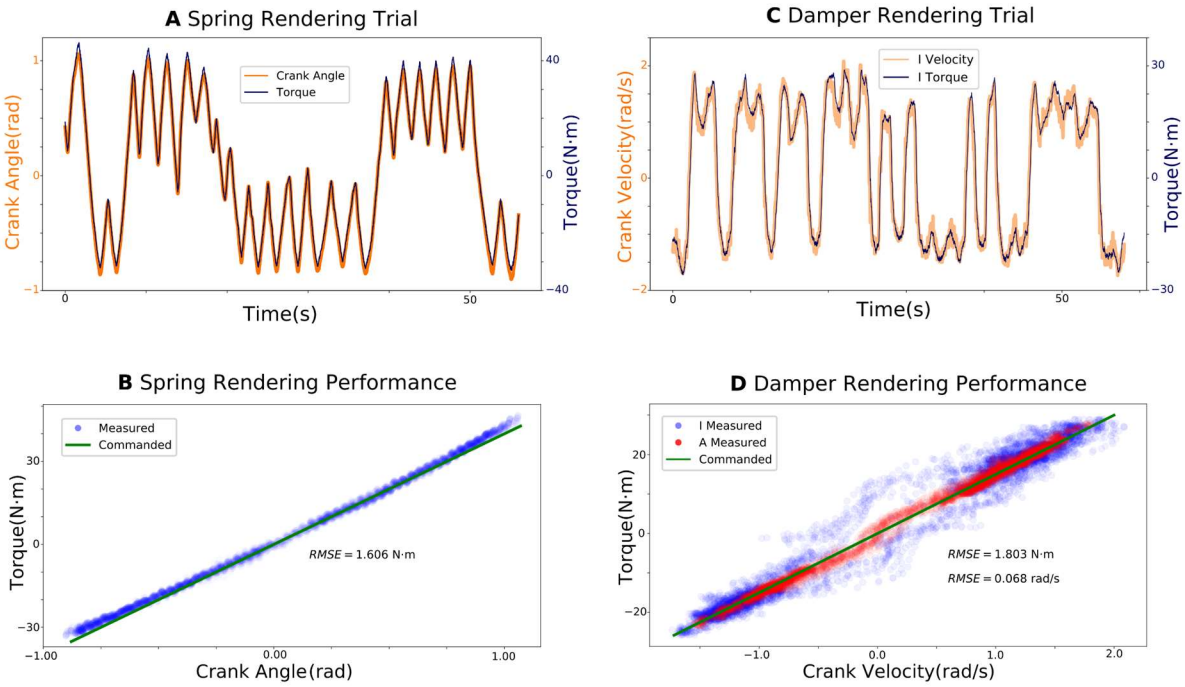

Fig 1.6. Rendering Performance During Human Interaction.
(A) Crank angle and torque over time during an impedance-based haptic rendering of a spring (k = 40 Nm/rad). (B) Regression between measured torque and measured crank angle for the spring of part A. (C) Crank velocity and crank torque vs. time during an impedance-based rendering of a damper (c = 15 Nm(rad/s)$^{-1}$) (D) Regression between measured torque and crank velocity for both impedance- and admittance-based haptic damper renderings.

Haptic env	Target parameter	Rendered parameter	Correlation coefficient	RMSE
I-spring	k = 10 Nm/rad	10.09	0.9945	0.92 Nm
	k = 40 Nm/rad	39.82	0.9987	1.60 Nm
	k = 70 Nm/rad	69.35	0.9990	1.96 Nm
I-damper	c = 5 Nm(rad/s)$^{-1}$	5.32	0.9866	1.22 Nm
	c = 15 Nm(rad/s)$^{-1}$	14.98	0.9811	1.80 Nm
	c = 25 Nm(rad/s)$^{-1}$	23.83	0.9568	3.37 Nm
A-damper	c = 5 Nm(rad/s)$^{-1}$	5.08	0.9970	0.100 rad/s
	c = 15 Nm(rad/s)$^{-1}$	15.32	0.9973	0.068 rad/s
	c = 25 Nm(rad/s)$^{-1}$	25.55	0.9950	0.079 rad/s

Table 1.1. Assessing the Quality of Haptic Rendering
Admittance and impedance-based renderings of springs and dampers, notice the high correlation coefficients and low root mean square errors of the renderings.

Finally, we calculated the frequency response function (FRF) for velocity control. We applied 10 linear chirps sequentially. Each chirp signal had duration 90 seconds, starting frequency 0.05Hz, terminal frequency 50Hz, and amplitude 2.09 rad/s with a baseline of 1.05rad/s. We calculated and plotted the velocity FRF using the same approach described in the torque section (Fig 1.5C).

1.3.5 Evaluation – Human Interaction Testing

We conducted a series of tests to quantitatively evaluate the ability of the robot to render different impedance- and admittance-based haptic environments during human machine interaction. Since the robot is instrumented with both kinematic and kinetic sensors, we can render a haptic environment with one sensor and assess environment accuracy with the other. We evaluated human interaction with an impedance-based spring, an impedance-based damper, and an admittance-based damper, with parameters that fall within a range useful for neuromuscular investigation and therapeutic intervention. The interaction testing setup was visually identical to that demonstrated in Fig 1.1. Research was performed under the oversight of the University of Wisconsin-Madison Health Sciences IRB submission ID# 2016-1279-CP001. Informed consent was received for all human subjects involved in testing. These tests establish the suitability of NOTTABIKE for the study of motor control and rehabilitation.

An impedance-based spring measures the crank angle θ and commands a motor torque τ computed from a mathematical representation of a torsional spring, $\tau = k\theta$. A single subject interacted with three impedance-based spring environments with stiffnesses of $k = \{10, 40, 70\}$ Nm/rad for one minute each. The subject was told to move freely back and forth within each environment. We recorded the measured crank angle and the torque calculated from the

instrumented pedals for each condition. We plotted the measured crank angle and measured torque over time in figure 1.6A for $k = 40$ Nm/rad to demonstrate their correspondence visually. We also used least-squares linear regression to estimate the apparent external stiffness of the rendered virtual spring. (Fig 1.6B).

An impedance-based damper relates the measured crank velocity ω to commanded motor torque τ through the mathematical expression $\tau = c\omega$. The controller estimates crank velocity using a backward difference method and a 50Hz linear IIR filter. We evaluated and analyzed damping coefficients $c = \{5, 15, 25\}$ Nm(rad/s)$^{-1}$ in the same fashion as the impedance-based spring (Fig 1.6C and 1.6D).

An admittance-based damper relates torque applied externally to the pedals to commanded servomotor velocity through the equation $\omega = \frac{\tau}{c}$. In this case, the controller estimates torque from the instrumented pedals and commands angular velocity ω. We evaluated the admittance-based damper for $c = \{5, 15, 25\}$ Nm(rad/s)$^{-1}$. We used measured crank kinematics as validation data. We estimated velocity with the central difference method and applied a 50 Hz linear filter. We plotted the regression between measured force and measured velocity on the same plot as the impedance-based trial to facilitate direct comparison (Fig 1.6D). Only the $c = 15$ Nm(rad/s)$^{-1}$ trial was plotted, for visual clarity. A summary of the results of human testing is provided in Table

1.4 Results

For the torque ramp test, error between the commanded (open loop) and measured torque was 1.33 Nm RMS. Error was negligible at low torque, increasing to a modest overestimate at higher torque values (roughly 6% at 45 N command). The torque step rise time was 29 ± 1 ms (mean ± SD), and the settling time was 125 ± 50 ms. Torque frequency response did not exhibit

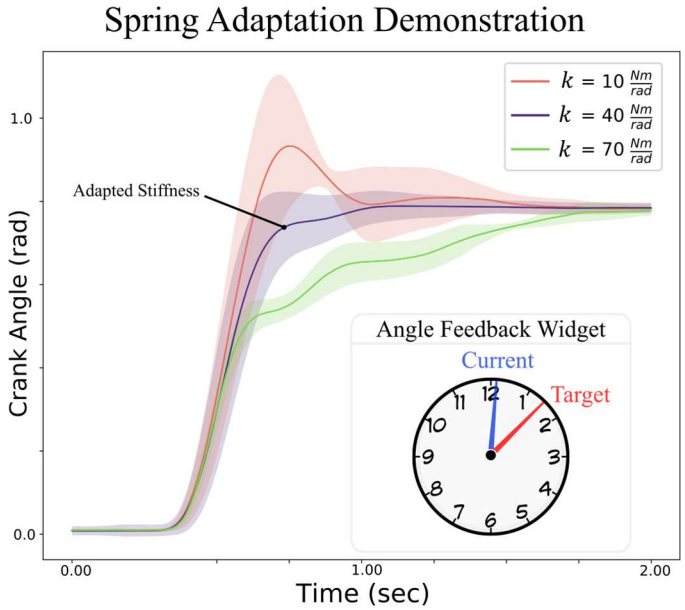

Fig 1.7. Motor Adaptation to Springs of Different stiffnesses.
In a single subject under visual feedback of performance with a clock widget (inset). 50 reaching trials were performed: 80% with the medium stiffness $k = 40$ Nm/rad and 10% catch trials to each of $k = \{10, 70\}$ Nm/rad. Subject attempted to reach 45deg (.78rad) in the least time possible.

magnitude roll-off within the 50 Hz command bandwidth (limited due to 100 Hz command update frequency). A key result from the torque frequency analysis is that the magnitude ratio is unity up to 10 Hz with only 29 degrees phase lag.

For the velocity ramp test, error between commanded (open loop) and measured signals was 0.051 rad/s RMS, with uniform accuracy throughout the commanded range (0-30 rad/s). The velocity step rise time was 36 ± 7 ms and settling time was 90 ± 35 ms. Magnitude ratio was within 1 dB of unity at all frequencies below 10 Hz, with less than 59 degrees phase lag.

Results of the haptic rendering tests during human interaction are displayed in Table 1. All three springs rendered within 1% of the desired spring constant, with RMS torque error less than 2 Nm within the range tested (roughly -50 to +70 Nm). Damping environments performed similarly on average when rendered using impedance-control and admittance-control, with larger torque variability using impedance-control. Impedance-controlled dampers rendered within 6% of the desired damping constant, with RMS torque error less than 3.4 Nm. Admittance-controlled dampers performed within 2.5% of the desired damping constant, with RMS velocity error less than 0.1 rad/s.

1.5 Discussion

1.5.1 Interpretation of Results and System Design

The results presented here confirm that the torque, velocity, and haptic rendering performance of NOTTABIKE are suitable for studying motor control and rehabilitation in the lower limb. Haptic environments for human interaction testing are rendered within a few percent of desired parameters, across a wide range of stiffness and damping. Both the torque and velocity control modes have near unity magnitude ratio and small phase loss up to 10 Hz, exceeding the bandwidth

of other lower limb rehabilitation robots [48]. For context, humans' ability to track unpredictable stimuli deteriorates around 1-2 Hz [49], and the control bandwidth of the human leg is roughly 2 Hz [2].

The phase loss is likely attributable to a time lag resulting from drive train compliance. The source of the compliance is the deflection of transmission mounting forks under tension and backlash from residual slack in the drive train. The time lag can most readily be seen in the torque and velocity step response plots, in the time between when torque or velocity is commanded and when the robot responds. This time is 16ms and 18ms respectively. Thus, in this respect, the performance of the robot is most limited by the drive train.

At first glance, there appears to be a discrepancy between the torque step and chirp responses. While the step response shows a gain slightly greater than unity, the chirp response shows magnitude below 0 dB. This may be explained by two factors. First, the chirp response and step response were conducted at different torque amplitudes, and the slight nonlinearity in the pedal measurements (see Fig 1.4A) could cause different amplitude measurements. Second, the measurements are experimental in nature, so slow drift in the strain gauges or motor behavior (e.g. due to temperature) could cause the two results to differ slightly.

From the torque frequency and step responses it appears the robot resonates around 40 Hz. This may be an artifact of the cantilever beam setup used to evaluate the frequency response. The amplification of the velocity before the magnitude roll-off observed in the velocity chirp response may be due to a resonance of the pedal mass connected through the compliance of the drivetrain. The authors do not believe this negatively impacts machine performance or safety in any practical manner as the peak amplification is 1dB or 12% amplification. None of these features adversely

affect the rendering capability of the robot within the frequency range necessary for the study of motor learning.

A limitation of our analysis is that the human's effect on the torque and velocity controllers was not directly analyzed in the frequency domain. Humans contribute mass which will lower system bandwidth, and human joint impedance can vary over two orders of magnitude depending on level of muscular co-contraction[50] and limb posture, making the experimental determination of the human's effect on a controller difficult to determine. As such, the human's effect on the controller likely contributed to the tracking error in the human interaction tests. Because the time domain and regression results fell within our desired performance limits, this analysis was not undertaken.

In addition to the stiffness and damping performance analyzed above, the third component of rendering haptic environments is inertia – the relationship between torque and angular acceleration, as in the traditional mass-spring-damper system. NOTTABIKE can render inertia, but assessing the performance of inertia rendering proved difficult because the only available estimate of angular acceleration is from double differentiation of the crank angle signal. The resulting acceleration signal is very noisy, so we did not use it to assess inertia rendering quantitatively. Qualitatively, subjects interacting with simulated inertias report that they are "smooth" and "feel like normal pedaling" when combined with light damping. Subjects were able to easily perceive the difference among inertias of $I = \{5, 10, 40\}$ kg-m^2.

The design of the control system is unusual for a robotic system, in that it includes a Windows desktop computer in the control loop. The desktop computer cannot perform high-bandwidth motor control, so it was also crucial to incorporate the integrated servo controller. Thus, parameters updated relatively slowly by the desktop computer's virtual environment model (100

Hz) produce motor commands (torque or velocity) that are tightly controlled at much higher bandwidth by the servomotor controller. This design decision had important benefits. Programming on a desktop with a high-level language enables rapid control law prototyping, easy data storage and sophisticated data visualization for biofeedback – here, through the Unity gaming engine. It also opens the possibility of creating control paradigms that incorporate data from patient history rather than just the current system state, for example by using patient specific models and machine learning approaches.

1.5.2 Importance of Approach

NOTTABIKE was built to enable different styles of lower-limb rehabilitation, based on rehabilitating volitional control of the leg in goal-directed movements rather than task-specific gait training. The use of haptic environments provides a means to create demanding motor tasks and incentivize them in a controlled way, by tuning task difficulty and success rates for optimal challenge and motivation [8]. Task incentives in the form of minimal encouragement toward volitional activity [12] or as a firm requirement for task completion [51] have been successful in the upper limb. These precedents suggest that explicitly rewarding volitional control of a targeted motor task may lead to increased motor learning and neuromotor recovery.

Haptic rendering may be combined with visual feedback to create multimodal learning environments. The addition of task-relevant visual feedback can increase motivation by making the task demands more understandable and intuitive[52]. NOTTABIKE uses a series of 2 and 3 dimensional widgets to provide real-time performance information about task parameters to the subject (Fig 1.3). Training effects arise when the human uses this information to reduce error and

learn new control strategies. Figure 1.7 demonstrates subjects using visual feedback to reach a target angle against haptically rendered springs of different stiffnesses.

NOTTABIKE uses a recumbent posture to separate the targeted tasks of motor coordination from the confounding demands of upright balance and weight support. The recumbent posture could also enable robotic rehabilitation earlier in the process of recovery from injuries such as stroke compared to treadmill training or exoskeleton walking. The approach is intended to redevelop motor coordination through a progressive series of subtasks, rather than all at once. It is envisioned as an early intervention to prepare the motor system for later task-specific gait and balance training.

NOTTABIKE also embodies an inversion of the usual paradigm for lower-limb rehabilitation robots. Exoskeletal robots are often designed to control many kinematic degrees of freedom, often with minimal measurement of interaction forces with the user [53] . The underlying assumption in such cases is that the movement itself is rehabilitative and the robot can drive it with minimal response to the user [54]. In contrast, our view of rehabilitation is that only user-generated actions (forces, movements) are rehabilitative – and therefore that the primary action of the robot should be to respond to the user, not to initiate movement. Therefore sensing, not actuation, is the focus of NOTTABIKE, and the exercises it prescribes use its one degree of freedom to provide kinematic or kinetic responses to many potential inputs. The one degree-of-freedom design results in a mechanically simple device that can still create complex virtual environments that require volitional engagement and elicit motor learning.

This single degree of freedom does present the obvious limitation that movement can only occur along a circular path; therefore NOTTABIKE cannot create true multidimensional haptic environments like viscous curl [2]. However, force-driven control can still occur along dimensions

that are kinematically constrained. For instance, forward motion of the crank can be controlled by the magnitude of lateral force produced by the user. Environments may be arbitrarily precise to target specific changes. For example, left dorsiflexor modulation can be targeted by controlling crank velocity in proportion to EMG activation of the left tibialis anterior muscle at specific ranges of crank angle. Or bilateral abductor control can be targeted by controlling crank angle in proportion to symmetric abductor force measured at the pedals. Environments such as these may enable the exploration of lower limb motor synergies, believed to be important in pathological movement after stroke [55]. NOTTABIKE may even render Virtual environments with nonphysical properties that can only be realized through simulation, such as negative mass that accelerates backward when it is pushed forward. The novelty of such environments is critical for motor-learning studies because of the importance of testing activities which do not have a basis in the test subject's past experience.

Another limitation of a single degree of freedom robot is that it cannot elicit kinematic movement deviations as an indicator of motor adaptation or motor learning. Thus, path errors and spatial convergence cannot be observed. However, there remains a great deal of information available about motor performance in the force, position, velocity and time domains, which may be used to quantify task performance. For example, the overshoot and undershoot shown in figure 1.7 provide strong evidence of imperfect adaptation to the soft and stiff virtual springs, respectively, due to training focused on the medium stiffness spring. The amount of a movement completed within the initial sub movement is also a key indicator of motor adaptation [46]. Thus, methods from psychophysics based on time and movement extent can be adapted to elucidate findings on motor control.

1.5.3 Future Directions

NOTTABIKE provides an effective platform to train and test a variety of motor tasks that could be useful for basic science in motor control as well as rehabilitation. Our first study will investigate motor adaptation in the lower limb through a series of reaching tasks in haptic spring, damper, and mass environments with healthy subjects. This will allow us to establish normative metrics for adaptation in the lower-limb, and evaluate the extent to which principles established in the upper-limb [1] generalize. We will also investigate the time course of long-term motor learning in healthy subjects through repeated testing experiments across multiple days and weeks. We will further investigate the ability to train novel tasks that require new motor patterns, using novel environments such as half-reversed pedaling (reversing the sign of the torque generated by one leg), and inverse-curl fields (setting crank velocity in proportion to lateral force).

Following these and other motor experiments in healthy subjects, we will compare the capacity for motor adaptation in a clinical population of patients recovering from stroke. We anticipate that these tests may lead to methods for quantifying deficit and differentiating those individuals with a greater or lesser capacity for improvement (responders vs. non-responders). We will further investigate how training on NOTTABIKE can improve motor function in a clinical population, using those tasks most successful in provoking motor learning in movements targeted to overcome common deficits due to stroke.

1.6 Conclusion

NOTTABIKE can render both impedance- and admittance-based haptic environments with accuracy and responsiveness that are useful for the study of human coordination and the delivery of rehabilitative therapy. Future work using this robot will explore motor adaptation in the lower

limb in intact subjects and haptic environments with therapeutic value to a clinical population. The ability to test goal-directed movements in the lower limb will enable comparison of how motor learning principles and techniques for the lower limb relate to those established previously in the upper limb.

1.7 References

[1] D. J. Reinkensmeyer, J. L. Emken, and S. C. Cramer, "Robotics, Motor Learning, and Neurologic Recovery," *Annual Review of Biomedical Engineering*, vol. 6, no. 1, pp. 497–525, 2004, doi: 10.1146/annurev.bioeng.6.040803.140223.

[2] R. Shadmehr and F. Mussa-Ivaldi, "Adaptive representation of dynamics during learning of a motor task," *The Journal of Neuroscience*, vol. 14, no. 5, pp. 3208–3224, May 1994, Accessed: Aug. 12, 2011. [Online]. Available: http://www.jneurosci.org/content/14/5/3208.abstract

[3] F. Abdollahi *et al.*, "Error augmentation enhancing arm recovery in individuals with chronic stroke a randomized crossover design," *Neurorehabilitation and neural repair*, p. 1545968313498649, 2013, Accessed: Oct. 17, 2016. [Online]. Available: http://nnr.sagepub.com/content/early/2013/08/07/1545968313498649.abstract

[4] J. L. Patton, M. E. Stoykov, M. Kovic, and F. A. Mussa-Ivaldi, "Evaluation of robotic training forces that either enhance or reduce error in chronic hemiparetic stroke survivors," *Experimental Brain Research*, vol. 168, no. 3, pp. 368–383, 2006, Accessed: May 17, 2013. [Online]. Available: http://link.springer.com/article/10.1007/s00221-005-0097-8

[5] F. Abdollahi *et al.*, "Error Augmentation Enhancing Arm Recovery in Individuals With Chronic Stroke: A Randomized Crossover Design," *Neurorehabil Neural Repair*, vol. 28, no. 2, pp. 120–128, Feb. 2014, doi: 10.1177/1545968313498649.

[6] D. A. Brown, T. D. Lee, D. J. Reinkensmeyer, and J. E. Duarte, "Designing Robots That Challenge to Optimize Motor Learning," in *Neurorehabilitation Technology*, D. J. Reinkensmeyer and V. Dietz, Eds. Springer International Publishing, 2016, pp. 39–58. doi: 10.1007/978-3-319-28603-7_3.

[7] D. J. Reinkensmeyer and S. J. Housman, "'If I can't do it once, why do it a hundred times?': Connecting volition to movement success in a virtual environment motivates people to exercise the arm after stroke," in *2007 Virtual Rehabilitation*, 2007, pp. 44–48. Accessed: Aug. 01, 2016. [Online]. Available: http://ieeexplore.ieee.org/xpls/abs_all.jsp?arnumber=4362128

[8] J. E. Duarte and D. J. Reinkensmeyer, “Effects of robotically modulating kinematic variability on motor skill learning and motivation,” *Journal of neurophysiology*, vol. 113, no. 7, pp. 2682–2691, 2015.

[9] J. E. Duarte and D. J. Reinkensmeyer, “The Real-World Challenge Point Hypothesis: Predicting the consequences of challenge for unsupervised motor training,” presented at the Biomechanics and Neural Control of Movement 2016, Mt. Sterling, Ohio, USA, Jun. 2016.

[10] S. Srivastava *et al.*, “Assist-as-Needed Robot-Aided Gait Training Improves Walking Function in Individuals Following Stroke,” *IEEE Trans Neural Syst Rehabil Eng*, vol. 23, no. 6, pp. 956–963, Nov. 2015, doi: 10.1109/TNSRE.2014.2360822.

[11] J. L. Emken, R. Benitez, and D. J. Reinkensmeyer, “Human-robot cooperative movement training: learning a novel sensory motor transformation during walking with robotic assistance-as-needed,” *Journal of NeuroEngineering and Rehabilitation*, vol. 4, no. 1, p. 1, 2007.

[12] E. T. Wolbrecht, V. Chan, D. J. Reinkensmeyer, and J. E. Bobrow, “Optimizing Compliant, Model-Based Robotic Assistance to Promote Neurorehabilitation,” *IEEE Transactions on Neural Systems and Rehabilitation Engineering*, vol. 16, no. 3, pp. 286–297, Jun. 2008, doi: 10.1109/TNSRE.2008.918389.

[13] A. A. Blank, J. A. French, A. U. Pehlivan, and M. K. O’Malley, “Current Trends in Robot-Assisted Upper-Limb Stroke Rehabilitation: Promoting Patient Engagement in Therapy,” *Curr Phys Med Rehabil Rep*, vol. 2, no. 3, pp. 184–195, Sep. 2014, doi: 10.1007/s40141-014-0056-z.

[14] E. Dayan and L. G. Cohen, “Neuroplasticity subserving motor skill learning,” *Neuron*, vol. 72, no. 3, pp. 443–454, 2011.

[15] B. Draganski, C. Gaser, V. Busch, G. Schuierer, U. Bogdahn, and A. May, “Neuroplasticity: changes in grey matter induced by training,” *Nature*, vol. 427, no. 6972, p. 311, 2004.

[16] “Lokomat®,” *Hocoma*. https://www.hocoma.com/solutions/lokomat/ (accessed Jul. 20, 2017).

[17] K. P. Westlake and C. Patten, “Pilot study of Lokomat versus manual-assisted treadmill training for locomotor recovery post-stroke,” *Journal of NeuroEngineering and Rehabilitation*, vol. 6, no. 1, p. 18, Dec. 2009, doi: 10.1186/1743-0003-6-18.

[18] W. Meng, Q. Liu, Z. Zhou, Q. Ai, B. Sheng, and S. (Shane) Xie, “Recent development of mechanisms and control strategies for robot-assisted lower limb rehabilitation,” *Mechatronics*, vol. 31, pp. 132–145, Oct. 2015, doi: 10.1016/j.mechatronics.2015.04.005.

[19] A. J. Young and D. P. Ferris, “State of the Art and Future Directions for Lower Limb Robotic Exoskeletons,” *IEEE Transactions on Neural Systems and Rehabilitation Engineering*, vol. 25, no. 2, pp. 171–182, Feb. 2017, doi: 10.1109/TNSRE.2016.2521160.

[20] R. G. Ranky, M. L. Sivak, J. A. Lewis, V. K. Gade, J. E. Deutsch, and C. Mavroidis, “Modular mechatronic system for stationary bicycles interfaced with virtual environment for rehabilitation,” *Journal of NeuroEngineering and Rehabilitation*, vol. 11, no. 1, p. 93, Jun. 2014, doi: 10.1186/1743-0003-11-93.

[21] Reck, “MOTOmed viva2,” *MOTOmed viva2*. http://www.motomed.com/en/models/motomed-viva2.html (accessed Sep. 01, 2015).

[22] “RT300 series FES powered rehabilitation therapy systems.” http://restorative-therapies.com/rt300_series (accessed Sep. 01, 2015).

[23] L. H. Ting, S. A. Kautz, D. A. Brown, and F. E. Zajac, “Phase Reversal of Biomechanical Functions and Muscle Activity in Backward Pedaling,” *Journal of Neurophysiology*, vol. 81, no. 2, pp. 544–551, Feb. 1999.

[24] C. C. Raasch and F. E. Zajac, “Locomotor strategy for pedaling: muscle groups and biomechanical functions,” *J. Neurophysiol.*, vol. 82, no. 2, pp. 515–525, Aug. 1999, doi: 10.1152/jn.1999.82.2.515.

[25] H. F. M. Van der Loos, L. Worthen-Chaudhari, D. Schwandt, D. M. Bevly, and S. A. Kautz, “A Split-Crank Bicycle Ergometer Uses Servomotors to Provide Programmable Pedal Forces for Studies in Human Biomechanics,” *IEEE Transactions on Neural Systems and Rehabilitation Engineering*, vol. 18, no. 4, pp. 445–452, Aug. 2010, doi: 10.1109/TNSRE.2010.2047586.

[26] L. H. Ting, C. C. Raasch, D. A. Brown, S. A. Kautz, and F. E. Zajac, “Sensorimotor state of the contralateral leg affects ipsilateral muscle coordination of pedaling,” *Journal of Neurophysiology*, vol. 80, no. 3, pp. 1341–1351, 1998.

[27] L. H. Ting, S. A. Kautz, D. A. Brown, and F. E. Zajac, “Contralateral movement and extensor force generation alter flexion phase muscle coordination in pedaling,” *Journal of Neurophysiology*, vol. 83, no. 6, pp. 3351–3365, 2000.

[28] T. Tatemoto, S. Tanaka, K. Maeda, S. Tanabe, K. Kondo, and T. Yamaguchi, “Skillful Cycling Training Induces Cortical Plasticity in the Lower Extremity Motor Cortex Area in Healthy Persons,” *Front. Neurosci.*, vol. 13, 2019, doi: 10.3389/fnins.2019.00927.

[29] “NuStep,” *NuStep, LLC*, Oct. 24, 2016. https://www.nustep.com/ (accessed Aug. 13, 2019).

[30] H. J. Huang and D. P. Ferris, “Neural coupling between upper and lower limbs during recumbent stepping,” *Journal of Applied Physiology*, vol. 97, no. 4, pp. 1299–1308, Oct. 2004, doi: 10.1152/japplphysiol.01350.2003.

[31] D. P. Ferris, H. J. Huang, and P.-C. Kao, “Moving the Arms to Activate the Legs:,” *Exercise and Sport Sciences Reviews*, vol. 34, no. 3, pp. 113–120, Jul. 2006, doi: 10.1249/00003677-200607000-00005.

[32] S. A. Kautz and D. A. Brown, “Relationships between timing of muscle excitation and impaired motor performance during cyclical lower extremity movement in post-stroke hemiplegia.,” *Brain*, vol. 121, no. 3, pp. 515–526, Mar. 1998, doi: 10.1093/brain/121.3.515.

[33] D. A. Brown and S. A. Kautz, “Speed-Dependent Reductions of Force Output in People With Poststroke Hemiparesis,” *Phys Ther*, vol. 79, no. 10, pp. 919–930, Oct. 1999, doi: 10.1093/ptj/79.10.919.

[34] D. A. Brown and S. Kautz, “Increased workload enhances force output during pedaling exercise in persons with poststroke hemiplegia,” *Stroke*, vol. 29, no. 3, pp. 598–606, 1998.

[35] L. M. Rogers, D. A. Brown, and K. G. Gruben, “Foot force direction control during leg pushes against fixed and moving pedals in persons post-stroke,” *Gait & Posture*, vol. 19, no. 1, pp. 58–68, Feb. 2004, doi: 10.1016/S0966-6362(03)00009-2.

[36] M. R. Dimitrijevic, Y. Gerasimenko, and M. M. Pinter, “Evidence for a Spinal Central Pattern Generator in Humans,” *Annals of the New York Academy of Sciences*, vol. 860, no. 1, pp. 360–376, 1998.

[37] D. J. Reinkensmeyer *et al.*, “Computational neurorehabilitation: modeling plasticity and learning to predict recovery,” *J Neuroeng Rehabil*, vol. 13, no. 1, p. 42, 2016, doi: 10.1186/s12984-016-0148-3.

[38] E. H. F. van Asseldonk, M. Wessels, A. H. A. Stienen, F. C. T. van der Helm, and H. van der Kooij, “Influence of haptic guidance in learning a novel visuomotor task,” *Journal of Physiology-Paris*, vol. 103, no. 3, pp. 276–285, May 2009, doi: 10.1016/j.jphysparis.2009.08.010.

[39] F. Abdollahi *et al.*, “Arm control recovery enhanced by error augmentation,” in *2011 IEEE International Conference on Rehabilitation Robotics*, Jun. 2011, pp. 1–6. doi: 10.1109/ICORR.2011.5975504.

[40] H. Schmidt, S. Hesse, R. Bernhardt, and J. Krüger, “HapticWalker---a novel haptic foot device,” *ACM Trans. Appl. Percept.*, vol. 2, no. 2, pp. 166–180, Apr. 2005, doi: 10.1145/1060581.1060589.

[41] J. F. Veneman, R. Kruidhof, E. E. G. Hekman, R. Ekkelenkamp, E. H. F. Van Asseldonk, and H. van der Kooij, “Design and evaluation of the LOPES exoskeleton robot for

interactive gait rehabilitation," *IEEE Trans Neural Syst Rehabil Eng*, vol. 15, no. 3, pp. 379–386, Sep. 2007, doi: 10.1109/TNSRE.2003.818185.

[42] M. Girone, G. Burdea, M. Bouzit, V. Popescu, and J. E. Deutsch, "A Stewart Platform-Based System for Ankle Telerehabilitation," *Autonomous Robots*, vol. 10, no. 2, pp. 203–212, Mar. 2001, doi: 10.1023/A:1008938121020.

[43] A. R. Dawson-Elli and P. G. Adamczyk, "NOTTABIKE - a haptic robot for studying motor control and applying rehabilitation in the lower limb," presented at the International Society of Biomechanics, Calgary, Aug. 2019.

[44] C. Parthiban and M. Zinn, "Performance and stability limitations of admittance-based haptic interfaces," in *2018 IEEE Haptics Symposium (HAPTICS)*, San Francisco, CA, Mar. 2018, pp. 58–65. doi: 10.1109/HAPTICS.2018.8357153.

[45] D. J. Reinkensmeyer, O. Akoner, D. P. Ferris, and K. E. Gordon, "Slacking by the human motor system: computational models and implications for robotic orthoses," *Conf Proc IEEE Eng Med Biol Soc*, vol. 2009, pp. 2129–2132, 2009, doi: 10.1109/IEMBS.2009.5333978.

[46] M. Casadio and V. Sanguineti, "Learning, Retention, and Slacking: A Model of the Dynamics of Recovery in Robot Therapy," *IEEE Transactions on Neural Systems and Rehabilitation Engineering*, vol. 20, no. 3, pp. 286–296, May 2012, doi: 10.1109/TNSRE.2012.2190827.

[47] J. L. Emken, R. Benitez, A. Sideris, J. E. Bobrow, and D. J. Reinkensmeyer, "Motor Adaptation as a Greedy Optimization of Error and Effort," *Journal of Neurophysiology*, vol. 97, no. 6, pp. 3997–4006, Jun. 2007, doi: 10.1152/jn.01095.2006.

[48] J. L. Emken, J. H. Wynne, S. J. Harkema, and D. J. Reinkensmeyer, "A robotic device for manipulating human stepping," *IEEE Transactions on Robotics*, vol. 22, no. 1, pp. 185–189, Feb. 2006, doi: 10.1109/TRO.2005.861481.

[49] I. D. Loram, H. Gollee, M. Lakie, and P. J. Gawthrop, "Human control of an inverted pendulum: Is continuous control necessary? Is intermittent control effective? Is intermittent control physiological?," *The Journal of Physiology*, vol. 589, no. 2, pp. 307–324, 2011, doi: 10.1113/jphysiol.2010.194712.

[50] N. Hogan, "Controlling impedance at the man/machine interface," in *Proceedings, 1989 International Conference on Robotics and Automation*, Scottsdale, AZ, USA, 1989, pp. 1626–1631. doi: 10.1109/ROBOT.1989.100210.

[51] E. B. Brokaw, T. Murray, T. Nef, and P. S. Lum, "Retraining of interjoint arm coordination after stroke using robot-assisted time-independent functional training," *J Rehabil Res Dev*, vol. 48, no. 4, pp. 299–316, 2011.

[52] H. Huang, S. L. Wolf, and J. He, “Recent developments in biofeedback for neuromotor rehabilitation,” *J NeuroEngineering Rehabil*, vol. 3, no. 1, p. 11, Jun. 2006, doi: 10.1186/1743-0003-3-11.

[53] G. Chen, C. K. Chan, Z. Guo, and H. Yu, “A Review of Lower Extremity Assistive Robotic Exoskeletons in Rehabilitation Therapy,” *CRB*, vol. 41, no. 4–5, 2013, doi: 10.1615/CritRevBiomedEng.2014010453.

[54] A. Esquenazi *et al.*, “Clinical Application of Robotics and Technology in the Restoration of Walking,” in *Neurorehabilitation Technology*,Springer International Publishing, 2016, pp. 223–248. doi: 10.1007/978-3-319-28603-7_12.

[55] Hayes Cruz Theresa and Dhaher Yasin Y., “Evidence of Abnormal Lower-Limb Torque Coupling After Stroke,” *Stroke*, vol. 39, no. 1, pp. 139–147, Jan. 2008, doi: 10.1161/STROKEAHA.107.492413.

Chapter 2

Lower-Limb Reaching in a Haptically Rendered Spring Environment

Alexander R. Dawson-Elli and Peter G. Adamczyk
(In Preparation for Publication in Human Movement Science)

2.1 Abstract

In this study, we investigate the performance of healthy subjects performing a reaching task on the haptic robot NOTTABIKE against a spring environment. Subjects reached with their right leg located at top dead center (0 deg) to a known location (45 degrees) as indicated by visual real-time visual feedback. The objective of the subject was to reach the defined destination in the least time without compromising accuracy. On any given reach, the subject could encounter one of 3 spring stiffnesses, 10, 20, and 30 Nm/rad. In all but one experimental block, subjects were not aware of which of these stiffnesses they would encounter on any given trial. Subject performance was defined in terms of features extracted from the crank angle vs. time curve such as settling time, rise time to 30 and 40 degrees, and curve extrema. The values of these features varied dramatically depending on the training environment – the fraction of high, medium, and low stiffnesses withing a training block. More specifically, we found that the feature differences were explainable as an evolving process which could be predicted via an autoregressive exogeneous input (ARX) model. Subjects maintained consistent settling time performance across blocks, meaning subjects that tended to reach fast stayed that way, as did slower-reaching subjects. Using principal component analysis (PCA) we found that variation along a single dimension in feature space could explain 88% of the performance variation between subjects. This led to the development of an optimal control framework which incorporated a single parameter λ to control

the tradeoff between end-point accuracy and actuator effort. The model was able to reproduce salient features differentiating fast from slow reachers. Finally, subjects were able to incorporate visual information about the stiffness of the next trial to improve their performance but could not fully mitigate the effect of adaptation on reaching performance.

2.2 Introduction

Rehabilitative robots have been useful tools for studying motor control in the upper-limb for several decades. Starting with the seminal work of Shadmehr and Mussa-Ivaldi in 1994 [1], the ability of simulated dynamic environments to elicit strong adaptive responses began to be appreciated. Investigation focused on goal-oriented and reaching type tasks in a 2D plane [2]–[6], as this was envisioned to be – and is – a primary use of the upper-limb. An interesting set of principles emerged from these investigations, concepts like error augmentation [7] and optimal control as a feasible framework for understanding motor control [8]–[10]. In many cases it was found that adaptive responses could be predicted using linear models such as ARX models, simply based on the previous performance and the next perturbation [11].

Robots have also been used to study motor control over the lower-limb, but from a different vantage point. Here the emphasis was placed on cyclic movements, rather than goal behaviors. Investigators used a variety of cycling robots, lower-limb exoskeletons, and split belt treadmills [12]–[16]. From these investigations and others [17]–[19] an interesting picture emerged which focused on the lower-limb as being an extremity whose control was mediated primarily by subcortical structures. Concepts like central pattern generators [20] inter-limb coupling between ipsilateral sensorimotor state and contralateral flexion phase muscle coordination [19] painted a

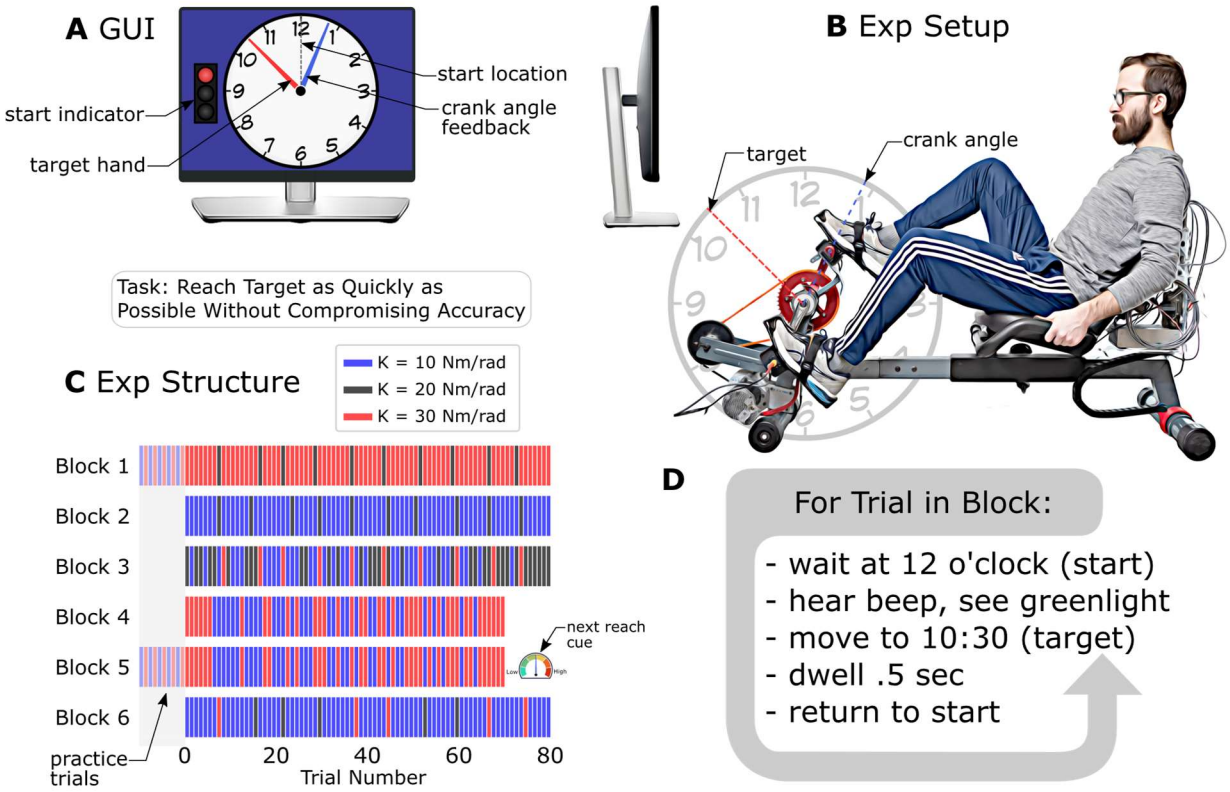

Fig 3.1. Overview of experimental setup and structure.
(A) The NOTTABIKE lower-limb haptic robot was used to render an impedance based virtual spring with rest position x0 located 12 O'clock for the right foot. (A) A screen showing a virtual clock indicating the target and actual locations of the crank was placed in front of the subject. (C) The experiment was broken into 6 blocks of between 70 and 80 reaches. A 5-minute rest period was given between blocks. On each reach, one of 3 stiffnesses was rendered (D) When the red target hand moved to the target location (45 degrees), the subject performed a reach with their right foot against the force of the rendered spring, to settle as quickly as possible at the target location without compromising accuracy.

picture of a limb whose action was primarily automatic and cyclical. Adaptation was studied in the lower-limb in the context of walking using the split-belt treadmill [21] – investigating both basic science questions, and clinical questions of whether repeated exposure to the stimulus that elicit adaptation in stride length could have therapeutic effect when repeated [22]. Investigations into adaptation in the lower-limb during goal directive activities has been relatively understudied by comparison. Here we present an investigation into reaching activities in the lower-limb towards targets using the NOTTABIKE platform.

2.3 Methods

2.3.1 Subject Recruitment

Twelve healthy subjects (age: 28.8 ±10.5, range: 22 – 59 years, 6 female, 6 male) participated in the study. The protocol was approved by the University of Wisconsin-Madison Health Science Institutional Review Board, and all subjects provided written informed consent before participating.

2.3.2 Setup and Instrumentation

Each subject was fitted individually to NOTTABIKE robotic system in the following ways. Subject's feet were situated on the instrumented pedal such that the first MTP joint of the big toe aligned with the center of the pedal axis. An adjustable toe strap and heel cup were used to maintain this positional arrangement, and a Velcro strap ensured the subjects' shoe and foot remained connected to the pedal. Subject seating distance was selected with the help of the experimenter to target about a 160 degree knee angle at the most extended point in the cycle (about 135 degrees

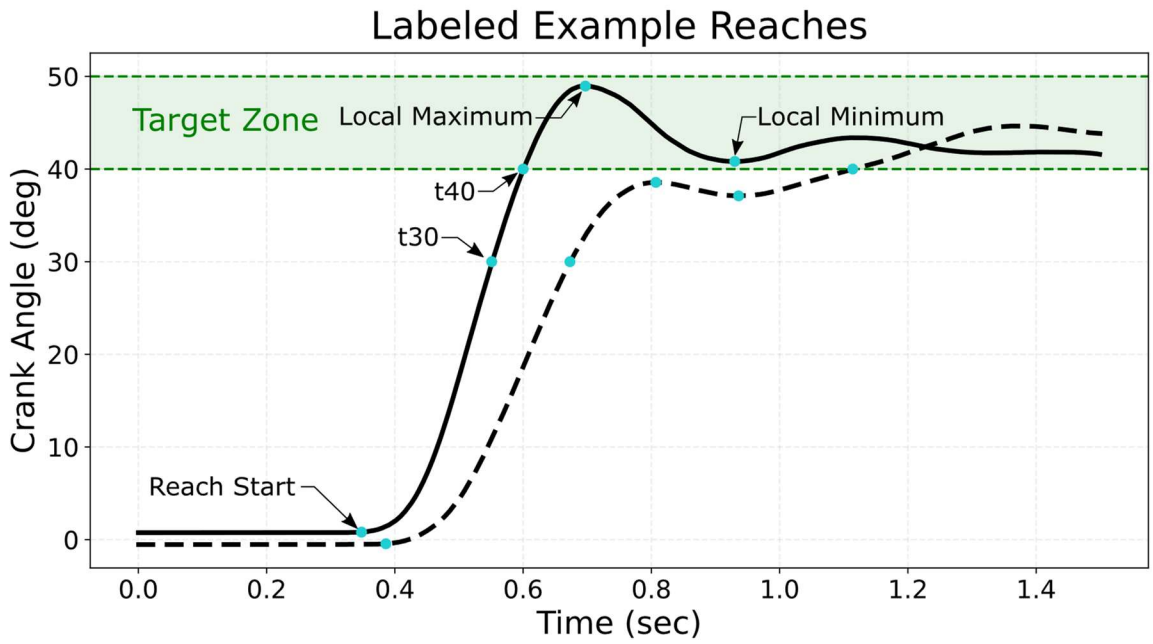

Fig 2.2. Example reaches with labeled features.
The Target zone indicated in green was 45 ± 5 for each reach. The labeled features were used to assess subject reaching performance across different trials and spring stiffnesses. Time based included rise times to 30 and 40 degrees, denoted t30 and t40 respectively, and position-based features such as the angular location of local minima and maxima. Features not depicted on this graph include settling time and peak velocity.

forward from top dead center). The NOTTABIKE robotic system recorded crank angle and foot interaction forces at 1000Hz for analysis.

2.3.3 Reaching Experimental Procedure

The reaching experiment was structured into 6 blocks, each block consisted of approximately 80 reach trials (Fig 2.1C). Between blocks, subjects were encouraged to get up from the robot and walk around, with a minimum rest period of 3 minutes and a maximum rest period of about 10 minutes. The blocked structure of the experiment was as follows: Block 1 consisted of 10 warm-up trials that were discarded, 70 trials of low stiffness (K = 10Nm/rad) with 10 medium stiffness (20 Nm/rad) catch trials dispersed throughout the block. For the blocks which included catch trials, the catch trials were uniformly distributed ± a randomization factor of several trials. This approach was used to guarantee that none of the catch trials were too close to one another, as was likely to happen with a purely random sequence. Block 2 was structured with 80 trials, 70 high stiffness (K = 30Nm/rad) with 10 medium stiffness (20 Nm/rad) catch trials. Block 3 consisted of a mixture of 35 low stiffness, 35 medium stiffness, and 10 high stiffness trials. Blocks 4 and 5 used a sequence known as a Debruijn (2,6) sequence. The Debruijn sequence is a cyclic sequence from combinatorial math in which every possible length-n string occurs exactly once as a substring. This is a useful characteristic for our experiment, as it allowed us to guarantee that each time history of 5 trials was encountered exactly once for the two stiffness conditions, high and low. Block 5 is identical to block 4 in trial sequence but has visual cuing of the next stiffness to be encountered provided by a visual widget on the subject-facing display. 10 throw-away trials were prepended to block 5 to give subjects practice integrating visual information into their

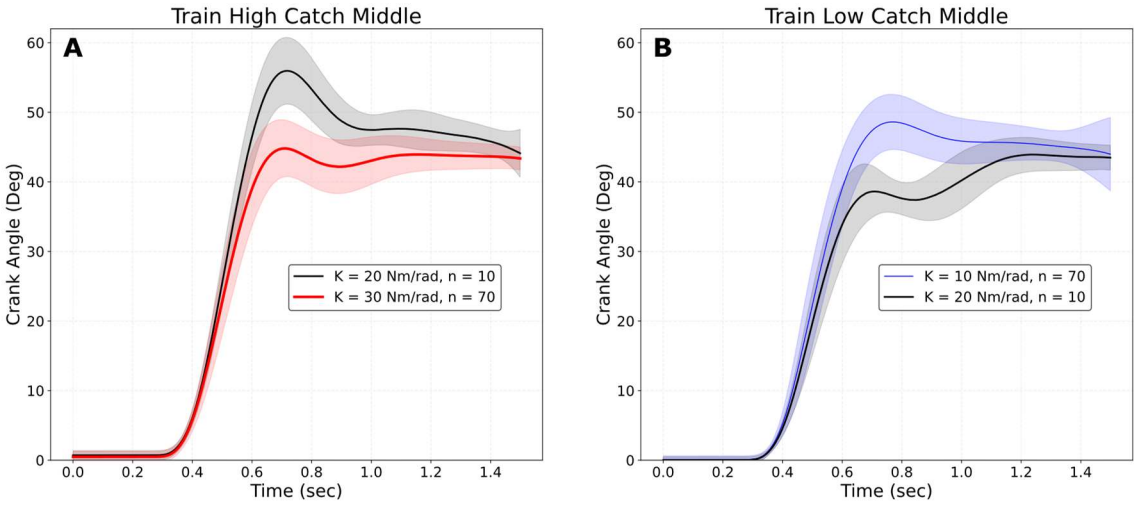

Fig 2.3. Average Reaching Performance is affected by Training Environment. Figures A and B show composite curves, generated by aligning each trial of the same stiffness within a block to factor out variable reaction time, then averaging across trials. (A) Block 1 performance for an example subject. Note the high local maximum, short t30, t40 for k = 20 Nm/rad (medium) trial in an environment which featured predominantly high stiffness springs. (B) Block 2 performance for example subject. The same k = 20 Nm/rad (medium) stiffness, in an environment which predominantly contains low stiffness springs. The local maximum is much lower there is a pronounced local minimum, and the t30 and t40 times are much slower than the same stiffness performance in block 1.

reaching performance. Finally in block 6, subjects encountered 70 low trials, with 5 catch trials of medium and 5 of high.

The trial structure was as follows (Fig 2.1D). Each trial was triggered to start when the subject had dwelled with the right crank arm at top dead center (0 degrees) for a variable amount of time of between 3.5 and 5 seconds, selected randomly from a uniform distribution. The red target indicator on the clock visual feedback widget would then move to the fixed target location of 45 degrees. Seeing the changing indicator, the subject would then respond by performing a reaching trial against an unknown (except for block 5) spring environment. Subjects would dwell within ± 5 degrees of the target location for .5 seconds, and the red target clock hand would return to the base position. Subjects would then retract their foot and wait for the next trial.

To keep subjects engaged and avoid slacking during the experiment, a motivational system was used which rewarded the subjects for their performance. Performance was scored by the motivational system as the amount of time required to settle within ± 5 degrees of the target location for at least .5 seconds. Descriptive statistics of the subjects' previous 20 reach performances were maintained and used to trigger either a neutral, reward or punishment sound. Time scores that were in the top 25% for time were rewarded, while scores in the bottom 20% were punished; the rest received a neutral sound. Subjects were informed that the motivational system was only relative to their own performance, rather than normative data, and that they were being judged on settling time, rather than some other metric such as overshoot. Subjects were given the explicit instruction that the objective of the task was to reach for the target as quickly as possible without compromising accuracy.

Time-Based Features (seconds)

	reaction time(M1-M2)	t30(M1-M2)	t40(M1-M2)	settling time(M1-H1)	settling time(M2-L2)
condition1: mean(sd)	0.366(±0.038)	0.537(±0.039)	0.592(±0.051)	1.29(±0.079)	1.40(±0.096)
condition2: mean(sd)	0.375(±0.037)	0.605(±0.080)	0.869(±0.12)	1.21(±0.068)	1.24(±0.071)
p-val	0.27	**<.001**	**<.001**	**0.01**	**<.001**

Position-Based features (degrees)

	local min(M1-M2)	local max(M1-M2)
condition1: mean(sd)	45.1(±2.3)	52.4(±2.6)
condition2: mean(sd)	37.7(±2.1)	40.6(±2.6)
p-val	**0.04**	**<.001**

Table 2.1. Inferential Statistical Analysis Comparing Block 1 and Block 2 performance.

Inferential statistical analysis to establish differences between subject performance on block 1 vs. block 2 using paired t-tests with false discovery rate (FDR) corrections.

Note: Column labels may be read as follows: "feature name (stiffnessBlock-stiffnessBlock)". Example: "local min(M1-M2)" compares the value of the local min feature on medium stiffness reaches in block 1 to medium stiffness features in block 2.

2.3.4 Analysis – primary feature extraction

In this section, we describe how the primary features were calculated from crank angle vs. time curves. Those features which are easily depicted graphically are labeled in figure 2.2. *Reach start* is the point in time, after the reaction time, in which the crank begins moving. To determine reach start, The crank velocity signal was filtered using a 5^{th} order forwards, backwards Butterworth filter with cutoff frequency of 30Hz. The reach start detection algorithm started at the point of maximum velocity and worked backwards in time until it found the point closest to a velocity threshold of 5 deg / second, which was defined as the threshold for starting the reach. It should be noted at this point that for each time-based feature, the reaction time (time between beginning of trial and reach start) was factored out and replaced by a fictitious reaction time of .3 seconds. This was done so that the effect of each feature could be evaluated independently of reaction time. There were 2 rise time features in the analysis, *t30* and *t40* which correspond to the time at which the reach curve hits these respective values. *Curve extrema* were computed using a zero velocity condition and determined to be either a local max or min. *Settling time* was computed as follows, and was the feature directly optimized by the subjects and rewarded by the motivational system. Settling time was determined as the amount of time required to accumulate .5 seconds within 5 degrees of the target 45 degrees. This was computed by iteration: while the accumulator was less than .5 seconds, move thorough the points in the crank angle vs. time curve and if the point was in the target zone, add to the accumulator.

Botched trials due to inattention or early action were removed from the analysis via the following criteria: reaction times greater than 1 second and less than .15 seconds, respectively. Additionally, any trials that had not finished within 6 seconds were removed. In practice, no more than 1% of trials were categorized as botched.

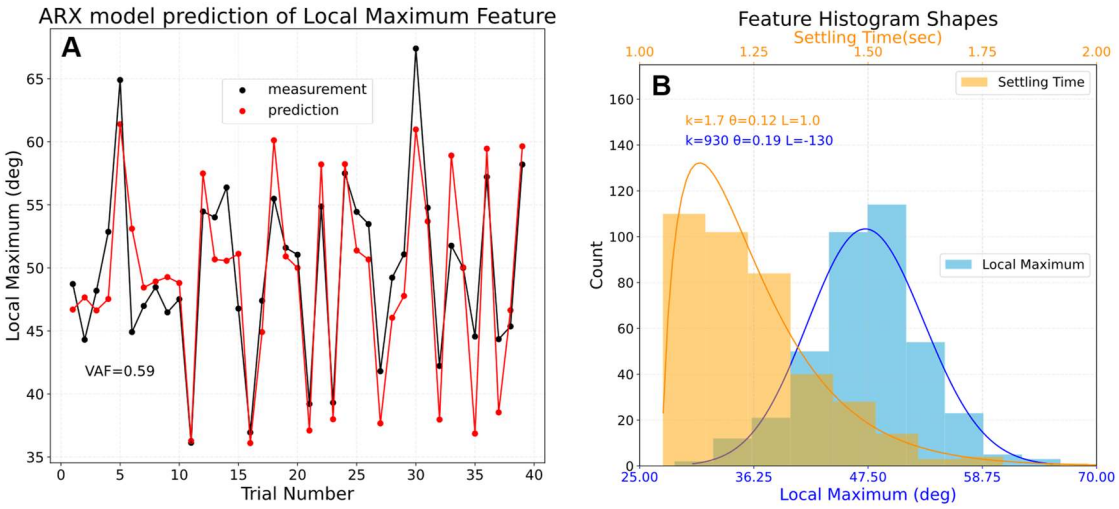

Fig 2.4. ARX model prediction performance and feature histogram shapes. (A) Example of ARX model performance for prediction of the Local Maximum feature for an example subject on the first 40 reaches of block 4. The ARX model incorporates a linear combination of the previous feature value and past and current spring stiffness values to form a prediction what the subjects' performance will be on the current reach. The model was trained on data from blocks (1,2,3) and was tested on blocks (4,6). Variance Accounted For (VAF) this subject was 59%. (B) Histograms of the local maximum and settling time features from every reach taken by an example subject. While spatial features like local maximum tend to be normally distributed, temporal features such as settling time tend to have longer right tails which makes fitting linear models difficult. Parameters of a gamma distribution were fit to the histograms using maximum likelihood estimation.

2.3.5 Analysis – composite curve generation

Composite curves are used throughout the analysis as a way of determining and visualizing average subject behavior. Here we describe how a composite curve was created. A composite curve is a representation of the average reach for a particular stiffness in a particular block. The reach curves from a block of trials are sorted into groups by stiffness. Each curve is brought into register with the same .3 second fictitious reaction time as described in the previous section. Then, for each time point, average and standard deviation statistics are computed across reaches. The composite plot shows this registered and averaged reach curve plus and minus the standard deviation for that timepoint. The result is a curve which characterizes average subject reaching performance binned by condition and is used in figures 2.2, 2.5, 2.6, and 2.7.

2.3.6 Analysis – inferential statistics

Inferential statistical analysis was used to establish differences between the values of features across different experimental conditions. For example, inferential statistics were used to substantiate the performance differences between blocks with (block 4) and without (block 5) visual cues. Inferential statistics form the basis of the analyses described in tables 1,3, and 4. In each case, the approach taken was the same. Feature statistics were calculated for each reach in a block and condition for each subject (example, t30 in the high stiffness reaches of block 4 for subject 3). To evaluate whether 2 conditions were different a paired-t test was undertaken between those two conditions. The following label was used to connote such a comparison: feature name (stiffness_block – stiffness_block). To continue with the previous example, t30(H4-H5) is a statistical test, evaluating the difference between the value of the *t30* feature in the high stiffness condition of block 4 and the value of the *t30* feature in the high stiffness condition of block 5, for

each subject, in a paired fashion. Labeling for table 2.4 was slightly different, as that analysis compared reaches only within block 5, but with different reaching histories. An example label for table 4 would be t30(HH-LH) which compares t30 for high reaches where the previous reach was high, to high reaches where the previous reach was low. The data in the inferential statistical analysis are justifiably paired, as the same subject underwent each test. Every pairwise comparison that was undertaken has been reported here, and a false discovery rate (FDR) correction has been applied to the p-values of each resulting statistic to avoid the multiple comparisons problem.

2.3.7 Analysis – ARX modeling

To model the temporal dynamics of adaptation, time series analysis using an Autoregressive Exogeneous input (ARX Model) was performed. An ARX model linearly combines past performance values (the autoregressive term) with exogeneous input terms, in this case the value of the spring environment, to predict future performance. The mathematical formula of the ARX model used in this analysis was

$\hat{y}_t = c + p_0(y_{t-1}) + b_0(x_{t-1}) + b_1(x_t)$ where $\hat{y}_t$ is the feature value to be predicted, c is a constant term p_0 is the coefficient on the autoregressive terms, and b_0 , b_1 are the coefficients of the exogeneous terms of the past and current stiffness. 4 features were fit with ARX models, with one model fit per feature per subject. The features fit were *t30,t40,settling time, local max.* Data was separated into training and testing sets, with data from blocks [1,2,3] being used for training / fitting the model ,and data from blocks [4,6] was used for evaluating the fit of the model. The quality of the model fit was evaluated using the criteria variance accounted for (VAF) which is calculated as the ratio of the measured to predicted variance. Here, a perfect prediction produces a VAF of 1, and a prediction which accounts for none of the variance results in a VAF of 0.

	t30	t40	settling time	local max
VAF	0.243959	0.351904	-0.046580468	0.391593

Table 2.2. ARX modeling test set Variance Accounted For (VAF) by feature
The average test set variance accounted for across the 12 subjects. The ARX models were fit on blocks (1,2,3) and tested on blocks (4,6) Temporal features had lower VAF than positional features.

2.3.8 Composite curve analysis of block 3: secondary features, regression, PCA

Composite curve analysis was undertaken to investigate subject reaching strategy (Fig 2.7). Analysis block 3 was used in this analysis because all 3 stiffnesses, high medium and low, were represented in this block. A set of 8 secondary features were created to characterize each subjects' block 3 performance and establish patterns of performance. The naming convention followed by the secondary feature was [feature name (stiffnesses involved)]. Here we will describe how the secondary features were computed and justify why they might provide useful information for understanding subject reaching performance. In all subjects the medium stiffness composite curve had the best performance in terms of settling time, and so frequently this was chosen as a reasonable curve to use in the characterization of subject reaching strategy. The secondary features *t30(M), settling time(M), and peak velocity(M)* were all looked at for this reason. *L2loss(M)* was defined as the sum of the square of the difference (L2 loss) between the subjects' medium stiffness composite curve and a step function. This offers a precisely defined mathematical expression for how fast and smoothly a subject arrived at the target location. *Local max t(L)* and *Local max y(L)* generally look at the overshoot behavior of the lower stiffness condition. The following 2 features characterize the nature of the undershoot response for of the higher stiffness curve*: n_extrema(H)* and *backtracking(H)*. *n_extrema(H)* is a count of the number of extra points in the H composite curve which varied between 0 and 2. *Backtracking(H)* is only defined when the *n_extrema(H)* is 2 and represents the difference between the local maximum of the H composite curve and the local minimum that follows, in degrees. Lastly, the *t30 dispersion (LH)* secondary feature was defined as the *t30(H)* time minus the *t30(L)* value, which is an indication of how tightly clumped together or widely dispersed the *t30* time was the different response curves.

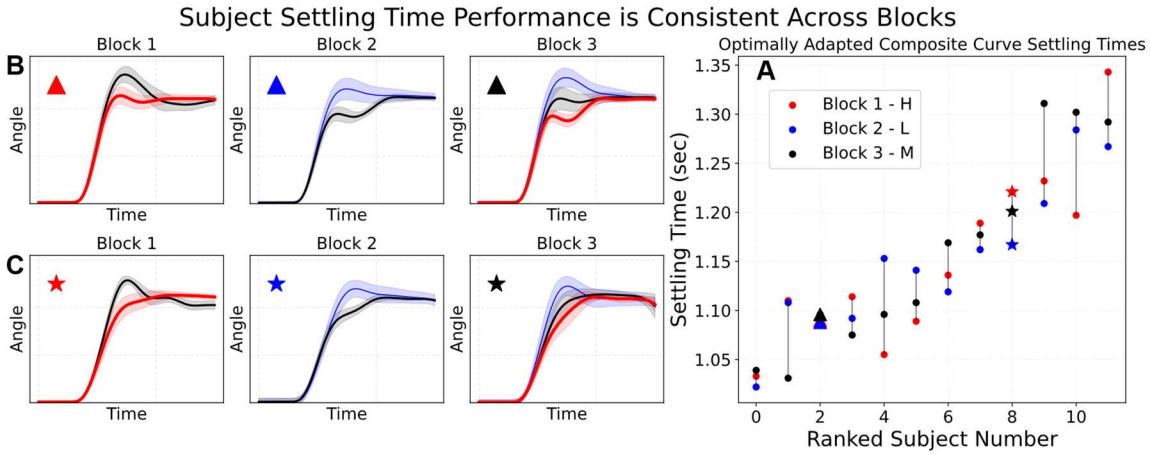

Fig 2.5. Subject Settling Time Performance is Consistent Across Blocks
(A) subjects were ranked in terms of the settling time performance of their composite curves on optimally adapted trials. Here optimally adapted was defined as the stiffness with the fastest settling time in a block. Subjects who were the fast reachers tended to reach fast in all blocks while those who were slow reachers tended to reach slowly in all blocks. Put another way, variance across subjects was much greater than variance within subjects. (B) Composite curves of a fast reacher for blocks 1,2, and 3. The subject consistently demonstrated features characteristic of the fast reacher such as low stiffness overshoot, low t30 dispersion, presence of a local min and max. (C) Composite curves of a slow reacher for blocks 1,2 and 3. The subject consistently demonstrated features characteristic of a slow reacher such as high t30 dispersion, low overshoot on low stiffnesses, absence of local min in sub optimally adapted curves.

A series of regressions were undertaken to establish relationships between secondary features. Several interesting regressions are featured in figure 2.7. P-value and correlation coefficients were calculated and reported for each regression. Lastly principal component analysis (PCA) was performed on the secondary features, and explained variance was plotted as a function of principle component index.

2.3.9 Model Identification Adaptive Control (MIAC)

An optimal control framework called Model Identification Adaptive Control (MIAC) was implemented to simulate lower-limb reaching behavior. The objective of the analysis was to explore whether the dispersion of features seen experimentally might be explained in terms of an optimal trade-off between competing objective functions. The results of the analysis are shown in figure 2.8.

Figure 2.8B shows the MIAC control system architecture. A model predictive controller (MPC) generates a torque sequence which represents the control action of the human. The torque interacts with a plant model, which represents the physical system being rendered by the NOTTABIKE robot. Finally, an optimal parameter estimator represents the ability of the human to adapt the estimate of the system they are interacting based on feedback. It takes in a copy of the torque trajectory generated by the MPC (efference copy), and sensory data from how the physical plant actually behaved and forms the best estimate for the spring being rendered. This estimate is used on the next iteration torque generation by the MPC.

We begin by a description of the plant model. A continuous time state-space model of a 1 degree of freedom rotational mass-spring system was created and is depicted graphically and numerically in figure 2.8A. The state vector of input of this system is torque u and the output is

the state vector $x = [\theta\omega]'$. For computability, the continuous time system representation was discretized using sample time $T = .01$ and 5 terms in the Taylor-Series expansion of the matrix exponential. This model constitutes the plant block in figure 2.8B.

The model predictive controller (MPC) (see Fig 2.8B) generates a torque trajectory using a technique called direct-collocation. In direct collocation, an objective function is optimized subject to a set of constraints which constitute the dynamics of the system. Here the dynamics of the system come from the discretized dynamics of the plant model estimate over the planning horizon. We used a 1.5 second planning horizon with a time grid of $T = .01$. We used a MPC period of .3 seconds except for where specified (see discussion) so that while an entire trajectory is planned, only a fraction of it is executed through the plant model at any control loop iteration. The objective function trades off 2 competing objectives using a single parameter λ. The first objective is integral actuation cost, which is computed as the sum of the square of the torque trajectory. This objective function makes using high torques expensive. The second is integral end-point error, which mathematically is defined as the sum of the difference between the current location and target location over the specified time interval. This objective function encourages fast reaching towards the target. Trading off between these 2 objectives with the parameter lambda λ specifies mathematically what a modeled subject values during their reach.

The optimal parameter estimator uses measured data from the plant and information about the torque trajectory u to formulate an optimal estimate for k, denoted $\hat{k}$. The optimal parameter estimator was implemented using a shooting method which varied $\hat{k}$ to minimize the difference L2 norm between the measured and simulated state vectors x_n.

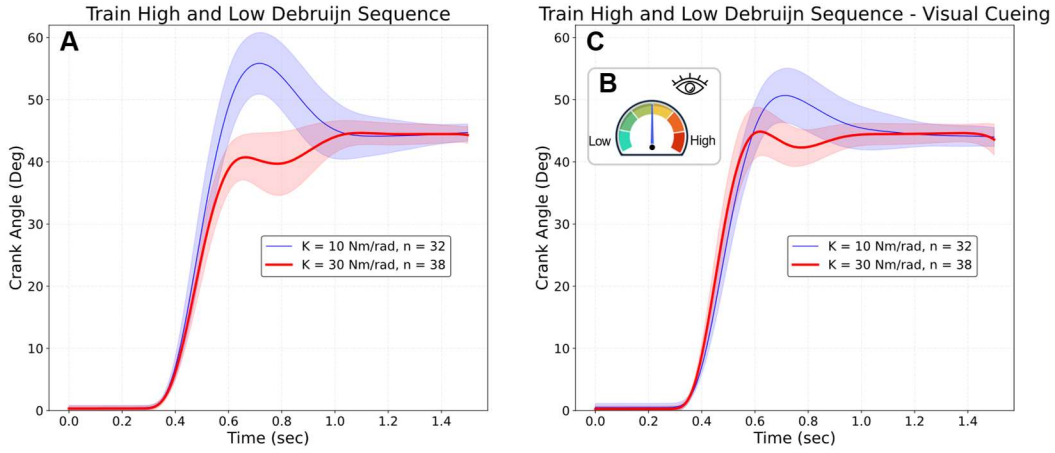

Fig 2.6. Visual Cueing Impacts Reach Performance.
(A) Without visual cueing, large differences were observed between the composite curve of high stiffnesses and low stiffness reaching trials in block 4. (C) A dial indicator was added to the visual display to inform the subject which stiffness was going to be encountered next in block 5. (C) With this additional information, subjects could reduce overshoot on low stiffnesses and undershoot on high stiffnesses. Interestingly, timing statistics (t30,t40) of high stiffness reaches were impacted to a greater extent than low stiffness reaches. (see table 2.1.3)

2.4 Results

Inferential statistical analysis was performed to establish the difference in performance between block 1 and block 2 across different stiffness conditions (Table 2.1). Recall that block 1 featured predominantly high stiffnesses while block 2 featured predominantly low stiffnesses, with 10 medium catch trials (Fig 2.1.C). All comparisons in table 2.1 were found to be statistically significant besides that of reaction time.

ARX models were fit to a time series of each subjects' performance for the features *t30,t40,settling time,* and *local max* (Table 2.2). Time based features tended to poorer performance on variance accounted for than the angular feature *local max*. The extent to which ARX models fit the data for a particular subject varied from .2 to .7 VAF.

To establish whether subject settling time performance was consistent over time, settling time performance was evaluated on blocks 1,2,3 for the most frequently presented stiffness in that block. Subjects were ranked in terms of their average settling time, and the results were plotted in figure 2.5. *Settling time* variance across subjects was greater than *settling time* variance within subjects, indicating that fast reachers remained fast, and slow reachers remained slow over time.

Table 2.3 establishes the effect that visual cueing has on reaching performance by comparing block 4 and block 5 performance features for both high and low stiffnesses. Subjects showed lower overshoot on both high trials and low trials ($p = .008$ and $p < .001$ respectively). Temporally, subjects showed faster *t30* and *t40* rise times, but only on the high stiffness trials ($p < .001$ for both). Low stiffness trial rise times were unaffected.

The results of an analysis to evaluate if visual cueing could cancel the effect of adaptation are presented in table 2.4. Block 5 trials were sorted by their 1 trial histories (what the previous

trial was) and compared statistically. Those reaches where the previous reach was of a different stiffness had a slower *settling time*, and statistically different *local max* than reaches where the previous reach was of the same stiffness.

An analysis of block 3 composite curve performance was undertaken to evaluate subject reaching strategy (Fig 2.7). 8 secondary features were created to characterize (see section 2.8 for details) block level subject performance. Regression analysis revealed relationships between these secondary features. The time of overshoot was negatively correlated with angle of overshoot ($r = -.81$, $p = .001$). Subjects who had a higher peak reaching velocity on their medium stiffness curves, also had a tighter t30 dispersion across curves ($r = -.93$, $p < .001$). Principal component analysis revealed that the majority (88%) of the explained variance among the 8 secondary features could be accounted for by a single principal component dimension.

The MIAC model simulated reaching in uncertain environments for simulated subjects with different weights in their multi-objective reaching function. When the simulation placed more value on reaching fast (minimizing end-point cost), secondary features characteristic of fast reachers emerged such as a high *Local max(L),* a small *t30 dispersion*, a high stiffness reach with a local max and min. When the simulation placed more value on using low torque (minimizing actuation cost), secondary features characteristic of slow reachers emerged, such as low *Local max(L),* a large *t30 dispersion*, and a high stiffness reach without a local max or min.

Time-Based Features (seconds)

	t30(L4-L5)	t30(H4-H5)	t40(L4-L5)	t40(H4-H5)
condition1: mean(sd)	0.537(±0.047)	0.571(±0.070)	0.598(±0.066)	0.741(±0.082)
condition2: mean(sd)	0.539(±0.050)	0.524(±0.051)	0.609(±0.073)	0.620(±0.077)
p-val	1	**<.001**	0.54	**<.001**

	reaction time(4-5)	settling time(4-5)
condition1: mean(sd)	0.369(±0.043)	1.28(±0.053)
condition2: mean(sd)	0.363(±0.044)	1.19(±0.061)
p-val	0.09	**<.001**

Position-Based Features (seconds)

	local max(H4-H5)	local max(L4-L5)
condition1: mean(sd)	43.8(±1.9)	52.0(±2.5)
condition2: mean(sd)	45.4(±1.1)	49.5(±1.9)
p-val	**0.008**	**<.001**

Table 2.3. Evaluating Subject performance with and without Visual Cue.
Inferential statistical analysis evaluated the effect of visual cueing on subject performance for the above features by comparing block 4 (deBruijn with no visual cue) to block 5 (deBruijn with visual cue) performance.

Note: Column labels may be read as follows: "feature name(stiffnessBlock-stiffnessBlock)". Example: "local max(H4-H5)" compares the value of the local max feature on high stiffness reaches in block 4 to high stiffness features in block 5. If no stiffness is listed, all reaches in the block are pooled for the analysis.

2.5 Discussion

2.5.1 Average reaching performance is affected by training environment

When considered together, figure 2.3 A and B shows the impact of training environment on the shape of a medium stiffness reach composite curve. In the predominantly high stiffness environment of block 1, the medium stiffness response on average show characteristic features such as a high local max (52.4 degrees) fast t30 (.537 sec) and t40 (.592 sec) rise times. These features suggest that the human motor control system was on average anticipating encountering the more prevalent (7:1 ratio) higher stiffness and was mis-calibrated when encountering the medium stiffness trial.

By contrast, the medium stiffness composite curves of block 2 in which low stiffness predominated showed the opposite characteristics. Local max undershoots the target (40.6 degrees) and t30 (.605sec) and t40 (.869sec) are slow – suggesting mis-calibration in the opposite direction. These results are consistent with the results of adaptive processes from other movement modalities such as the upper-limb, fingers, and saccadic movements of eye muscles. It is important to note that the human controller is not responding by calculating an evenly weighted running average, but instead the recalibration is more strongly influenced by proximal past performances. In the next section, we explore more precisely how mis-calibrations are related to previous performance and encountered stiffness using time series analysis techniques.

2.5.2 ARX model prediction performance and feature histogram shapes

An Autoregressive Moving Average model (ARX) was used to predict feature performance on the current trial from a linear combination of a constant, feature performance on the previous

trial, and the current and previous spring stiffnesses (see section 2.7 for details). As an example, we will look at the average coefficients for an ARX model of the *local max* feature and interpret their meaning. The base formula of the ARX model is $\hat{y}_t = c + p_0(y_{t-1}) + b_0(x_{t-1}) + b_1(x_t)$. The average fit across all subject training data was calculated as $\hat{y}_t = 40.5 + .165(y_{t-1}) + .472(x_{t-1}) - .558(x_t)$. If we consider the first two terms together, then just the AR part of the model is defined as $\hat{y}_t = c + p_0(y_{t-1})$. This is recursive discrete time function which causes exponential decay towards a steady state value. c moves the value up and down, and p_0 has a combined effect of adjusting the steady state value and the rate of exponential decay, with larger p_0 values resulting in slower rates, and smaller p_0 values resulting in faster decay rates. For our model the steady state value was 48.2, and the exponential decay rate, which might be thought of as a forgetting rate was .165.

The last two terms in the model, $.472(x_{t-1}) - .558(x_t)$, form the exogeneous input. Notice that the terms are nearly the same magnitude and opposite in sign. Thus, when the previous stiffness and current stiffness are the same, the sum of these two terms is small and nearly offset. When the previous stiffness is low for example (10Nm/rad) and then current stiffness is high (30Nm/rad), this part of the model predicts that there should be an undershoot of about 12 degrees. Conversely if the previous stiffness was high and the current stiffness low, then there should be an overshoot of about 8 degrees.

As should be expected, the quality of the ARX model training fits were much higher than the testing fits as determined by the VAF criterion. The quality of fit as quantified by VAF was more variable from subject to subject than we expected. For instance, when modeling the *local max* feature, some test fits were as high as 0.67, while others were as low as 0.1. One reason for this discrepancy could have been that linear least squares is sensitive to outliers during the fitting

	localMax_y(HH-LH)	localMax_y(LL-HL)	settlingTime(HH-LH)	settlingTime(LL-HL)
condition1: mean(sd)	46.0(±0.99)	48.6(±1.1)	1.14(±0.070)	1.19(±0.079)
condition2: mean(sd)	44.5(±1.8)	50.3(±2.9)	1.19(±0.067)	1.24(±0.072)
p-val	**0.02**	**0.03**	**0.006**	**0.03**

Table 2.4. Visual Cueing Cannot Cancel Adaptation.
To evaluate if visual cueing completely cancels the effect of adaptation, an inferential statistical analysis was performed on data from block 5 performance. Local max and settling time statistics were calculated using paired t-tests with FDR corrections, to evaluate the effect that previous trial had on current trial performance. Performance on each metric was better (lower overshoot, faster settling time) in the condition when the previous trial stiffness matched the current trial stiffness, indicating that an adaptive mechanism was still at play even when the next stiffness was known before the reach.

Note: Column labels may be read as follows: "feature name(previousStiffnessCurrentStiffness – previousStiffnessCurrentStiffness)". Example: "settling Time(HH-LH)" compares the settling time of High stiffness where the previous stiffness was high to high stiffness trial where the previous stiffness was low. All analysis in this table was performed on block 5 trial.

process, and so it's possible for a small number of non-representative datapoint to skew the fitting process. Spatial features like local max tend to be normally distributed, while temporal features are gamma distributed with right skew (Fig 2.4B) this could be a reason why test VAF was higher in spatial than temporal features.

2.5.3 Settling Time Performance is Consistent Across Blocks

The analysis shown in figure 2.5A was undertaken to assess whether subjects maintained a consistent level of performance throughout the duration of the experiment. Other investigators have noted the existence of slacking – a phenomenon in which subject performance worsens over time. We did not observe this phenomenon, which would have been indicated by earlier blocks consistently having lower settling times than later blocks in figure 2.5A. This could have been due to the motivational system keeping subjects engaged with the task.

2.5.4 Visual Cueing Impacts but cannot cancel reach adaptation

The analyses were undertaken to establish the impact that visual cueing of environment stiffness has on lower-limb reaching performance. The results are compared graphically in figure 2.6 and statistically in tables 2.3 and 2.4. Subjects showed an ability to utilize stiffness cues to improve performance features, but improvements were not the same for every feature or every stiffness condition. For the *local max* feature, undershoot of the high stiffness trials was decreased while overshoot of low stiffness trial increased with visual cueing, likely indicating a change to motor preplanning and environmental expectation. The improvement in *local max* characteristics led to a statistically significant improvement in *settling time* for all conditions ($p<.001$).

Temporal features such as *t30* and *t40* were significantly different ($p < .001$) on high stiffnesses, but not low stiffnesses. This means that despite information about the environment to

be encountered, subjects choose not to modify the temporal characteristics of their reach in the low stiffness condition. One possible reason for this choice could be that pushing the low stiffness reach to be faster could compromise endpoint accuracy as specified by Fitts law. Signal-dependent noise, or increased variance as a function of control signal magnitude, has been suggested as the mechanism behind Fitts law. As the speed of the reach gets faster with brief periods of large accelerations, the contribution of force required to accelerate the inertia of the legs becomes larger, and the timing requirements for those forces becomes tighter. It's possible in the low stiffness case, subjects were already closer to their timing limits, and so no change in timing characteristics was observed despite the subject having access to cueing information.

By contrast, when subjects were interacting with an unknown high stiffness environment, their behavior was significantly slowed by the force required to overcome the spring. When subjects were cued about encountering the high stiffness environment, they were willing to offset the cost of pushing against the high stiffness spring to improve their temporal performance characteristics, up to the point the timing characteristics of the high and low stiffness were about equal.

Finally, we performed an analysis which demonstrated that while visual cueing can improve performance features of reaching curves, it cannot cancel the effects of adaptation. Table 4 shows an inferential statistical analysis that makes this point. *Local max* and *settling time* were significantly better in the block 5 (with visual cue) conditions where the previous trial was the same as the current trial. To understand why this might be, it's important to examine how a subject uses cues to improve reaching performance. The subject must translate between the visual image of an indicator dial on the screen indicating high or low and then call up a motor memory of what it was like to interact with that environment and integrate that information into their motor plan

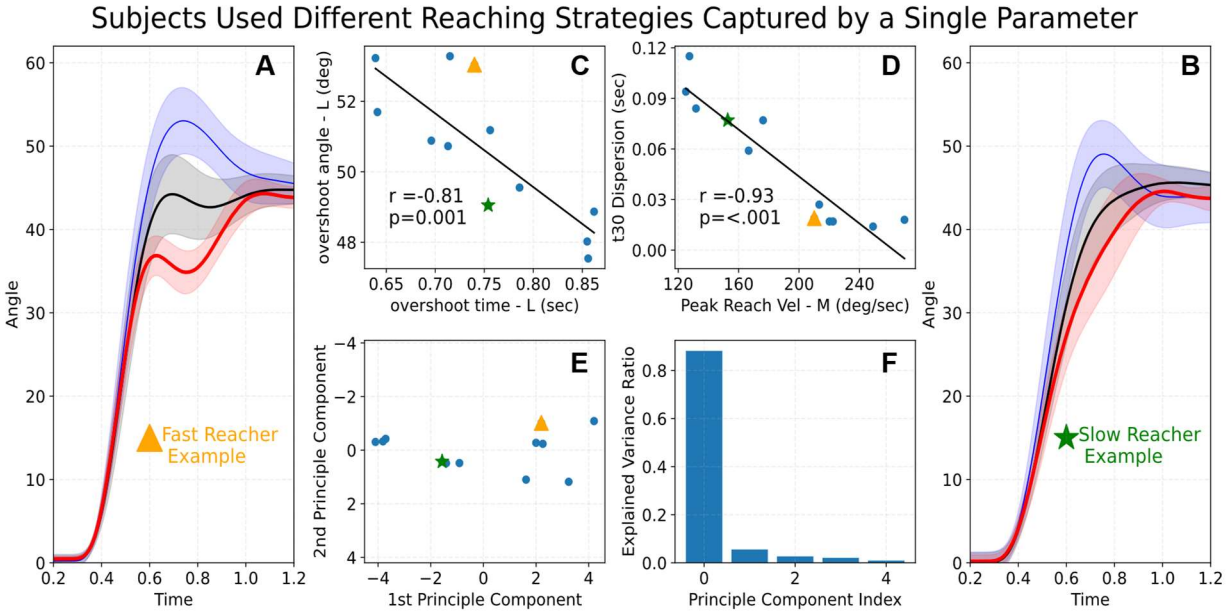

Fig 2.7. Subjects used Different Reaching strategies captured by a single parameter 8 features were extracted from the composite curves of the block 3 performance of each subject and were used in regression and principal component analysis (A) An example faster reacher as determined by settling time performance of the medium stiffness condition (B) An example slow reacher as determined by settling time performance of the medium stiffness. (C) Regression analysis which demonstrates that faster reachers tend to overshoot more on the low stiffness. (D) regression analysis which show that faster reachers, as determined by their peak velocities tend to have lower t30 dispersion. (E) Data sliced along the first and second principal components, demonstrating the maximum variation of the dataset (F) PCA revealed that 88% of the variance of these features could be explained by the first principal component, which suggests a single parameter can be used capture the different subject reaching strategies.

for the next reach. Such conceptual manipulation requires frontal lobe involvement. In parallel, there is an adaptive process going on when is driven largely by motor prediction error. This adaptation process which is believed to be mediated by the cerebellum. Thus, while visual cueing can greatly improve aspects of reaching performance, it can't cancel the effects of the adaptation process that is happening concurrently.

2.5.5 Subjects used Different Reaching Strategies Captured by a Single Parameter

An analysis of block 3 performance was undertaken to try and understand how subject reaching performances were different from one another, and to what extent curve features correlated. A set of 8 secondary features was created to quantify subject composite curve performance and the rational and implementation of those features is listed in section 2.8. From the Principal Component Analysis of these 8 features across all 12 subjects, it was found that only 1 dimension was required to explain 88% of the experimental variance (Fig 2.7 E and F). This result indicated that strong correlations existed between the salient features of the reaching curves and variation along a single parameter might be able to explain the different features observed in the experimental data and motivated the construction of an optimal control model of reaching.

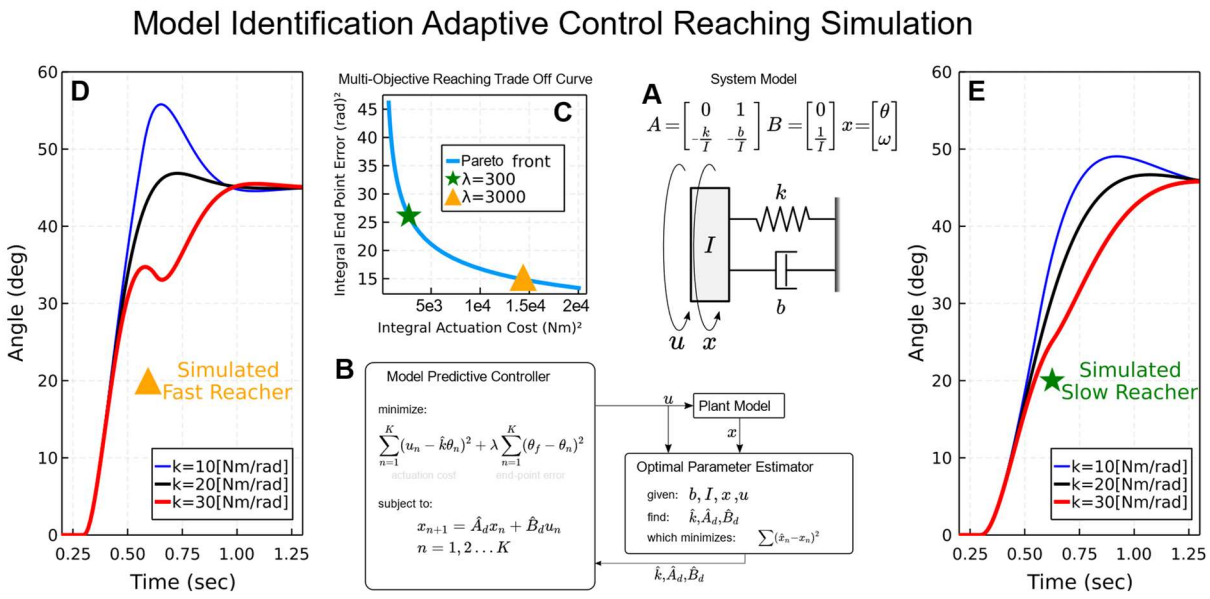

Fig 2.8. Model Identification Adaptive Control (MIAC) Simulation Results
We created an optimal control framework to model lower-limb reaching. (A) the dynamics of the model were based on a 1 DOF rotational system with input torque u and output kinematics $x = [\theta\omega]'$. (B) an optimal controller solves for a torque trajectory u over a planning horizon. The trajectory minimizes a 2-term cost function trading off actuation cost and end-point accuracy while being constrained by the dynamics of the estimated system. A single parameter λ defines the relative tradeoff between the two cost functions. Each MPC cycle, u is input into the plant model which generates $x(t)$. u and x are then passed to an optimal parameter estimator which updates the estimate of k, $\hat{k}$ used by the controller. (C) By plotting the controller performance over range of λ values, a pareto optimal frontier is generated. High values of λ favor lower integral end-point error, while low values of λ favor lower actuation cost. (D and E) Simulated trajectories using the (MIAC) framework with, $\hat{k}$ = 20[Nm/rad] (medium stiffness) (D) The simulated fast reacher values end-point error at the expense of actuation cost. Notice characteristic features observed in the experimental results, such as low t30 dispersion, large overshoot on low stiffness, and a local minimum and maximum on the high stiffness curve. (E) The simulated slow reacher values low actuation cost at the expense of integral end-point error. Notice the high t30 dispersion, lack of local minima in the high stiffness response curve, and smaller overshoot in low stiffness curve.

2.5.6 Model Identification Adaptive Control (MIAC) Simulation Results

A Model Identification Adaptive Controller (MIAC) Simulation was developed to explain the salient features observed in the experimentally collected data in terms of variation along a single dimension. The single model parameter λ specifies a trade-off between 2 competing objectives - one for end-point accuracy and a second for actuation cost (see section 2.9 for details). Allowing lambda to vary changes which objective function is more highly valued and forms a curve known as a pareto front (Fig 2.8C).

Settling time of the most frequently encountered environment within a block forms a good proxy measurement for end-point error valuation, and figure 2.5 suggests this did not change over the course of the experiment. What factors might determine a subject's choice (constant) choice of λ value? Motivation and engagement with the task and recruitment of the dopaminergic system is one possibility. Subjects with higher engagement levels may place more importance on end-effector error as good settling time performance elicited enjoyable sounds from robot's motivational system. Risk aversion manifesting as a low tolerance for overshoot, undershoot, or unintended movements of the crank is another possibility, as subjects with faster reaching preferences had greater deviations of the crank angle when they were miss-adapted to the encountered environment (Fig 2.8 D and E). A third possibility is that the speed of the subjects' reach may be limited by the lag time of their sensory feedback and ability to integrate sensory information. Maximum overshoot and undershoot in miss-adapted cases was very sensitive to MPC loop time, so a subject with slower sensory feedback may elect to reach more slowly.

The MIAC model allowed for the investigation of the mechanisms behind some of the observed curve features. For instance, undershoot followed by a local minimum in the high stiffness response curve of fast reachers is due to a mechanical resonance between rendered spring

and limb mass. The human enacts a pre-planned force trajectory which is not sufficient to reach the target position. The spring begins to move the leg backwards when sensory feedback reaches the optimal parameter estimator. The actual stiffness of the environment is calculated updating $\hat{k}$ and corrective measures are taken to reach the desired target. Overshoot may be understood in a similar fashion.

The MIAC model also sheds light on the *t30 dispersion* feature. The early portion of fast reaches are dominated by the large forces required to accelerate the mass of the model. Force due to the small spring displacements of early reaching by comparison contribute very little to the total applied force, and so the early trajectories of all 3 curves in figure 2.8D (fast reaching) look the same. In slow reaching where high forces are strongly penalized, the early portion of the reach is much more gradual, and so pre-planned forces required to offset the spring stiffness represent a larger fraction of the total applied force u. Thus, when the encountered spring stiffness is different than anticipated, the resulting trajectory is different than planned.

2.5.7 Limitations and Future Investigations

In this investigation we explored adaptation during goal directed reaching in the lower-limb. While the study quantified may of the spatial and temporal performance characteristics of lower-limb adaptation, limitations and further questions remain.

The ARX models of features such as *local max, t30,* and *t40* proved to be excellent predictors of performance in the best case, but poor predictors for some subjects. Non-linear model fitting or outlier elimination techniques might be able to address these issues in the future. While *settling time* proved to be a reliable metric when averaged across condition as in the inferential

statistical analysis, a linear time series analysis model was not capable of producing satisfactory predicts of it.

The MIAC model generated simulated curves that contained many of the secondary features observed in experimental data such as *t30 Dispersion (LH),* the presence of backtracking in fast reachers, and others. There were however limitations to the model that could be addressed in future work. There is no way besides exhaustive search to know if the objective functions other than the two selected might provide a better description for human behavior. Perhaps smoothness and energetic cost are closer to human goals, or robustness to environmental variation? Our model can't answer these questions. The MIAC model implemented here doesn't incorporate the non-linear dynamics of the limb, or the temporal properties of muscle activation dynamics. Because of this, the model can't answer questions about muscle activation levels or timing. Future studies which wish to answer such questions would require more complex musculoskeletal modeling.

Reaching in this study was conducted along a kinematically constrained cyclic path, and between 2 locations only. Future reaching studies in the lower-limb could involve multiple reaching objective locations, and consider free-form reaching in the plane, as has been studied extensively in the upper-limb

2.6 Conclusion

Here we have demonstrated and quantified different features of adaptation during a lower-limb reaching task in healthy subjects against spring environments of different stiffnesses. The performance of the reach was shown to depend on the time history of the previously encountered trials via an ARX model of the previous performances. We additionally showed that visual

information about the next trial could be utilized in increasing performance on the next trial but could not fully overcome the effect of the time history of previously encountered trials. Future work will explore lower-limb reaching in a varied set of environments, including damper, mass, and spring-mass-damper systems.

2.7 References

[1] R. Shadmehr and F. A. Mussa-Ivaldi, "Adaptive representation of dynamics during learning of a motor task," *J. Neurosci.*, vol. 14, no. 5, pp. 3208–3224, May 1994, doi: 10.1523/JNEUROSCI.14-05-03208.1994.

[2] C. D. Takahashi, R. A. Scheidt, and D. J. Reinkensmeyer, "Impedance Control and Internal Model Formation When Reaching in a Randomly Varying Dynamical Environment," *J. Neurophysiol.*, vol. 86, no. 2, pp. 1047–1051, Aug. 2001, doi: 10.1152/jn.2001.86.2.1047.

[3] N. Bhushan and R. Shadmehr, "Computational nature of human adaptive control during learning of reaching movements in force fields," *Biol. Cybern.*, vol. 81, no. 1, pp. 39–60, Jul. 1999, doi: 10.1007/s004220050543.

[4] M. I. Mohamed Refai *et al.*, "Smoothness metrics for reaching performance after stroke. Part 1: which one to choose?," *J. NeuroEngineering Rehabil.*, vol. 18, no. 1, p. 154, Oct. 2021, doi: 10.1186/s12984-021-00949-6.

[5] J. L. Patton, M. E. Stoykov, M. Kovic, and F. A. Mussa-Ivaldi, "Evaluation of robotic training forces that either enhance or reduce error in chronic hemiparetic stroke survivors," *Exp. Brain Res.*, vol. 168, no. 3, pp. 368–383, 2006.

[6] E. B. Brokaw, D. Nichols, R. J. Holley, and P. S. Lum, "Robotic Therapy Provides a Stimulus for Upper Limb Motor Recovery After Stroke That Is Complementary to and Distinct From Conventional Therapy," *Neurorehabil. Neural Repair*, vol. 28, no. 4, pp. 367–376, May 2014, doi: 10.1177/1545968313510974.

[7] F. Abdollahi *et al.*, "Arm control recovery enhanced by error augmentation," in *2011 IEEE International Conference on Rehabilitation Robotics*, Jun. 2011, pp. 1–6. doi: 10.1109/ICORR.2011.5975504.

[8] E. Todorov and M. I. Jordan, "Optimal feedback control as a theory of motor coordination," *Nat. Neurosci.*, vol. 5, no. 11, pp. 1226–1235, Nov. 2002, doi: 10.1038/nn963.

[9] E. Todorov, "Optimality principles in sensorimotor control," *Nat. Neurosci.*, vol. 7, no. 9, pp. 907–915, Sep. 2004, doi: 10.1038/nn1309.

[10] T. Flash and N. Hogan, “The coordination of arm movements: an experimentally confirmed mathematical model,” *J. Neurosci.*, vol. 5, no. 7, pp. 1688–1703, Jul. 1985, doi: 10.1523/JNEUROSCI.05-07-01688.1985.

[11] R. A. Scheidt, J. B. Dingwell, and F. A. Mussa-Ivaldi, “Learning to Move Amid Uncertainty,” *J. Neurophysiol.*, vol. 86, no. 2, pp. 971–985, Aug. 2001, doi: 10.1152/jn.2001.86.2.971.

[12] H. F. Machiel Van der Loos, S. A. Kautz, D. F. Schwandt, J. Anderson, G. Chen, and D. M. Bevly, “A split-crank, servomotor-controlled bicycle ergometer design for studies in human biomechanics,” 2002, vol. 2, pp. 1409–1414. doi: 10.1109/IRDS.2002.1043952.

[13] D. A. Brown and S. A. Kautz, “Speed-Dependent Reductions of Force Output in People With Poststroke Hemiparesis,” *Phys. Ther.*, vol. 79, no. 10, pp. 919–930, Oct. 1999, doi: 10.1093/ptj/79.10.919.

[14] D. A. Brown and S. Kautz, “Increased workload enhances force output during pedaling exercise in persons with poststroke hemiplegia,” *Stroke*, vol. 29, no. 3, pp. 598–606, 1998.

[15] D. A. Brown, S. Nagpal, and S. Chi, “Limb-Loaded Cycling Program for Locomotor Intervention Following Stroke,” *Phys. Ther.*, vol. 85, no. 2, pp. 159–168, Feb. 2005, doi: 10.1093/ptj/85.2.159.

[16] M. Alcobendas-Maestro, “Lokomat Robotic-Assisted Versus Overground Training Within 3 to 6 Months of Incomplete Spinal Cord Lesion Randomized Controlled Trial,” *Neurorehabil Neural Repair*, vol. 26, no. 9, pp. 1058–1063, Nov. 2012.

[17] L. H. Ting, S. A. Kautz, D. A. Brown, and F. E. Zajac, “Phase Reversal of Biomechanical Functions and Muscle Activity in Backward Pedaling,” *J. Neurophysiol.*, vol. 81, no. 2, pp. 544–551, Feb. 1999, doi: 10.1152/jn.1999.81.2.544.

[18] L. H. Ting, C. C. Raasch, D. A. Brown, S. A. Kautz, and F. E. Zajac, “Sensorimotor state of the contralateral leg affects ipsilateral muscle coordination of pedaling,” *J. Neurophysiol.*, vol. 80, no. 3, pp. 1341–1351, 1998.

[19] L. H. Ting, S. A. Kautz, D. A. Brown, and F. E. Zajac, “Contralateral movement and extensor force generation alter flexion phase muscle coordination in pedaling,” *J. Neurophysiol.*, vol. 83, no. 6, pp. 3351–3365, 2000.

[20] M. R. Dimitrijevic, Y. Gerasimenko, and M. M. Pinter, “Evidence for a Spinal Central Pattern Generator in Humans,” *Ann. N. Y. Acad. Sci.*, vol. 860, no. 1, pp. 360–376, 1998.

[21] L. A. M. and A. J. Bastian, “Spatial and Temporal Asymmetries in Gait Predict Split-Belt Adaptation Behavior in Stroke,” *Neurorehabil Neural Repair*, vol. 28, no. 3, pp. 230–240, Mar. 2014.

[22] D. S. Reisman, H. McLean, J. Keller, K. A. Danks, and and A. J. Bastian, “Repeated Split-Belt Treadmill Training Improves Poststroke Step Length Asymmetry,” *Neurorehabil Neural Repair*, vol. 27, no. 5, pp. 460–468, Jun. 2013.

Chapter 3

Exploring the Role of Cognitive Models in Skill Acquisition for a Novel Half-Reversed Cycling Task

Alexander R. Dawson-Elli and Peter G. Adamczyk
(study is complete and manuscript is in preparation)

3.1 Abstract

While much work has been done to investigate goal-directed tasks in the upper-limb and cyclic tasks in the lower-limb using robotic systems, the role of cognitive models on skill learning with these systems is less known. In this study, we investigate the role of cognitive models in the acquisition of a novel skill in the lower-limb using the NOTTABIKE Robot. The learning environment, which we have termed Half-Reversed Cycling (HRC), reverses the relationship between direction of push and direction of acceleration for one leg using an admittance based haptic control law. This reversal has tremendous consequences for the timing and direction of force application required to successfully cycle forward. 20 healthy subjects were split into two groups, one received instructions on how to accomplish the task, and the other did not. Subject trained in the Half-Reversed Cycling environment for 5, 30-minute sessions over a 2-week period, during which time they learned coordination strategies to move the crank forward with a constant forward velocity of 20RPM. In a 6^{th} session the reversed side was switched from the right side to left side, and so subjects were challenged to transfer what they had learned to the other side. This experimental design compares learning performance in a Reinforcement Learning (RL) environment, where the only available feedback is a scalar value of instantaneous performance, and a Reinforcement learning plus Cognitive Model (RL+CM) learning environment, where

subjects are provided with reinforcement feedback and a cognitive model of how to accomplish the motor task. The results of this work have implications for the design and structuring of rehabilitation exercises in stroke affected populations.

3.2 Introduction

Rehabilitative robots have been useful tools for studying motor control in the upper-limb for several decades. Starting with the seminal work of Shadmehr and Mussa-Ivaldi in 1994 [1], the ability of simulated dynamic environments to elicit strong adaptive responses began to be appreciated. Investigation focused on goal-oriented and reaching type task in a 2D plane [2]–[6], as this was envisioned to be – and is – a primary use of the upper-limb. An interesting set of principles emerged from these investigations, concepts like error augmentation [7] and optimal control as a feasible framework for understanding motor control [8]–[10]. The behavior of adaptation is however relatively simple compared with the development of a new skill or control policy to suit a new environment [11]. In many cases it was found that adaptive responses could be predicted using linear models such as ARX models, simply based on the previous performance and the next perturbation [12]. A much smaller emphasis was placed on skilled movements, and whether a robot could be successfully used to teach such movements [13].

Running somewhat in parallel was an initiative to use robots in the rehabilitation of the lower-limb after stroke or other neurological damage. Here the emphasis was placed on cyclic movements, rather than goal directed behaviors. Investigators used robots a variety of cycles, lower-limb exoskeletons, and split belt treadmills [14]–[18]. From these investigations and others [19]–[21] an interesting picture emerged which focused on the lower-limb as being an extremity

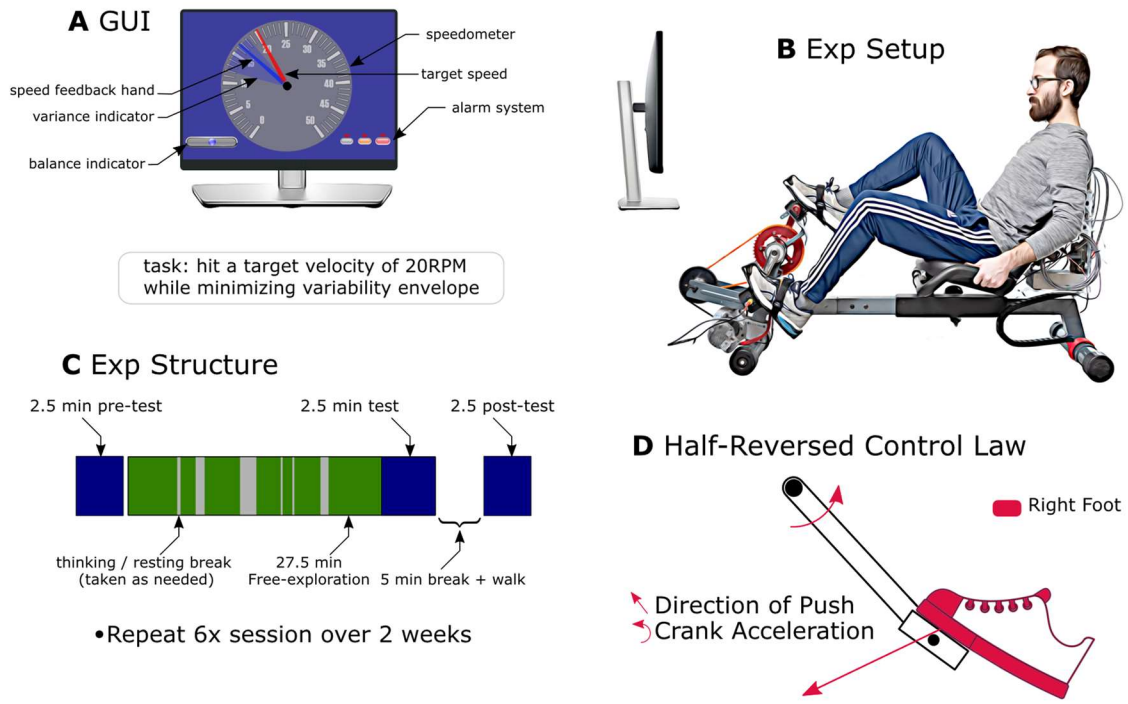

Fig 3.1. The Robot, Task, Experimental setup, GUI and haptic control law
(A) The graphical user interface displayed useful information to the participants while they were performing the study. The subject's goal was to pedal at a constant 20RPM while reducing their speed variance. Their speed was indicated by a blue clock hand, and speed variance was indicated by a translucent blue wedge. Subjects were also shown a balance indicator and alarm indicator. (B) The NOTTABIKE robot used to render the HRC environment. (C) Experimental structure. Each session began with a 2.5minute pretest to evaluate initial performance and retention. A 27min free-exploration period allowed subjects to investigate and learn coordination strategies. The session closed with a 2, 2.5min testing periods in which performance was to be evaluated, separated by a 5min break and walking period. Subjects came in for a total of 6 sessions. (D) Graphical representation of the HRC Control law. A force sensitive pedal measured magnitude and direction of pushing force and resulting torque about the crank. The direction of this torque was reversed in software and applied to an internal mass model, resulting in a crank acceleration. The result is a control law which is highly counter-intuitive and difficult to coordinate.

whose control was mediated primarily by subcortical structures. Concepts like central pattern generators [22], inter-limb coupling between ipsilateral sensorimotor state and contralateral flexion phase muscle coordination [21] painted a picture of a limb whose action was primarily automatic and cyclical. Adaptation was studied in the lower-limb in the context of walking using the split-belt treadmill [23] – investigating both basic science questions, and clinical questions of whether repeated exposure to the stimulus that elicit adaptation in stride length could have therapeutic effect when repeated [24]. Approaches such as assist-as-needed [25], where force was applied in order to guarantee kinematic objectives became the standard methodology.

Outside the field of rehabilitative robotics, motor skill development has been studied as a phenomenon which requires extended amounts of time and exposure to develop, and which can benefit from various types of coaching such as learning through demonstration, explicit instruction and implicit learning techniques [26], [27]. While the motor skill to be developed will eventually become implicit and automatic, explicit knowledge in the form of demonstrations, cognitive models, and analogies has been shown to improve the rate of novel skill acquisition for tasks in the upper-limb [28]. The pedagogical importance of scaffolding is appreciated, in which the learner is progressively challenged with more and more difficult tasks as they grow. Within the stroke literature, it's not yet agreed upon whether the ability to learn skilled movements implicitly is preserved after cortex damage. This elicits an interesting question: in those individuals who have sustained motor cortex damage but have their cognitive faculties preserved, might they benefit from the explicit instruction and cognitive models? As a prerequisite for answering this question, we have chosen to ask whether intact individuals can benefit from explicit models learning a novel skill in the lower-limb using a robotic platform.

A useful computational framework for understanding why cognitive models might be useful for the acquisition of new skills is reinforcement learning [29]. In the reinforcement learning framework, an agent interacts with an environment to optimize performance on an objective function. RL algorithms can provide high performance solutions to optimization problems, but in general efficient exploration of the solutions space is a difficult and unsolved problem [30]. For this reason, naive or unconstrained searches of the solution space tend to be long and time inefficient [31], [32]. The explicit knowledge generated by experts and codified in words and pictures might serve as an epi-function that limits the size of the search space which must be explored and suggests regions of the search space which are fruitful, leading to more efficient skill acquisition.

In this study, we use a lower-limb robot to train 2 groups of subjects on a novel skill called Half-Reversed Cycling. One group has access to cognitive models with potential utility in accomplishing the task, while the other is performing a pure reinforcement learning task. We expect that cognitive cues can be used to conceive of and formulate strategies of interaction, as well as limit the force, angle, and timing state-space over which the reinforcement learning process much search to optimize performance within the environment.

3.3 Methods

3.3.1 The Robot, Learning Environment, and Penalty Function.

In this section we describe the robot and its capabilities as a motor learning platform. We then detail the HRC haptic learning environment, the task objective given to subjects and the construction of a penalty function in the haptic environment designed to safeguard against pathological solutions.

The experiment was conducted on the NOTTABIKE robotic system. NOTTABIKE is a 1 Degree-of-Freedom robot capable of rendering impedance and admittance based haptic environments and used for interacting with the lower-limbs in a recumbent posture (Fig 3.1B). It is a fully integrated experimental robotic motor learning platform capable of rendering haptic environments, capturing kinematic and kinetic data, displaying real time visual performance feedback to the user, and prescribing precise experimental protocols via a scripting interface (Fig 3.1 AB).

Subjects interacted with the Half-Reversed Cycling environment. This unique environment is achieved using an admittance-based haptic approach. Force direction and magnitude and pedal configuration are recorded from the instrumented pedals of the NOTTABIKE robotic platform. A virtual Inertia and damping are rendered in software that define the relationship between applied torque, angular velocity, and angular acceleration. On the side that has been reversed, applying positive torque results in negative acceleration. On the other side, force from that pedal creates crank acceleration in the normal / anticipated way. The reversal i.e. the relationship between applied torque and crank acceleration, constitutes a novel environment that subjects must explore and determine how to control. It should be noted here that the crank is not split – but that the net crank acceleration is determined from the sum of the left and right pedal torques via the equation $\tau_{net} = F_L \; x \; r + (-)F_R \; x \; r$. *The negative sign on the right foot* constitutes the reversal of the "half reversed" environment.

A penalty function was created to ensure that subjects used both their right and left legs to accomplish the task. Without application of the penalty function, many of the subjects quickly discover the pathological solution of only using the non-reversed leg and abandon coordination of the leg they don't understand how to coordinate. The penalty function prevents this behavior from

happening. The penalty function measures the amount of angular impulse (torque * time) delivered by the right and left legs over the previous 10 seconds and forms a vector in an impulse plane. Only torques which moved the crank forwards were considered (quadrant 1) and the penalty function was only levied at forward velocities greater than 10RPM so as not to impede exploratory activity. If the impulse of one of the legs exceeded the impulse of the other leg by a ratio of 2:1 a penalty was levied against the offending leg and on the system as a whole by increasing the system damping coefficient.

The penalty itself was implemented by a first order system model (RC circuit) with different activation and deactivation time constants of $\tau_a = 5$ seconds and $\tau_d = 3$ seconds, respectively. The value of the penalty function varied from .2 (fully on) to 1 (fully off) and was used as a multiplier for effective moment arm, making pedaling on the penalized side up to 5 times as difficult as in the unpenalized state. System damping was also increased by this same penalty value. When the 10 second impulse measure was in an unbalanced state, subjects would get a warning light on their graphical user interface, the penalty function would start charging at the τ_a time constant. If the subject didn't correct their impulse balance, the penalty value would cross a threshold and activate the alarm, which would flash white and red at .5Hz and buzz annoyingly, while the force penalty was rendered. A blue bubble level widget encodes the instantaneous penalty value on the subject GUI.

A second alarm indicates to the user when they have exceeded the safe torque threshold of 40Nm. When the torque threshold is exceeded, the haptic environment is no longer being faithfully rendered, and is in effect torque-saturated. This alarm was included to prevent subjects from trying to "push through" the rendering, and serves as an indicator to the subject that there is a problem with his or her control strategy, and the robot is acting properly.

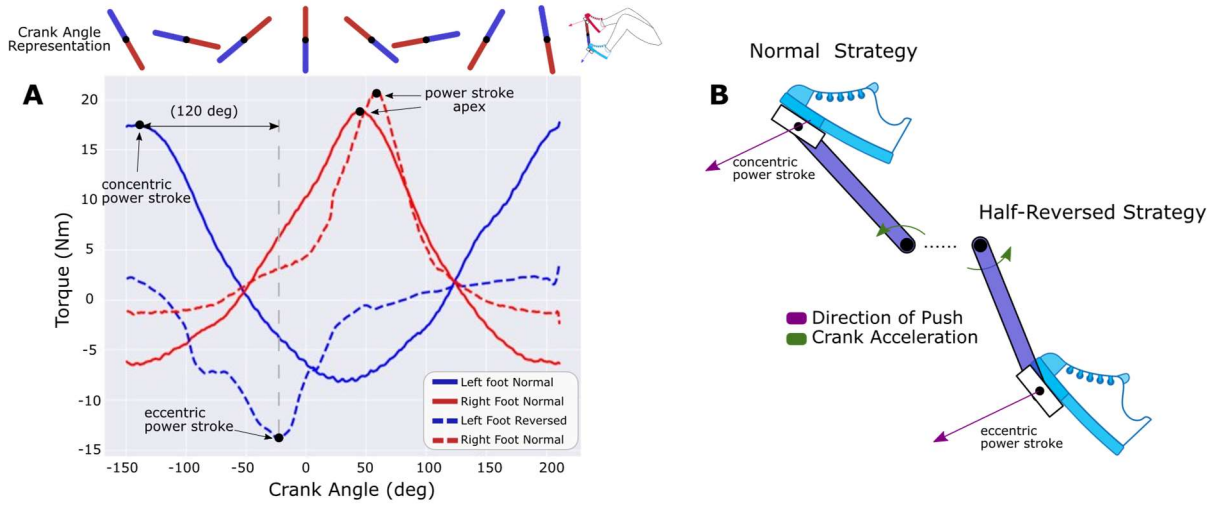

Fig 3.2. HRC Torque profile and coordination strategy

(A) Torque profile during normal cycling compared to HR Cycling. Solid lines represent the torque generated by the left and right feet during normal cycling. The crank angle representation on top provides a useful reference for interpretation. Peak torque is exerted by each foot when it is 45 degrees forward of vertical to create a strong concentric power stroke. These 2 power stroke phases are offset by 180 degrees. Compare this to the torque curves for HRC task. The apex of the power stroke on the (in this case, left) reversed leg has shifted 120 degrees from its normal location. Notice also that the direction of the measured torque is negative in the power stroke (due to the nature of the control law), and that it represents eccentric muscle activity. (B) Shows a schematic representation of the difference between the normal cycling strategy and the half reversed cycling strategy. In the normal case, the subject pushes forward at approximately +45 degrees from vertical and creates a large positive torque. This strategy will not work for the reversed control law however, and the subject must learn when, where, what direction, and how hard to push in order to successfully power the robot forwards.

3.3.2 Experimental protocol

In this section we detail the recruitment of subjects, the structure of the study groups, instruction sets, task objective and the experimental setup and protocol.

20 healthy subjects (ages 23-26, 10 females and 10 males) participated in this study. Subjects were randomly assigned to one of two study groups. Subjects gave written informed consent before participating, and the proposed protocol falls under the current University of Wisconsin-Madison Health Sciences IRB. These tests establish the suitability of NOTTABIKE for the study of motor control and rehabilitation.

The study participants were broken up into 2 experimental groups. The first group, termed the Reinforcement Learning (RL) group received only instructions of the task objective and safety information, while the second group, the Reinforcement Learning + Cognitive Models (RL+CM) group additionally received an instruction set containing cognitive models that were useful to achieving the task objective.

The reinforcement learning group was provided with the instruction set shown in appendix A. This instruction set contained a definition of the structure of the experiment, including the number of experimental sessions and the length of each session and the activity blocks within each session. Most importantly, it contains a description of the task objective: to achieve a target velocity of 20RPM over the crank cycle, while reducing the variance of the crank velocity. The instruction set further pictured the feedback subjects would receive (Fig 3.1B) a speedometer widget where a blue needle indicates their instantaneous velocity, and a translucent blue wedge represents the variance of their velocity over the past 5 seconds. It additionally provides the subject with an explanation of the safety features of the robot including a set of hand switches which cut

the power to the robot, and a quiz was included at the end of the instruction set that the subjects were required to complete at the beginning of each contact session.

The Reinforcement Learning + Cognitive Model group received the instruction set in appendix A, but additionally received the instruction set in appendix B. This instruction set included 12 strategies designed by an expert that were intended to give the subjects an explicit cognitive model of subskills required for the performance of HRC. The strategies avoided using advanced technical language and reference to physics or haptics, but instead focused on being understandable and practical. The strategies for skills were presented in order of increasing difficulty as determined by the expert performer and were labeled as such for the subject with the labels [beginner, intermediate, advanced].

Each subject in the study participated in 6 trainings of approximately 45 minutes including preparation time and rest time. The 6^{th} session differed from the previous only in that the rendering of the right and left foot flipped, so that transfer learning could be observed. On the 6th session, subjects in both groups were given an additional instruction set that said " the roles of the right and left foot have been reversed".

The subject would begin each session by reviewing the instruction set associated with their study group. They would then answer the quiz on the study sheet and hand their answers to the experimenter. The subject was fitted to the cycle, including strap-in foot connections which included a heel cup so that the subject could push or pull on the pedals. The experiment has a blocked architecture, shown in figure 3.1C. There are two types of blocks, testing blocks and free-exploration blocks. During the testing blocks, subjects exploit their current knowledge of the system to perform the best they can at the task objective, while during the free exploration blocks, they are free to explore different motor control strategies to gain skills that may lead to improved

performance. Subjects were encouraged to consult their instruction sheet and take frequent breaks during the free-exploration block, but during the testing block, they were instructed to keep the robot powered and perform at their best for the duration of the test. An experimental session consists of a 2.5 minute pre-testing block, a 27.5 minute free-exploration block, a 2.5 minute session testing block, a 5 minute rest block in which subjects were required to get up from the robot and walk around, and finally a 2.5 minute post-testing block.

On the first day of the experiment for each subject additional tests were conducted that were useful for future analysis. Each subject was fitted to the robot by the experimenter to be in such as position that the subject was comfortable, and still had bend left in their knee (approximately 160 degrees, where 180 is full knee extension) when at the point of maximal extension within the pedaling cycle and with the ankle in a natural position. Their seating distance from the crank axis was recorded and was used every session for the duration of the experiment.

Next the subjects performed a test on the robot to measure the passive weight of their legs. The robot actively drives the subjects' legs at 10RPM, while the subject was told to remain relaxed and allow the robot to drive them without exerting additional muscular effort. Finally, the subject performed a forward pedaling task while the robot rendered a "normal bike" which was based on an admittance-based rendering of a simulated mass-damper system with no half-reversal. Subjects were told the objective of this task was to attain 20RPM, the same target as the HRC task. All other parameters of the system were kept constant for this task.

3.3.3 Data Analysis

The data analysis will proceed in 3 stages, corresponding with figures 3.3, 3.4, and 3.5. In the first stage, features will be extracted from raw data where each feature represents a possible

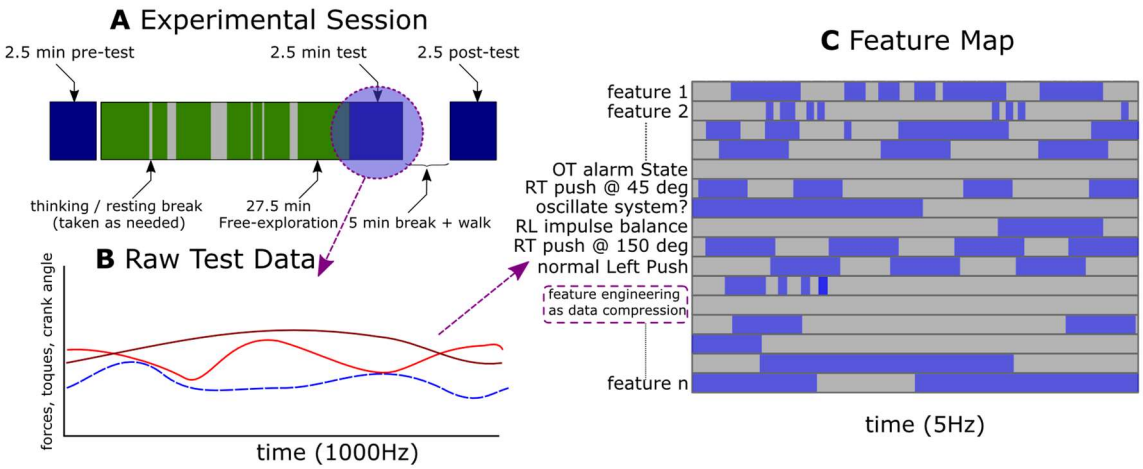

Fig 3.3. Analysis pipeline to form predictive features for subject performance
(A) From the experimental session data, we consider only the data from the testing sessions, where the subject was told explicitly that they were being evaluated for their ability to perform the task. The free exploration periods are discarded, as subjects were encouraged to explore, rest and otherwise perform sub optimally on the task during these periods. (B) Raw data from forces, torques, and crank angles, and internal system states are extracted from the test sets. (C) Engineered features are created from the raw data which compress raw data and extract (potentially) useful features which may be used to differentiate high from lower performers. These could represent performance on sub-skills which are necessary to learn before the overall skill of HRC can it learned. For each subject, a feature map is created and forms a unique signature of their performance.

subskill to be learned, culminating in the creation of a feature map. In phase 2 of the analysis pipeline, an unsupervised clustering algorithm will be used to segment performance classes from crank velocity vs angle plots, which is directly related to the task objective function. This analysis will allow us to classify individual performances as belonging to higher or lower performance strata. In the 3rd phase, the previous 2 analyses are combined with a decision tree classification algorithm to determine which features are most useful in separating, say high performers from low performers. These features may then be interpreted as necessary skills to elevate performance.

3.3.4 Engineered features

The engineered features which serve as candidate subskills were heuristically generated from observation of subjects interacting with the half-reversed pedaling environment, and from the opinions and interview with people skilled in performing the task. Below we describe the heuristics generated from these intuitions and interactions, and the process of translating from intuition to mathematical definition of a feature. A useful distinction is between a feature which is defined instantaneously, and one which is an aggregate feature over a time period, such as the entire testing period. Instantaneous features are computed at the sampling frequency of the data. For instance, if someone is currently oscillating, or the integral of the impulse of the push at a particular angle, is defined sample-by-sample. By comparison, an aggregate feature is formed as an aggregate of a set of instantaneous features. For example, average speed over the testing interval would be an aggregate feature and therefore constitutes a form of data compression.

Feature 1: can subjects oscillate the system about the stable point?

In the HRC environment, there is a stable system configuration position located at -45 degrees, with 0 degrees being to dead center for the right pedal. The position is difficult to get out of, because on the left leg forward propulsion can only be attained by the weak hip flexors, and on the right leg subjects have the tendency to try and pull, but this in fact causes movement in the wrong direction. For these reasons, novice subjects frequently get stuck here and spend considerable time trying to oscillate back and forth out of this stable location. A first indication that the subject is becoming proficient therefore is that they have enough understanding of the system that they can oscillate it back and forth with higher and higher amplitude.

We begin with a written description for how to mathematically define this feature. First, we want this feature to be active only when the subject is currently oscillating. Remember that we have access to the history and future performance of the subject. If the subject is oscillating, they are in effect located at a point on a sine curve of crank angle. Define a window around the current time over which to look. If a sine wave is a reasonable fit to the crank angle curve within that window, and if the point of oscillation (here, the offset of the sine wave) is approximately 135 degrees, the subject can be said to be oscillating at that time and the feature should be turned on, and should take on the value of the magnitude of the oscillation. This instantaneously defined feature could then be aggregated to form a feature such as "what fraction of the testing period was the subject oscillating over?"

Feature 2: Pedal the left side as you would a normal bike

How does the subject interact with the left pedal, at the position where they ought to be applying impulse to the mass-damper system (-145 degrees, see Fig 3.2 for reference) Recall that the left pedal is not reversed, and so the subject must interact in the same manner as a normal bike.

To define this feature mathematically, we will compare subject performance on HRC to their performance on the normal pedaling task. Using cross-correlation – how similar is the torque vs. angle curve from the HRC task to that of the normal comparison? This will define a continuous feature on 0-1.

Feature 3: when you get stuck, do you release the safety switches and reposition yourself?

This feature is defined only intermittently, and ideally is only defined during the free exploration sessions as subjects were instructed to avoid releasing safety switches during testing periods. It's easy to algorithmically test for the presence of this feature - if someone releases the safety switch and then moves the crank to the desirable position, then the feature is defined, and the behavior was performed.

Feature 4: resist the urge to push regularly with the right foot

Subjects will experience a strong desire to push with the right foot between 0 and 45 degrees. Learning to inhibit this behavior is a necessary prerequisite for performing the HRC task.

Mathematically, this feature may be phrased as follows: how frequently does the subject push in excess of their leg weight between 0 degrees and 45 degrees of crank angle? We have data on leg weight from the day 1 trials, so this is easy to compute via subtraction off the average torque in this range and then computing the angular impulse.

Feature 5: learn how to use the right foot to power the crank.

Subjects must learn how to coordinate the right foot in an eccentric power stroke if they want to pedal forward consistently without setting off the impulse balance alarm. The insight to power the bike in this way will emerge from a rare event, and then control will develop. Mathematically this may be defined from the shape of the torque angle curve between certain angles. Two different features may be defined here, such as the shape of the curve, the total impulse

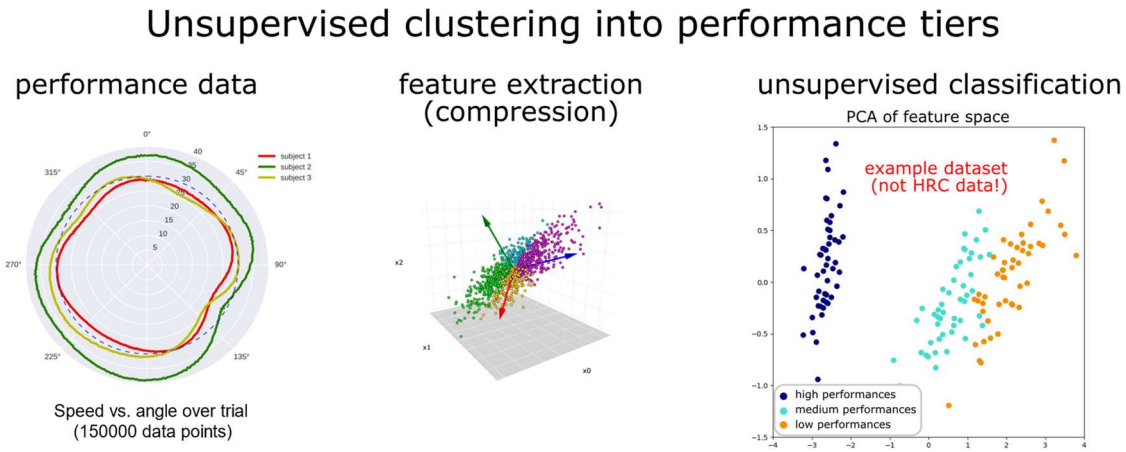

Fig 3.4. Unsupervised clustering into performance tiers.
In this activity, performance was defined by a crank velocity criterion – maintain crank velocity as close to 20RPM as possible, while also keeping crank velocity variance low. In this way the task may be viewed as an optimization problem: find the coordination strategy over time which minimizes crank speed deviation from 20RPM. Subject performance data was measured for analysis. From the measured data, we create a lower dimensional representation (compression) such as a spline fit to the crank angle vs. velocity plot. We then use PCA to further compress the data and a unsupervised clustering algorithm such as K-mean, mean-shift, or spectral clustering to determine how many performance clusters are natively in the data

delivered during a time or work performed over a specified angle, or average of these values over the test interval, normalized by the number of cycles.

Feature 6: avoid triggering the alarm using a balanced approach:

Remember that the impulse balance alarm is triggered when a subject generates impulse from one foot more than the other over by a 2:1 interval over a 10 second interval. This metric is recorded as calculated data and may be used directly as a feature to indicate proficiency with using a balanced approach.

Feature 7: to reduce speed variability, push less hard, for longer:

This feature evaluates the smoothness of the subjects' torque curve during the propulsive phases of their left and right legs. This might be defined as an aspect ratio, such as the peak torque amplitude compared to the width of the torque curve within a feasible window, or it could be computed as a moment of inertia of this curve.

Feature 8: for more control, power with the right leg then the left

This feature relates to a concept called individuation. Finer motor control is achievable by maximally separating the pushing phase of the left and right legs from one another. Calculating this metric would only be valid of there is a right and left pushing phase and may be defined as the difference between the location of the left push peak and the right push peak in terms of angle.

Feature 9: support the weight of the right leg to prevent a slowdown – 2 phase power

For maximum smoothness of performance, the subject must figure out how to use a 2 phase power stroke. This coordination strategy is very costly in terms of effort, because the subject must use their hip flexors to support the weight of their right leg at +45 degrees to prevent crank slowdown from the torque generated by said leg weight. We can test algorithmically for the presence of this coordination strategy by looking at the curve of torque vs. angle for the leg weight

measurement vs. the same curve in HRC. If there is less work delivered during this angular interval than in the passive weight measurement task, the subject is using the leg weight cancellation strategy to smooth their performance.

Feature 10: pull with the left leg.

Similar to the feature above, where smoother velocity performance could be achieved by powering the cycle not once per cycle, but twice, this last feature is an aspect of 2 phase power, but for the left leg. For the left leg to contribute to 2 phase power, it's useful to use it to pull and add torque at an angle 180 degrees offset from its push location. We can test if a subject uses this coordination strategy by comparing again to the leg weight torque curve. If there is torque in excess of leg weight over the test, the subject is pulling as part of their coordination strategy.

3.3.5 Unsupervised learning of performance clusters

In the 2nd part of the analysis pipeline, we will attempt to cluster subject performances into meaningful groups using unsupervised learning techniques. Clustering is important here, as we are trying to distinguish high performances from medium, medium from low, and so on. *A priori,* we don't have any information on how the performance data might cluster, besides physical intuition from watching subjects perform. Here I'll describe this physical intuition in a succinct way.

Subjects begin in an oscillatory phase, in which they cannot cycle the crank. They gradually learn how to oscillate the crank more and more. They might go through a phase of powering only with the left foot, which could be its own performance cluster. Next, they have a moment of insight that they can get power from the right reversed side. They tend at this point to go too fast rather than not being able to cycle at all. Finally, there is a phase of dialing in the timing and magnitude

of the motor control and moving from one phase power stroke to a 2 phase power stroke, which allows subjects to get close to 20RPM all the time.

This analysis is an attempt to formulate the number of total performance groups, and also the means of distinguishing higher levels of performance from lower levels. Recall that the objective of the task was specified to the subjects in a way that made quantification of performance easy. Objective functions by definition provide means of mapping from high dimensional space to lower dimension space $\mathbb{R}^n \rightarrow \mathbb{R}^1$. The objective function this experiment was to "hit a target velocity of 20RPM throughout the crank cycle while minimizing variance". Mathematically, this can be defined as the sum of the square of the difference between the subjects' current velocity and the target velocity. While this definition might be sufficient for scoring subject performance, it might not be enough to properly segment classes of performance, should such classes exist, and it certainly won't give insight into the nature of the kinematic improvements learned by subjects. So, while we will look at the low dimensional projection provided by the objective function, we will start with a slightly different technique.

Let's first look at the total dimensionality of an uncompressed testing trial. Let's assume that we down sample from 1000Hz to 100Hz, because we guess that nothing much interesting is happening faster than 100Hz. We have 120 seconds x 100Hz = 12000 dimensional space. We want to reduce this to a much more manageable number of dimensions before we attempt to form performance clusters. Here I see 2 ways of proceeding, from which we will pick one. First, we take the 2 min performance, which is itself a cyclic activity, and we remove the time dimension, instead only looking at the crank velocity vs. crank angle dimensions as a sort of scatter plot.

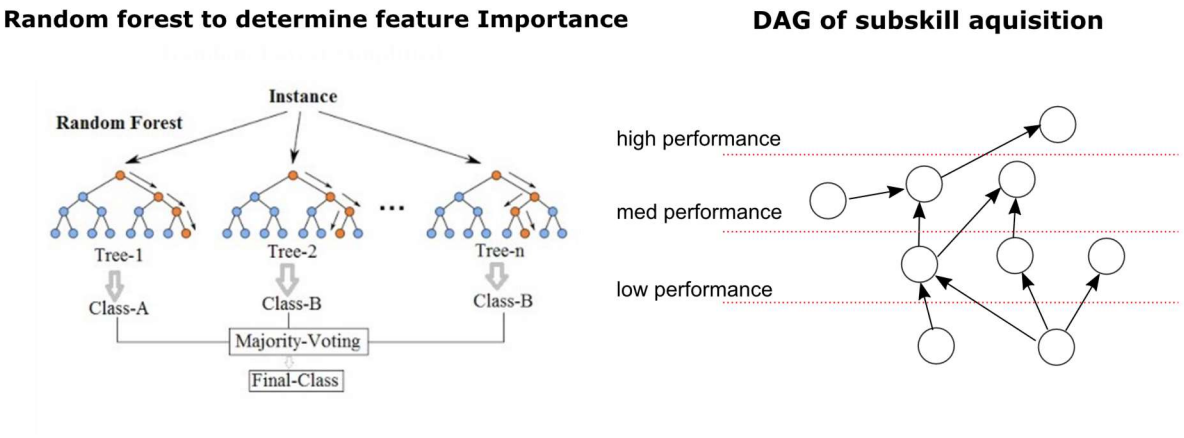

Fig 3.5. Determination of subskill order of acquisition and DAG formation

The fundamental question we would like to answer is this: what subskills, defined as the candidate features from the feature map, best predict the difference between performance levels we determined through clustering? We use a random forest classification technique because we can get classification accuracy from this, but more importantly, through the criteria information gain, we can determine which features were most helpful in determining the difference between performances of a particular class. A way of interpreting this is to ask “what features need to change for a subject performing at a low level to improve their performance to a high level?”

Now, using a least squares approach, we fit a 12 parameter spline to the crank velocity vs. crank position plot. This spline forms a low dimensional signature that could be useful in the clustering of performance. A second approach is less manual. We perform principal component analysis on all of our data instances simultaneously. We can think of each instance as a point in 12000 dimensional space, and each instance is a recorded test, so we have 10 subjects x 6 sessions x 3 tests / session or 180 instances per test group. We perform PCA on all these instances at once, and we are left with a reference frame which encodes the greatest amount of variance in the dataset. The positive aspect of the second approach is that it is highly automated. The difficult aspect is that the interpretability of the results might be lower than in the first approach.

Finally, once we have our lower dimensional representation, we can apply clustering algorithms to distinguish groups of performers. Because we are restricted by the fact that we don't have a number of ground truth classes, we are limited to approaches that either don't require this as a seed argument, or which can be run with multiple guesses for total number of classes and we can determine, using a function such as information loss, what number of classes best fits the data. K-means clustering and mean-shift clustering seems like good candidates for clustering at this time.

3.3.6 Random forest classification to determine feature importance

In the 3rd phase, the previous 2 analyses are combined with a random forest classification algorithm to determine which features are most useful in separating, say high performers from low performers. These features may then be interpreted as necessary skills to elevate performance.

From analysis 1, we have a set of features which are based on the kinetic performance of the subjects from a set of heuristically determined features. In phase 2, we attempted to learn the

performance features through dimensionality reduction techniques and unsupervised clustering. In this final phase of the analysis, we will train a classification algorithm called a random forest to separate members of high performing classes from members of lower performing classes using the hand tuned features from analysis 1 as predictors. We will use 10 fold cross validation to establish a prediction rate to establish model accuracy. Most importantly, we will use the features of highest importance within the decision trees of the random forest to establish which features are most useful in separating adjacent groups of performance. For instance, if we would like to separate low from medium performers, which data features are most predictive of that? This analysis will culminate in a tree like structure which shows which skills (kinetic / timing) were required to improve kinematic performance.

3.4 Results (projected)

It is projected that the subjects that had access to the structured cognitive model of the environment were able to integrate that model into their control strategy and gain proficiency with the novel skill more quickly. In particular, it's projected that they will be able to use this knowledge to bypass the early stage of getting stuck in the -45 degree stable location, will be able to quickly learn how to get out of that, and will learn how to deliver the eccentric power stroke to the right pedal at the appropriate time. It is projected that a greater fraction of the cognitive model group will have at least one of the 2 phase power coordination strategies that constitute advanced performance on the task. We project that while the learning rate will be longer for the reinforcement learning group, that the retention of the skill will not vary across groups. We project that transfer learning will be the same for the two groups, and that it will be dramatically faster to transfer learning than it was to learn in the first place for both groups.

3.5 Discussion

In the data analysis section, the acquisition of proficiency in the new skill of half-reversed cycling was broken down into a series of heuristically determined features that have dependencies upon one another, each building upon the former in a progressive fashion. It will be interesting to see if the subskills emerge in this order in all subjects, and at what rate they emerge. We suspect that the greatest variance will be in the amount of time required to figure out how to get unstuck form the stable position. When subjects are stuck in this position, the amount of information they can gain from the interaction with the environment is limited, because their muscles are so awkwardly positioned. They are at this point also limited by the models they possess of how one "should" interact with a "bike". It may be that unlearning and moving past this assumption is as big an obstacle to acquisition of the skill as acquiring aspects of the skill itself, when measured in terms of time.

It will be informative to see how many subjects in the RL group develop the useful strategy of de-energizing the robot, moving to a new position in the crank cycle, and exploring behavior in that new position. Subjects who do not do this will likely be very frustrated, while those that do, stand to more effectively use their free-exploration time to learn control over the right foot. Additionally, we will need to think carefully about the psychological factors involved in learning the skill. For instance, where the experimenter is positioned relative to the subject is important to their motivation in the activity. If the subject feels that their performance is being constantly judged, they may be hesitant to explore new strategies. One way to mitigate this is to explain to the subject that there is a free-exploration mode at the beginning of the trial that is not scored, and then at the end of the trial, there is a period that is scored. In reality, all of the information collected can in fact be used to evaluate subject performance, but it's important to acknowledge that subjects

might be hesitant to try out new strategies under time constraints, or when they feel that their performance always has to be good. This is the essence of the reinforcement learning problem, and the situation must be such that subjects are encouraged to explore as well as exploit.

3.6 Conclusion (projected)

In this chapter, we have described a study to investigate the importance of cognitive models in the acquisition of a novel skill on a lower-limb robotic training platform NOTTABIKE. It's projected that the subjects that had access to cognitive models of the environment were able to integrate the models into their control strategy and gain proficiency with the novel HRC skill more quickly. This work is important as it has implications for how a rehabilitation protocol ought to be thought about and structured. As rehabilitation engineers, we would like the therapeutic interventions we design have high efficiency – meaning the ratio of patient time and effort to marginal improvement. Ensuring that the subject has a cognitive model of what they are trying to do could be as important to their skill development as the quality of the and nature of the rendered environment.

3.7 References

[1] R. Shadmehr and F. A. Mussa-Ivaldi, "Adaptive representation of dynamics during learning of a motor task," *J. Neurosci.*, vol. 14, no. 5, pp. 3208–3224, May 1994, doi: 10.1523/JNEUROSCI.14-05-03208.1994.

[2] C. D. Takahashi, R. A. Scheidt, and D. J. Reinkensmeyer, "Impedance Control and Internal Model Formation When Reaching in a Randomly Varying Dynamical Environment," *J. Neurophysiol.*, vol. 86, no. 2, pp. 1047–1051, Aug. 2001, doi: 10.1152/jn.2001.86.2.1047.

[3] N. Bhushan and R. Shadmehr, "Computational nature of human adaptive control during learning of reaching movements in force fields," *Biol. Cybern.*, vol. 81, no. 1, pp. 39–60, Jul. 1999, doi: 10.1007/s004220050543.

[4] M. I. Mohamed Refai *et al.*, “Smoothness metrics for reaching performance after stroke. Part 1: which one to choose?,” *J. NeuroEngineering Rehabil.*, vol. 18, no. 1, p. 154, Oct. 2021, doi: 10.1186/s12984-021-00949-6.

[5] J. L. Patton, M. E. Stoykov, M. Kovic, and F. A. Mussa-Ivaldi, “Evaluation of robotic training forces that either enhance or reduce error in chronic hemiparetic stroke survivors,” *Exp. Brain Res.*, vol. 168, no. 3, pp. 368–383, 2006.

[6] E. B. Brokaw, D. Nichols, R. J. Holley, and P. S. Lum, “Robotic Therapy Provides a Stimulus for Upper Limb Motor Recovery After Stroke That Is Complementary to and Distinct From Conventional Therapy,” *Neurorehabil. Neural Repair*, vol. 28, no. 4, pp. 367–376, May 2014, doi: 10.1177/1545968313510974.

[7] F. Abdollahi *et al.*, “Arm control recovery enhanced by error augmentation,” in *2011 IEEE International Conference on Rehabilitation Robotics*, Jun. 2011, pp. 1–6. doi: 10.1109/ICORR.2011.5975504.

[8] E. Todorov and M. I. Jordan, “Optimal feedback control as a theory of motor coordination,” *Nat. Neurosci.*, vol. 5, no. 11, pp. 1226–1235, Nov. 2002, doi: 10.1038/nn963.

[9] E. Todorov, “Optimality principles in sensorimotor control,” *Nat. Neurosci.*, vol. 7, no. 9, pp. 907–915, Sep. 2004, doi: 10.1038/nn1309.

[10] T. Flash and N. Hogan, “The coordination of arm movements: an experimentally confirmed mathematical model,” *J. Neurosci.*, vol. 5, no. 7, pp. 1688–1703, Jul. 1985, doi: 10.1523/JNEUROSCI.05-07-01688.1985.

[11] D. M. Wolpert, J. Diedrichsen, and J. R. Flanagan, “Principles of sensorimotor learning,” *Nat. Rev. Neurosci.*, vol. 12, no. 12, pp. 739–751, Dec. 2011, doi: 10.1038/nrn3112.

[12] R. A. Scheidt, J. B. Dingwell, and F. A. Mussa-Ivaldi, “Learning to Move Amid Uncertainty,” *J. Neurophysiol.*, vol. 86, no. 2, pp. 971–985, Aug. 2001, doi: 10.1152/jn.2001.86.2.971.

[13] D. J. Reinkensmeyer and J. L. Patton, “Can Robots Help the Learning of Skilled Actions?,” *Exerc. Sport Sci. Rev.*, vol. 37, no. 1, p. 43, Jan. 2009, doi: 10.1097/JES.0b013e3181912108.

[14] H. F. Machiel Van der Loos, S. A. Kautz, D. F. Schwandt, J. Anderson, G. Chen, and D. M. Bevly, “A split-crank, servomotor-controlled bicycle ergometer design for studies in human biomechanics,” 2002, vol. 2, pp. 1409–1414. doi: 10.1109/IRDS.2002.1043952.

[15] D. A. Brown and S. A. Kautz, “Speed-Dependent Reductions of Force Output in People With Poststroke Hemiparesis,” *Phys. Ther.*, vol. 79, no. 10, pp. 919–930, Oct. 1999, doi: 10.1093/ptj/79.10.919.

[16] D. A. Brown and S. Kautz, "Increased workload enhances force output during pedaling exercise in persons with poststroke hemiplegia," *Stroke*, vol. 29, no. 3, pp. 598–606, 1998.

[17] D. A. Brown, S. Nagpal, and S. Chi, "Limb-Loaded Cycling Program for Locomotor Intervention Following Stroke," *Phys. Ther.*, vol. 85, no. 2, pp. 159–168, Feb. 2005, doi: 10.1093/ptj/85.2.159.

[18] M. Alcobendas-Maestro, "Lokomat Robotic-Assisted Versus Overground Training Within 3 to 6 Months of Incomplete Spinal Cord Lesion Randomized Controlled Trial," *Neurorehabil Neural Repair*, vol. 26, no. 9, pp. 1058–1063, Nov. 2012.

[19] L. H. Ting, S. A. Kautz, D. A. Brown, and F. E. Zajac, "Phase Reversal of Biomechanical Functions and Muscle Activity in Backward Pedaling," *J. Neurophysiol.*, vol. 81, no. 2, pp. 544–551, Feb. 1999, doi: 10.1152/jn.1999.81.2.544.

[20] L. H. Ting, C. C. Raasch, D. A. Brown, S. A. Kautz, and F. E. Zajac, "Sensorimotor state of the contralateral leg affects ipsilateral muscle coordination of pedaling," *J. Neurophysiol.*, vol. 80, no. 3, pp. 1341–1351, 1998.

[21] L. H. Ting, S. A. Kautz, D. A. Brown, and F. E. Zajac, "Contralateral movement and extensor force generation alter flexion phase muscle coordination in pedaling," *J. Neurophysiol.*, vol. 83, no. 6, pp. 3351–3365, 2000.

[22] M. R. Dimitrijevic, Y. Gerasimenko, and M. M. Pinter, "Evidence for a Spinal Central Pattern Generator in Humans," *Ann. N. Y. Acad. Sci.*, vol. 860, no. 1, pp. 360–376, 1998.

[23] L. A. M. and A. J. Bastian, "Spatial and Temporal Asymmetries in Gait Predict Split-Belt Adaptation Behavior in Stroke," *Neurorehabil Neural Repair*, vol. 28, no. 3, pp. 230–240, Mar. 2014.

[24] D. S. Reisman, H. McLean, J. Keller, K. A. Danks, and and A. J. Bastian, "Repeated Split-Belt Treadmill Training Improves Poststroke Step Length Asymmetry," *Neurorehabil Neural Repair*, vol. 27, no. 5, pp. 460–468, Jun. 2013.

[25] S. Srivastava, "Assist-as-Needed Robot-Aided Gait Training Improves Walking Function in Individuals Following Stroke," *IEEE Trans Neural Syst Rehabil Eng Publ IEEE Eng Med Biol Soc*, vol. 23, no. 6, pp. 956–963, Nov. 2015.

[26] T. S. Horn, "Coaching effectiveness in the sport domain," in *Advances in sport psychology, 3rd ed*, Champaign, IL, US: Human Kinetics, 2008, pp. 239-267,455-459.

[27] J. M. Poolton and T. L. Zachry, "So You Want to Learn Implicitly? Coaching and Learning through Implicit Motor Learning Techniques," *Int. J. Sports Sci. Coach.*, vol. 2, no. 1, pp. 67–78, Mar. 2007, doi: 10.1260/174795407780367177.

[28] N. J. Hodges and I. M. Franks, “Modelling coaching practice: the role of instruction and demonstration,” *J. Sports Sci.*, vol. 20, no. 10, pp. 793–811, Jan. 2002, doi: 10.1080/026404102320675648.

[29] L. P. Kaelbling, M. L. Littman, and A. W. Moore, “Reinforcement learning: A survey,” *J. Artif. Intell. Res.*, vol. 4, pp. 237–285, 1996.

[30] P. Shyam, W. Jaśkowski, and F. Gomez, “Model-Based Active Exploration,” in *Proceedings of the 36th International Conference on Machine Learning*, May 2019, pp. 5779–5788. Accessed: Oct. 17, 2022. [Online]. Available: https://proceedings.mlr.press/v97/shyam19a.html

[31] S. B. Thrun, “Efficient exploration in reinforcement learning,” 1992.

[32] P. Abbeel and A. Y. Ng, “Exploration and apprenticeship learning in reinforcement learning,” in *Proceedings of the 22nd international conference on Machine learning*, New York, NY, USA, Aug. 2005, pp. 1–8. doi: 10.1145/1102351.1102352.

Chapter 4

Optimal Design of a 2DOF Parallel Rehabilitation Robot for the Lower-Limb based on Force-Space Matching

Alexander R. Dawson-Elli and Peter G. Adamczyk

(This Chapter is in preparation for Publication)

4.1 Abstract

To date, serial robots like exoskeletons have been the dominant architecture used to probe motor control and deliver robotic therapy for the lower-limb. Serial robots offer the advantage of having large workspaces and congruent mechanics with the leg. By comparison, the application of parallel robots to lower-limb rehabilitation has been less explored. Parallel robots have many characteristics that make them desirable for rendering high-performance haptic environments. Due to their multiple connections to ground, they are stiff and may be actuated entirely using grounded motors (no motors on distal joints) and for this reason are also low inertia. The motivation for this simulation study is to design a parallel robot that has a high degree of force-space congruence with a human model, while retaining the desirable properties of a parallel robot. We developed a planar model of the inverse, forward, and instantaneous kinematics for a generalized 5-bar linkage and connected it to a data driven sagittal plane human model. We used a novel approach called force-space congruence matching to assess the ability of a parallel robot design to meet the force-space requirements of the human model. We then used the DIRECT optimization algorithm to design robot parameters based on the force-space matching criteria. Here we present the results of this simulation, a full dynamic model of the robot, and the overall design for our 2DOF parallel robot which will be used for the study of lower-limb motor control and the application of therapeutic interventions.

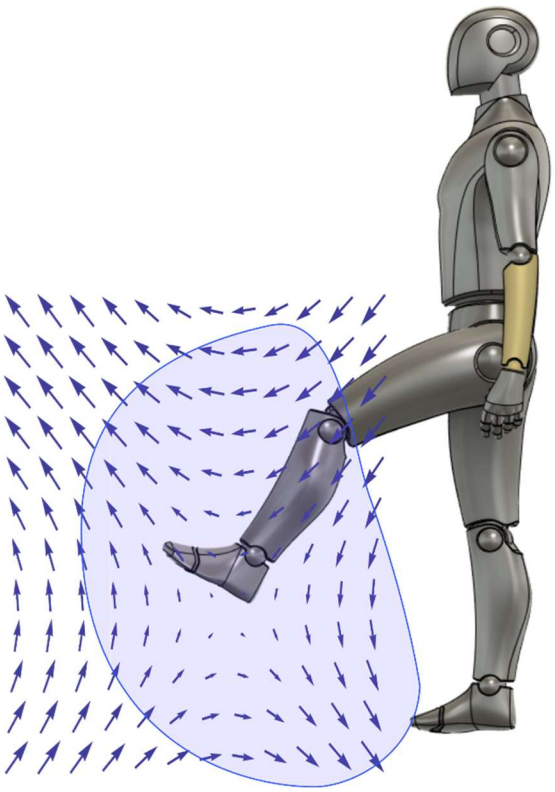

Fig 4.1. Rendering Objectives for the Design of a 2 DOF Lower-Limb Haptic Robot.
The Lower-Limb Haptic Robot must meet a series of design objectives. First, it must have a reachable workspace (blue shape) which is overlapping with that of the human leg, while still having a parallel architecture. Within the reachable workspace, the robot must be able to render a set of forces to match the requirements of the human subject. This compatibility is known as force-space congruence. These two objectives are most difficult in the sagittal plane, and so the design of the robot was undertaken using a sagittal plane simulation.

4.2 Introduction

The predominant robot architecture used to probe lower-limb motor control and deliver therapy are robotic exoskeletons such the Lokomat [1]. Serial robots like exoskeletons offer several advantages when interfacing with the lower-limb. They have large workspaces and congruent kinematics to the lower-limb. This is important due to the lower-limbs' ability to generate large forces. While robots meant for the upper limb often have total force capacities measured in tens of Newtons [2], robots meant for interaction with legs require significantly more force.

Optimization has been a useful tool in the design of the kinematics of robotic manipulators. Optimization in the space of kinematics can be non-convex, and so benefits from algorithms which are global in nature such as derivative free algorithms [3], genetic algorithms, and space division methods like the DIRECT algorithm [4], [5].

Measurements of the force polytope have been made in the upper-limb in 3 dimensions [6], and in the lower-limb in 2 dimensions at particular postures [7]. Force polytopes have also been a useful concept in understanding the effects of a robots' configuration on its output force, mapped through the Jacobian [8]

Here, we describe an approach which combines global optimization with the concept of the force-space polytope to design the kinematics of a parallel rehabilitation robot for the lower-limb.

4.3 Methods

4.3.1 Defining rendering objectives

The 2DOF lower limb haptic robot must meet a series of design objectives (Fig 4.1). First it must have a reachable workspace, defined in the sagittal plane, which is overlapping with a human. We defined this workspace by hand in the section on human model. Within the specified reachable workspace, it must be able to render a set of forces which match the requirements of the human. It's also preferable that the forces generated by the robot do not exceed the force requirements of the human in other directions. This is for two reasons. First, it opens up the possibility of rendering a force to the human which they cannot counter leading to potential injury. Second, mechanics which lead to excessive force production in a certain direction decrease force rendering resolution in that direction, as a smaller fraction of the feasible torque is usable. This problem stems from the digital nature of the torque command signal. For instance, if the torque controller is 8 bit (256 different torque levels) but the mechanics of the robot are such that 10% of the torque range maxes out the force requirement of the human, then there are only 25.6 different torque levels which are usable levels within that space, and therefore the force resolution is 10x decreased.

While the device is intended for usage in a variety of planes, its design in the sagittal plane is most critical. This is the case for a variety of reasons. First, the sagittal plane usage is arguable the most common and most important use case. Second, workspace required for natural

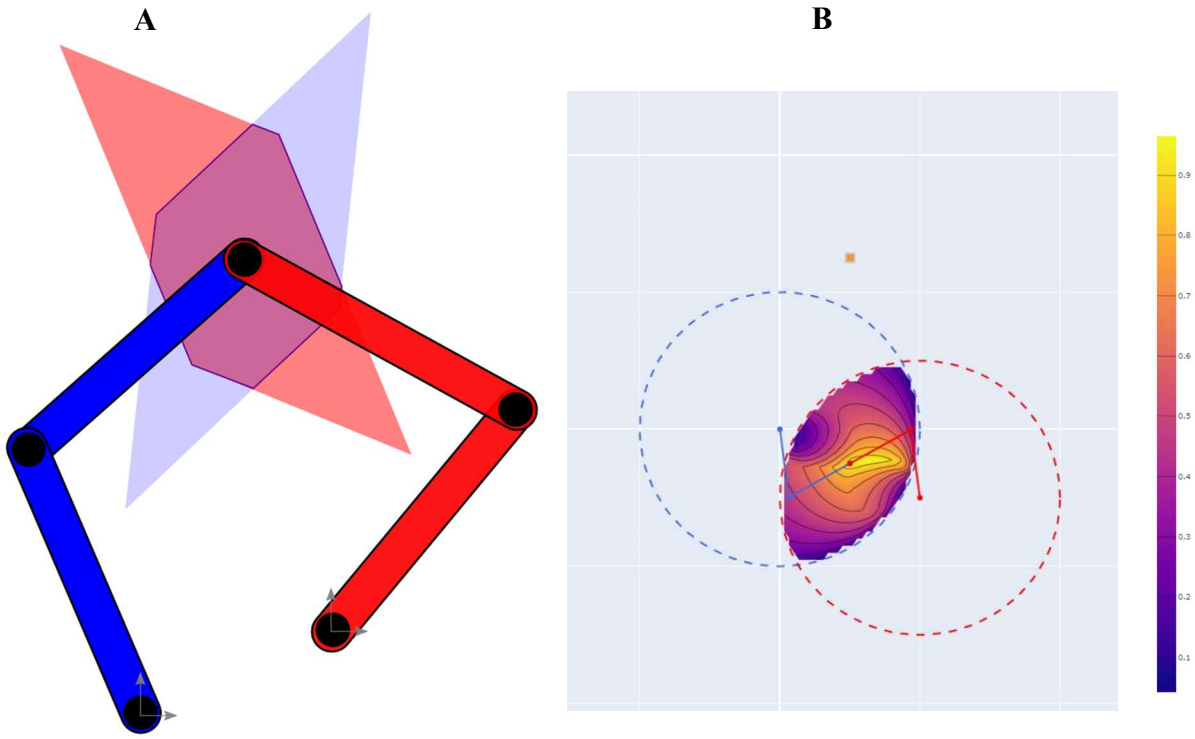

Fig 4.2. Exploration of the Force-Space Congruence Function.
To develop an intuition for the interaction of Force-Spaces, we developed a simulation of the static interaction of 2 Revolute-Revolute (RR) robots. Each robot was equally strong, in terms of its ability to develop torque at its 2 (one proximal and one distal) joints. The relationship between the square torque space, and the Force-Space as a function of robot configuration is found by mapping thorough the force Jacobian. A congruence function was defined as the quotient of the overlapping (purple) area to the size of the force space itself (A). The value of this function is always between 1 and 0. figure B shows a contour plot of the convergence function for 2 RR robots of equal strength and limb-length, but with different root locations. As the roots of the robots move further away from each other the average congruence score decreases.

interaction with an object is largest in the sagittal plane. Meaning the workspace requirements of every other plane of usage can fit inside the sagittal plane usage. Thirdly, the forces involved in other planes of usage, such as the frontal plane, are dramatically lower than the sagittal plane. For these reasons, design of the robot architecture in the sagittal plane was most natural.

4.3.2 Exploration of force-space congruence

From the concept of force-space requirements, we developed models for the overlap of two force-spaces - one force space representing the robot, and the other representing the human. We began by building a mathematical model of 2 interacting serial Rotation-Rotation (RR) robots with equal joint torque capabilities on all 4 driving joints (Fig 4.2). The force space of an RR robot may be calculated in the following way. Take the torque space plot, which is in this case a perfect square, with 4 corners located at ± 1Nm from the origin. Map each of these points through the force Jacobian which relates force and the end point of the robot to joint torques as a function of robot configuration. The resulting shape is a parallelogram. Near a singularity, the length of this parallelogram becomes infinite, in the same direction as the velocity capability of the robot drops to zero, and the Jacobian drops rank.

The feasible workspace of an RR robot is a perfect circle, and the intersection curve between the two robots is the intersection of two circles of equal radius, separated by an x,y offset that corresponds to the distance between the robot's grounded joint (called the root from here on). In the case where the offset is (0,0) the two robots have identical workspaces, and match perfectly in terms of force rendering capability. This is the case of a perfectly matched exoskeleton. As the roots of the two robots move away from each other however, the quality of the force-space

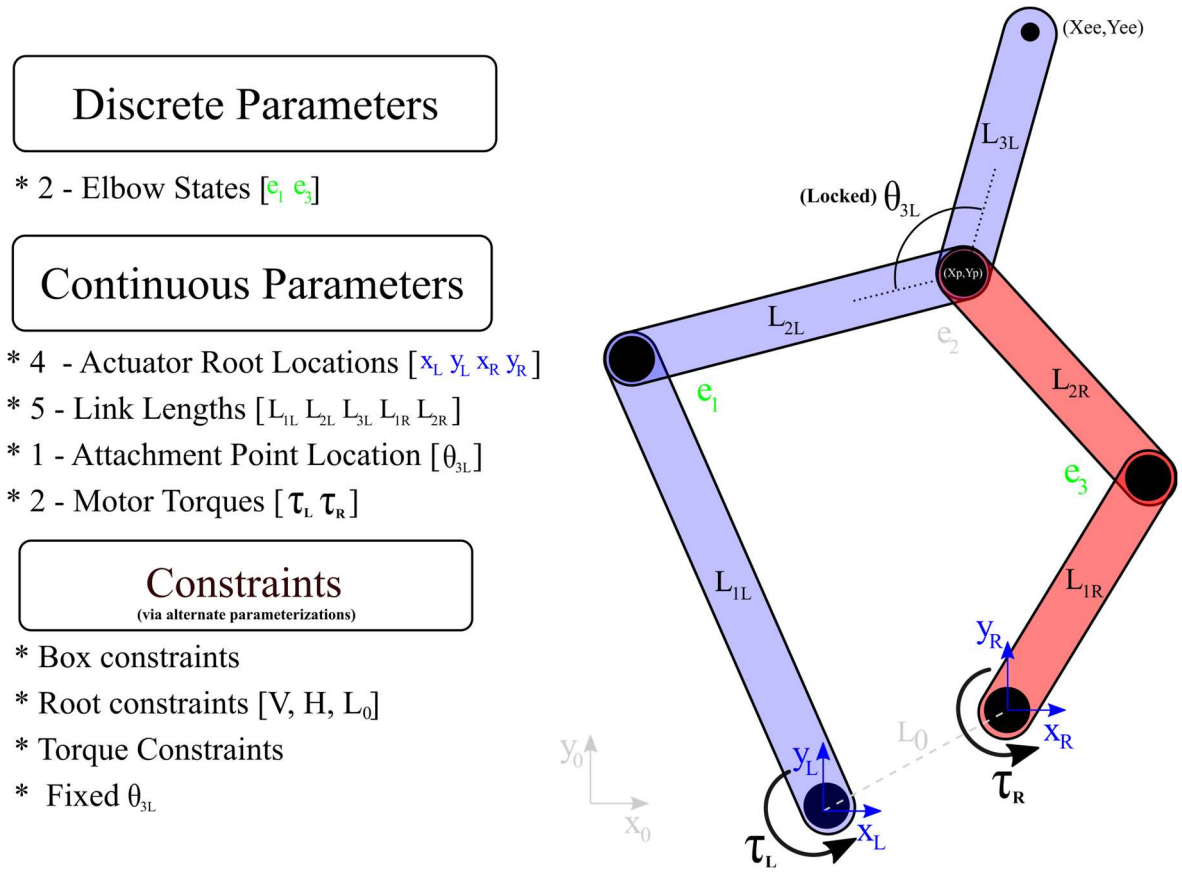

Fig 4.3. Parameterization of the Generalized 5-Bar Linkage.
We created a model of the forward kinematics, inverse kinematics and statics of a 5 bar linkage. We call the model a generalized 5-bar linkage, because the interface to the human at point (Xee,Yee) may be connected to link L2L at an arbitrary distance and angle represented in the model by parameters L3L and θ3L, respectively. Discrete parameters of the model include the elbow states being in or out. Continuous parameters of the model are the locations of the two roots of the parallel robot, the link lengths, the location of the attachment point, and the magnitude of the motor torques. Constraints were placed on the model which can limit the set of feasible robots designs. Constraints on the locations of the roots, combined with constraints on θ3L allowed for the construction of a robot which is symmetrical about the vertical axis, and constraints for L0 distance as well as maximum torque were used to enforce physical feasibility of design, and motor axis could not be collocated and motor torque was limited by available motor choices.

congruence diminishes. The force-space congruence may be defined from the perspective of one of the robots, as the fraction of area of the force-space which is overlapped by the other, servicing force-space. This is depicted as the purple area in Fig 4.2A. The force-space congruence function has a maximum value of 1, and a minimum value approaching 0, which is well behaved. It's worth noting that the area of the force-space of either robot is not a conserved quantity. What is conserved is the virtual work or instantaneous power of either robot. Alternatively, it's possible to define a force-space congruence function with a normalization factor by dividing the overlapping area by the total area.

From 4.2B, it's clear that as the roots of the two robots move away from each other, the average force-space congruence goes down. In fact, there is only one point, located at the center of the intersection where there is perfect congruence, every other point in the intersection is in some ways compromised, and in particular at the edges of the workspace intersection, where one of the robots is at its singularity, the force-space congruence approaches zero.

Even from this simple model of force-space interaction, it was possible to derive intuitions about the interaction of force-spaces and this enables the construction of more sophisticated models.

4.3.3 Human Model

The human model is constructed as a sagittal plane model with 3 degrees of freedom. We solved the IK problem as a minimization of potential energy of a set of 3 torque springs placed at each of the joints. We tuned the resting position and the stiffness until the IK performance appeared to be realistic. Data about the force production capacity of a human interacting with a force plate was taken from literature [7]. An ellipse was fit to this data, resulting in an attachment point to the

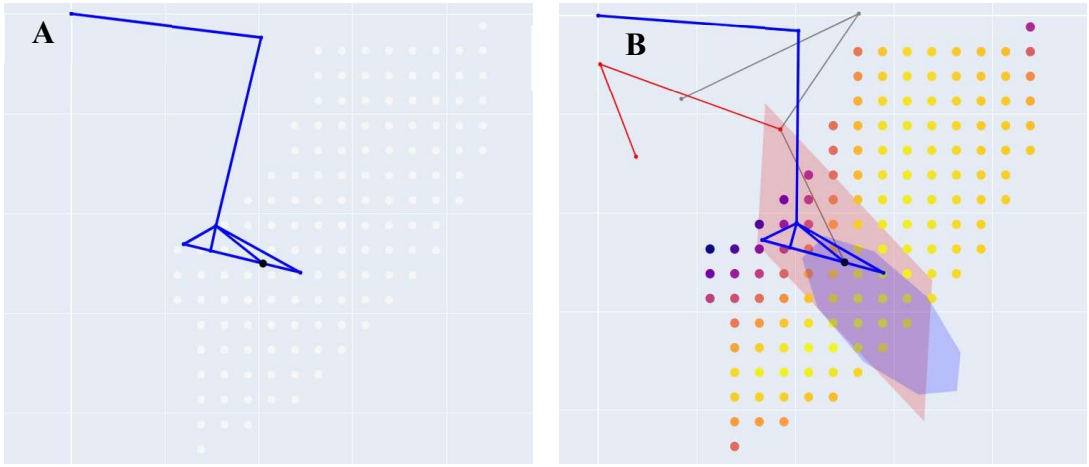

Fig 4.4 Objective Function and Optimization Process.
The Generalized 5-bar linkage Model was combined with a Sagittal plane human model to form a joint human-robot system. The force-space of the human was taken from literature values [7]. A Cartesian sampling grid was formed within the workspace of the human (A). For a proposed robot design, the congruence score was calculated over the workspace at each sampled point. The sum of the congruence scores over the sample grid defines the value of the objective function for that set of robot parameters. The DIvided RECTangles (DIRECT) Optimization algorithm was used to explore the state space of possible robot linkage designs to find an optimal force space congruence with the human model.

foot that was biased to reflect the asymmetrical strength of the flexor vs. extensor muscles, with the latter being stronger than the former. A simplifying assumption was made that this force ellipsoid could be rotated with about the hip, through a line which connected the ankle joint to the hip joint. This simplifying assumption alleviated the need to record data from all over the human workspace.

4.3.4 Robot Model

The 2DOF parallel robot was parameterized as a generalized 5-bar linkage (Fig 4.3). We have chosen this name to indicate that the attachment point between the robot and the human can occur anywhere in the plane on L2L – not just at the pin-joint connecting the left and right branches of the parallel robot. This general attachment point to L2L is parameterized by the (locked) angle θ3L and link L3L. The robot has 2 discrete parameters, which are the states of the elbow of the robot e1 and e3. State e2 is a calculated state and is determined by the IK solution once the elbows are fixed. The robot also has a set of continuous parameters. 4 parameters determine the location of the robot roots, (xl,yl), (xr,yr). 5 parameters determine the link lengths of the robot, and the motor torques can vary.

A set of constraints have been implemented on the robot to limit the feasible space to a subset of possible robots. The relationship between the roots of the left and right robot may be constrained to a vertical or horizontal orientation. L0 may also be used to specify a minimum distance between the roots. This is used to ensure that the resulting designs are physically realizable, as the design must have both motors on the same side or there is a minimum separation distance due to physical interference of the motors. Additionally, θ3L may be set to 0, which in combination with the vertical orientation of the roots, ensures the robot is symmetrical about a

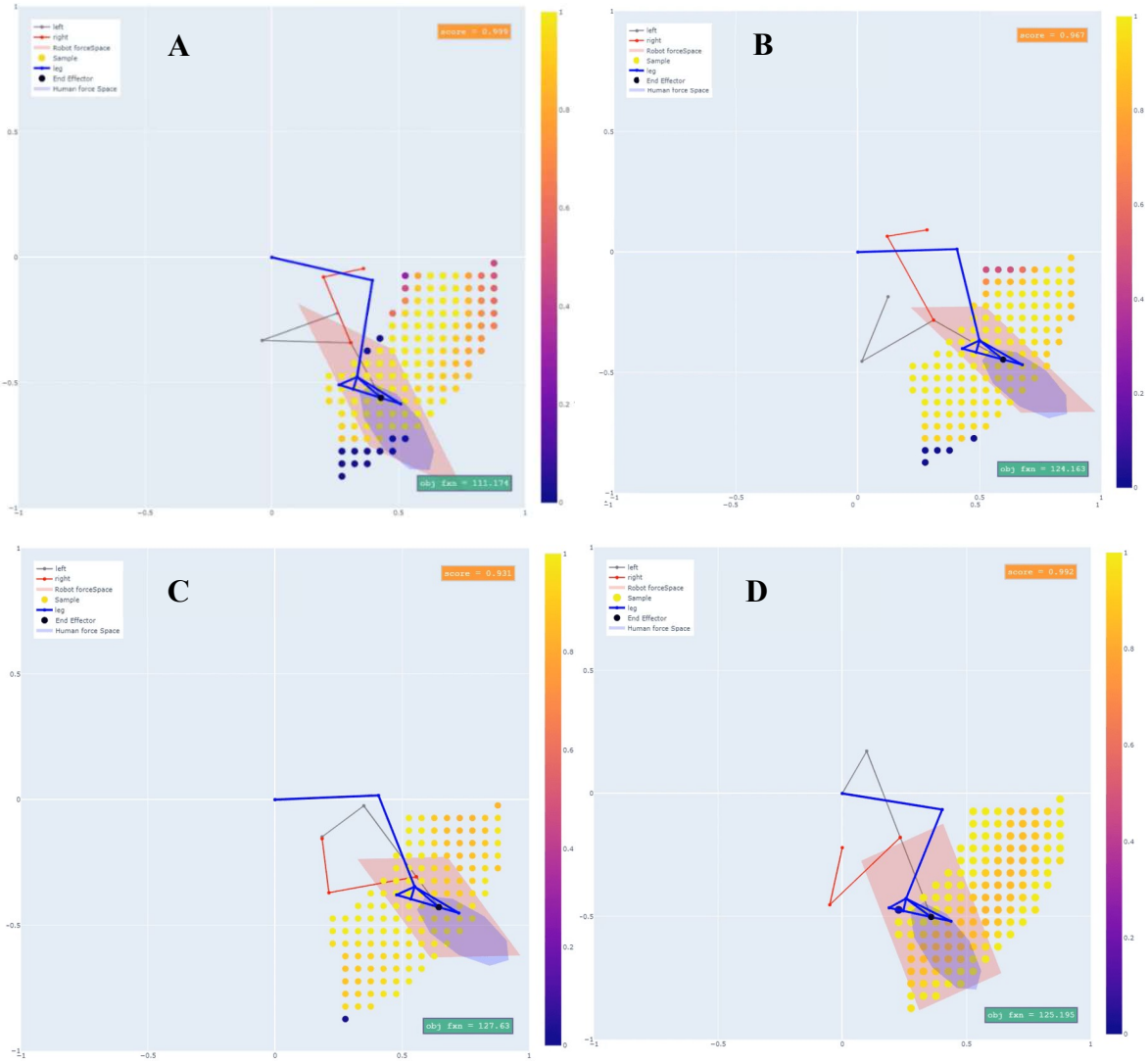

Fig 4.5. Optimization Results.
A set of numerical experiments was conducted to determine the best robot designs under different constraints. (A). shows a design after n=4000 iterations with no constraints (B) shows the same simulation after n=250,000 Notice that the score has increased and the link lengths have changed but the fundamental shape remains similar to (A). in (C) the constraint that the roots of the robot must lie vertically is introduced. This constraint narrows the searchable space, and causes the optimizer to discover a better solution than B more quickly n=4000, but the solution it comes up with is not physically realizable. (D) shows a design which came out of the optimizer when symmetry constraints were added ($\theta 3L = 0$) and when the roots of the robot were constrained to be vertical, and spaced at least 22cm apart – a requirement that comes from the mechanical constraint of designing a physical robotic system, as designing co-axial which drive from the same side is prohibitively difficult.

vertical axis and so can be used from the right or left sides.

Forward kinematics were solved for each branch individually. IK was solved for the left branch, and then the location of the right branch top was calculated. IK was then performed to that point. The Force Jacobian of the generalized 5 bar linkage was calculated numerically using the method of finite differences on the inverse kinematic solution. The force space was then calculated by mapping the torque space corner points through the force space Jacobian.

4.3.5 Joint objective function and optimization

The joint objective function is formed as follows: a sampling grid was constructed on the human model that represented that workspace over which matching was to be scored. This workspace could be seen in figure. 4.4A. The resulting shape and location were calculated and cached at each of the 135 discrete points in this workspace. A parameter set defining a potential robot design is specified. For each of the sampled points in the workspace, IK is performed on the robot model. If IK cannot be solved, a score of zero is returned for that point. If IK solves, then the force-space can be calculated for the robot at that configuration. The force space is calculated via the force Jacobian resulting in a parallelogram which at least partially overlaps the human force space ellipsoid. The area of overlap was calculated using a geometric numerical library, and a congruence score is calculated for that point in space. The sum of these scores over the sampled points in the human workspace, represents the value of the objective function for that robot design.

Using the DIRECT (Divided Rectangles) optimization method [2], we calculated the robot design with maximal congruence summed over the sampling grid. Different parameterizations of the robotic model allow for constraining the solution space of robot.

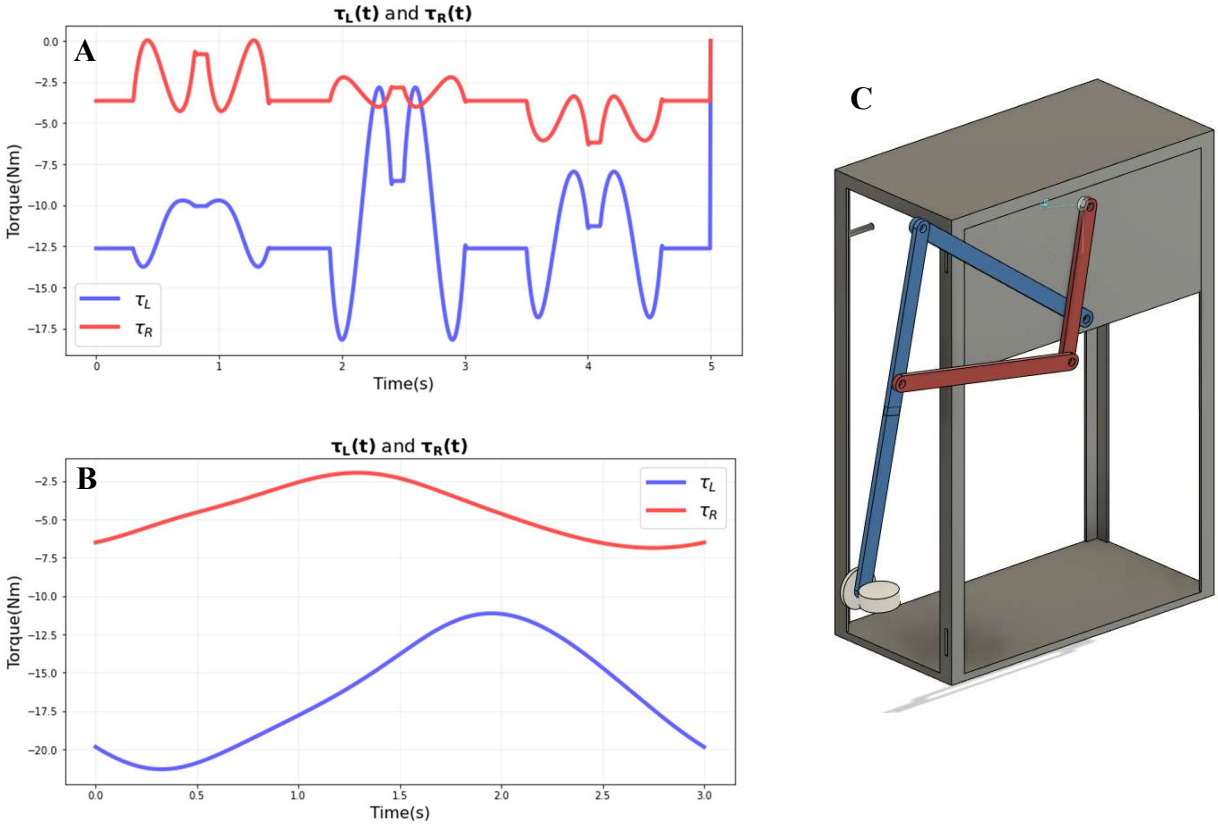

Fig 4.6 Trajectory Curves from a Dynamic Model of the Robotic System.
Using the Chrono engine, we constructed a Dynamic model of a robot design developed from the static optimizer. We constructed a CAD model of the robot and calculated inertial properties for the link segments. We built a library of minimum-jerk trajectory paths for the end effector (Xee,Yee) location and ran Inverse Kinematic and Inverse Dynamic simulations to assess torque usage from inertial loads and gravity. Figure A shows the torque requirement for a star reach pattern, which figure B shows the torque requirement for the right and left motors during a circular path of radius .2 meters.

4.4 Results

Four robot designs are pictured in figure 4.5 in order from least to most constrained. The first solution (A) resulted after 4000 iterations of the DIRECT optimization method with no constraints on parameters. This robot scored 111 on the congruence objective function, has an e1=down, e2=down configuration, and utilized to some extent differential joint torques. It's easy to tell that this robot is sub optimal, as IK cannot solve in the bottom left of the space, as indicated by the dark blue circles. Solution (B) is similarly unconstrained but was run for 250,000 iterations. The basic design remained unchanged, but the locations of the roots, and the link lengths have changed such that the score has increased to 124. There are still a few points at the bottom that don't solve however. In (C) the vertical constraint was added, so that the roots of the right and left robot had to be on top of one another. The simulation was run for 4000 iterations, and scores 127. This indicates that adding the constraint of verticality actually helped the optimizer to search a more fruitful region of space, but there is a slight problem. The design that the optimizer selected is not physically realizable, as the motors roots cannot be right on top of each other. Adding a L0 minimum separation distance constraint, as well as $\theta 3L=0$ symmetry constraint to guarantee vertical axis symmetry, we arrive at a solution that scores almost as highly as the previous one, at 125, but is physically realizable.

Figure 4.6 shows the results of a dynamic simulation made in the chrono engine. Trajectory generation functions were constructed, and this analysis demonstrated that inertial forces were low during moments that were programmed with velocities one might encounter when rendering rehabilitative environments.

4.5 Discussion

The DIRECT optimization algorithm was chosen because although the optimization space appeared smooth, there were many local minima, possibly due to the presence of many trigonometric functions within the static equations. Gradient based methods then were not appropriate for such a landscape.

The four solutions presented in the results section were not the only solutions by any means but were meant to demonstrate points and insights that came out of the analysis. Constraints seemed to help the optimizer get out of regions of space were there were good, but not great solutions. It's possible these solutions would have been found given enough computation budget, or if the right exploration – exploitation compromise had been made.

High congruence between the force-space requirements of the human and robot increases the inherent safety of human-robot interaction. The robot designed by our optimization routine allowed us to select a parallel robot which best matches the experimentally determined force-space. High force space congruence is not the only factor to consider, however. Machine transparency is also a factor that is worth consideration and hasn't been factored into the development of this geometry. This could be added as an additional factor in the objective function and explored through a multi-objective optimization process. This point is also valid for the consideration of other use cases beside the sagittal plane. The difficulty to such an approach is the correct selection of the weighting functions for multiple objects which define the pareto optimal trade-off curve.

The dynamics analysis was important to explore as the optimization was purely static and didn't take into consideration inertial effects. Future dynamic models could explore the complex interaction between a parallel robot such as this and the leg it's meant to interact with.

4.6 Conclusion

The objective of this study was to meet the force requirements of a human leg in the sagittal plane under realistic constraints on actuator placement, while retaining the advantages of a parallel robotic architecture. Starting from the geometry of intersecting force-spaces, our approach led to a parallel robot architecture design that was intuitive, performant, and realizable. This method may be useful to the robotics community in designing other parallel robots for human interaction, or more broadly in machine design where a parallel mechanism must achieve a force objective within a specified workspace.

4.7 References

[1] M. Alcobendas-Maestro, "Lokomat Robotic-Assisted Versus Overground Training Within 3 to 6 Months of Incomplete Spinal Cord Lesion Randomized Controlled Trial," *Neurorehabil Neural Repair*, vol. 26, no. 9, pp. 1058–1063, Nov. 2012.

[2] N. Hogan, H. I. Krebs, J. Charnnarong, P. Srikrishna, and A. Sharon, "MIT-MANUS: a workstation for manual therapy and training. I," in *[1992] Proceedings IEEE International Workshop on Robot and Human Communication*, 1992, pp. 161–165. doi: 10.1109/ROMAN.1992.253895.

[3] L. M. Rios and N. V. Sahinidis, "Derivative-free optimization: a review of algorithms and comparison of software implementations," *J. Glob. Optim.*, vol. 56, no. 3, pp. 1247–1293, Jul. 2013, doi: 10.1007/s10898-012-9951-y.

[4] "DIRECT Optimization Algorithm User Guide", Accessed: Nov. 13, 2020. [Online]. Available: https://repository.lib.ncsu.edu/bitstream/handle/1840.4/484/crsc-tr03-11.pdf?sequence=1

[5] J. M. Gablonsky and C. T. Kelley, "A Locally-Biased form of the DIRECT Algorithm," *J. Glob. Optim.*, vol. 21, no. 1, pp. 27–37, Sep. 2001, doi: 10.1023/A:1017930332101.

[6] N. Rezzoug, V. Hernandez, and P. Gorce, "Upper-Limb Isometric Force Feasible Set: Evaluation of Joint Torque-Based Models," *Biomechanics*, vol. 1, no. 1, pp. 102–117, Apr. 2021, doi: 10.3390/biomechanics1010008.

[7] K. G. Gruben, C. López-Ortiz, and M. W. Schmidt, “The control of foot force during pushing efforts against a moving pedal,” *Exp. Brain Res.*, vol. 148, no. 1, pp. 50–61, Jan. 2003, doi: 10.1007/s00221-002-1276-5.

[8] A. Skuric, V. Padois, and D. Daney, “On-line force capability evaluation based on efficient polytope vertex search,” *arXiv* 2011.05226v1

Conclusion and Future Directions

In the course of this research program, I've developed a novel robotic platform and used it to study adaptation and skill learning in the lower-limb. Beyond the completion of my degree, the BADGER Lab Rehab Robotics research program will continue its mission to develop goal-directed therapies for the lower-limb, building on the foundation established by this body of work. Unequivocally, the direction going forward will be to complement the motor control studies performed in healthy controls, with therapeutic investigations *in stroke affected populations*. In the short term, this may entail comparing the results from the lower-limb reaching studies detailed in chapter 2 with comparable studies in a stroke affected population.

Ultimately though, the goal isn't to simply affect adaptation, but to deliver interventions that challenge subjects and increase motor capability. A necessary step towards this end is to develop methods for characterizing the individual deficits unique to each stroke patient. Each task performance is a potential window into the coordination malfunction of a stroke patient. But how do we distinguish between what is fundamental from what is extraneous? What is signal from what is noise? I suspect that will be a big part of the program going forward.

One of the things I would like to see explored is what I call co-learning algorithms. In most haptic renderings, the objective of the robot is to faithfully render an environment defined by a set of differential equations. The robot is in a sense indifferent to the time history of who or what is interacting with it (apart from a possible integral term). In a co-learning algorithm by contrast, the robot is actively probing the human to learn about their capabilities (and deficits) while at the same time, the human is trying to understand their task and how to interact with the robot. It seems likely to me that this is an approach stands to yield a rich understanding of human motor control.

Finishing the 2DOF robot, a task left to the next cohort of students, will significantly expand the capabilities of the research program, allowing for planar haptic rendering in the sagittal, frontal, transverse, and intermediate planes. It will be rewarding to see the vision for this multi-use robotic architecture come to fruition.

Appendix: Instruction Set

Group A and B shared instruction set

Summary: Thank you for participating in this experiment on how people learn new movements with their legs. Before you get started with the experiment, let's quickly discuss the robot's safety system, what you will be trying to do, and the overall structure of the experiment.

How the Safety System Works

The robotic cycle (pictured to the right) is equipped with an electric motor that allows it to respond to your actions in both familiar and new/unfamiliar ways. To ensure your safety, there are two safety switches located on the hand rests of the robot. For the motor to be powered, *both* the left-hand and the right-hand switch must be *gently* squeezed at the same time. Releasing either hand will depower the robot. A button in the upper right-hand corner of the computer monitor in front of you shows whether the system is powered. When depowered, the robot enters a low-resistance coasting mode

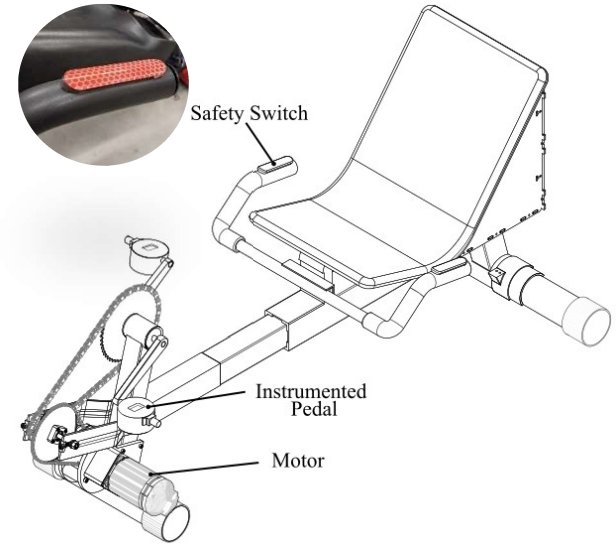

What you are trying to do:

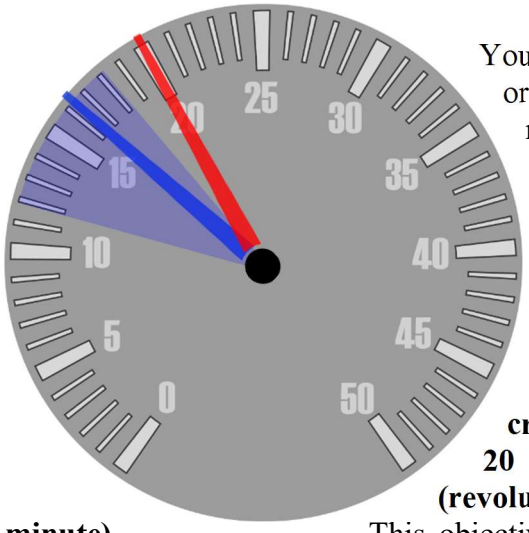

You will be interacting with a robot that relates how you push or pull on the pedals to the rotation of the crank (the solid metal piece that the pedals thread into). This relationship is constant, but unknown to you and must therefore be learned by experience. Your task is to coordinate the forces you exert on the pedals to produce a **forward crank speed of 20 RPM (revolutions per minute).** This objective is indicated by the red target needle on the speedometer. Feedback of your instantaneous speed will be supplied to you via a blue needle. Once you have achieved a consistent forward crank movement, a secondary

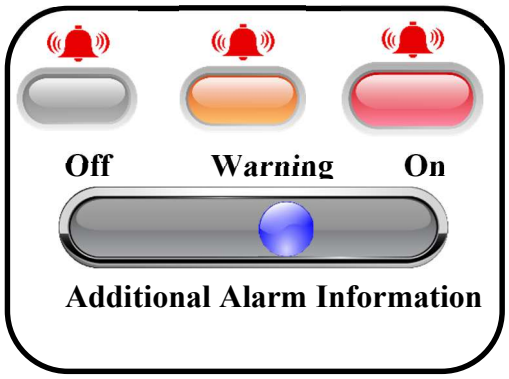

objective will be to **reduce the variability of your forward crank speed**. The variability of your forward speed will be indicated by the size of a translucent blue circular wedge which you will try to make as small as possible. Additionally, there is an alarm system (pictured on the right) which is set off by incorrect coordination patterns. *It is possible to coordinate your legs in such a way which moves the crank forward at 20 RPM, does not set off the alarms, and uses low to moderate muscle effort. This is a test of coordination, not strength.*

Structure of the Experiment

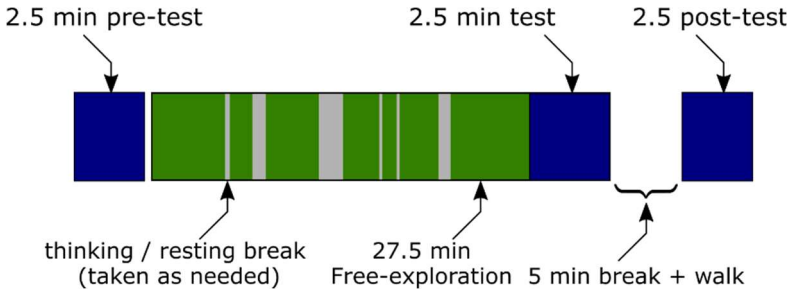

The study consists of 6 separate sessions, conducted on 6 different days. During each session, there is a 2.5 minute pre-test block to evaluate your initial performance, a 27.5 minute free-exploration block for you to learn the task, a 2.5 minute test session, and a 2.5 minute post-testing block. Your goal during the testing blocks is to perform your very best on the forward pedaling task, while your goal during the free-exploration block is to explore new ways of moving your legs and to learn how to control the robot. During the free-exploration period, you **should** take intermittent breaks to think, rest, or as you see fit, but during the testing periods you should strive do you best at the task **without disengaging the power**.

Tips for Free Exploration:

Exploring different crank angles, force directions, and focusing on one leg at a time are useful strategies for exploration

Quiz:

1. Only one safety switch needs to be pressed down for the robot's power to be engaged
2. When the indicator in the upper right-hand corner is green, the motor is powered.
3. My objective is to produce a constant crank speed 30 rpm
4. A secondary objective is to decrease the variability of the crank speed
5. I can deactivate the power to the robot if I feel unsafe, or whenever I choose to, including If I feel it's a useful strategy for learning.
6. It's impossible to prevent the alarm from going off
7. the point of the free-exploration session is to explore different ways of moving your legs
8. the point of the testing period is to perform your best at forward pedaling
9. I should aim to not let go of the power during the testing blocks

To protect the integrity of the study, please don't discuss details or learning strategies with other participants!

Group B instruction Set

The below instruction set was given only to the cognitive model group.

Cycling Environment Description

The robot has been programmed to respond to you in a way we call "half-reversed cycling "or HRC for short. In HRC, the left pedal functions as a normal bike does. This means when you push the left pedal forward and away from you, the crank will speed up in the forward direction. The right pedal operates differently, however. On the right side, the relationship between the direction you push, and the motion of the crank has been **reversed**. So, pushing on the right pedal as you normally would to pedal forward will actually slow the crank down and make it come back at you. Below are a set of strategies and skills that will help you become proficient in half-reversed cycling.

Strategies and skills

Strategy 1: Practice strategies in order from beginner -> intermediate -> advanced.
To avoid being overwhelmed, work on developing strategies in order of increasing difficulty

Strategy 2: Consult this manual.
You are allowed to consult this manual during the 30min free-exploration period of each session. If you forget the details of a strategy, you can always come back here to remind yourself.

Strategy 3: Learn to oscillate the pedals back and forth first before cycling forward (Beginner)
The first time you interact with the environment will be very confusing. Before you start trying to pedal forward, see if you can get the system to oscillate back and forth.

Strategy 4: Pedal the left side as you would a normal bike. (Beginner)
The left pedal functions identically to a normal bike so push on this side as you normally would. But, be aware that if you only use the left leg, you will set off the alarm (see strategy 7 at appropriate time).

Strategy 5: When you get stuck, release the safety switches and reposition yourself. (Beginner)
One of the consequences of reversing the behavior of the right pedal is that it creates a "sticky" or stable location of the crank which is difficult to escape! This location of the crank is pictured to the right. When you are learning and you get stuck in this position, you could try to fight your way out of it, but it is better to *deactivate the power* and reset the crank to a location where you can push with your left (non-reversed) foot to move the crank forward. You can deactivate power

by letting go of one of the safety switches. This is especially important during the free-exploration phase where you are trying new things out.

Strategy 6: Resist the urge to push with your right (reversed) leg. (Beginner)
All of your instincts will tell you to push with your right foot as you would on a normal bike. This will **NOT** work, and crank will move the opposite way from what you intend. You will have to unlearn this habit to perform well at the HRC.

Strategy 7: Learn to use the right foot to move the crank forward. (Intermediate)

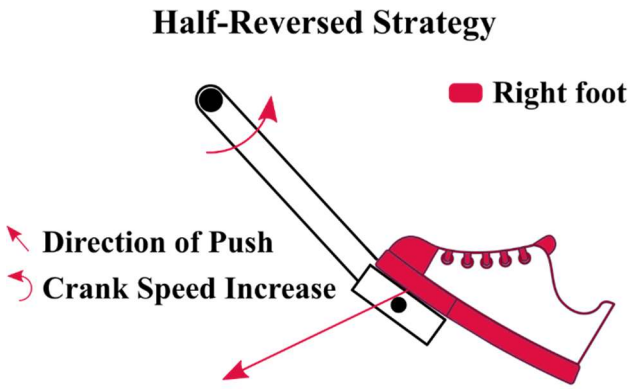

To make the half-reversed cycle go forward with the right (reversed) foot, you must push into the pedal at the location depicted, and the crank will come back at you! Instead of powering the bike, you should think of it as allowing the bike to power you!

Strategy 8: Avoid triggering the alarm by using a balanced approach. (Intermediate)
The robot has an alarm system to ensure that you use both feet to make it move forward. If you only use one leg or the other to make it move forward, the robot will become progressively more difficult to operate, and will eventually set off the alarm. As long as you use both legs to move forward, you won't set off the alarm. There is also a short alarm that is just auditory (sounds like unnnt -unnnt) that is set off by using too much torque and can be avoid using strategy 9.

Strategy 9: To reduce speed variability, push less hard, for longer. (Intermediate)
Large forces cause the crank speed to spike. Try to power the bike with smaller forces, but smoother and applied over a longer time.
Strategy 10: For more control, power with the right leg and then the left. (Advanced)
You know now how to push on the robot and make it go forward. Consider starting the push earlier with the right foot, and finish the push later with the left foot. This makes the power stroke of the right and left legs more distinct and easier to control finely.

Strategy 11: Support weight of the right leg to prevent slowdown in crank position shown (Advanced)
In the crank position shown, the weight of the leg on the reversed side (right) will cause the crank to slow down. Consider lifting the weight of the right leg off the pedal slightly in this position.

Strategy 12: for smoothest operation, pull with the left leg. (Advanced)

In the crank position shown below consider moving the crank forward by pulling with your left leg. Think about pulling your left heel towards your left glute / the seat. (the dotted blue vector)

Strategy 11: Support Right Leg Weight / Strategy 12: Pull With Left Leg

Quiz:

1. Strategies are arranged from beginner to advanced as number increases
2. I'm allowed to consult the manual during the free-exploration block only
3. The right side of the robot pedals like a normal bike
4. If I'm stuck, I can depower the robot and reposition the crank to somewhere easier during the free-exploration, but should try to maintain power all the time and do my best during the testing blocks.
5. I should practice "not pushing" on the right side, to unlearn my normal cycling habits
6. I can avoid triggering the alarm by using a balanced pushing approach, where I use both the right and left leg to accomplish the activity.
7. To reduce crank speed variability, I should push harder, but for shorter periods of time
8. To maximize performance, I should use advanced strategies like supporting the weight of my right leg, and pulling with my left leg